AN INVESTIGATION OF WING BUFFETING RESPONSE AT SUBSONIC AND TRANSONIC SPEEDS: PHASE II F-111A FLIGHT DATA ANALYSIS

VOLUME I - SUMMARY OF TECHNICAL APPROACH, RESULTS AND CONCLUSIONS

by

David B. Benepe, Atlee M. Cunningham, Jr., Sam Traylor, Jr., and W. David Dunmyer

Prepared under Contract No. NAS 2-7091 by
GENERAL DYNAMICS CORPORATION
Fort Worth Division
Fort Worth, Texas

for

AMES RESEARCH CENTER
NATIONAL AERONAUTICS AND SPACE ADMINISTRATION

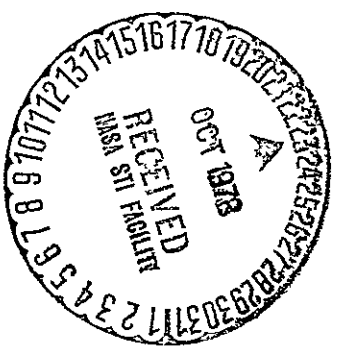

NASA CR-152112

AN INVESTIGATION OF WING BUFFETING RESPONSE AT SUBSONIC AND TRANSONIC SPEEDS: PHASE II F-111A FLIGHT DATA ANALYSIS

VOLUME I - SUMMARY OF TECHNICAL APPROACH, RESULTS AND CONCLUSIONS

by

David B. Benepe, Atlee M. Cunningham, Jr.,
Sam Traylor, Jr., and W. David Dunmyer

Prepared under Contract No. NAS 2-7091 by
GENERAL DYNAMICS CORPORATION
Fort Worth Division
Fort Worth, Texas

for

AMES RESEARCH CENTER
NATIONAL AERONAUTICS AND SPACE ADMINISTRATION

OUTLINE &
TABLE OF CONTENTS

OUTLINE &
TABLE OF CONTENTS, Continued

LIST OF TABLES

LIST OF TABLES, Continued

LIST OF FIGURES

LIST OF FIGURES (Cont'd)

LIST OF FIGURES, Continued

LIST OF FIGURES, Continued

SUMMARY

A detailed investigation of the flight buffeting response of the F-111A was performed in two phases In Phase I stochastic analysis techniques were applied to wing and fuselage responses for maneuvers flown at subsonic speeds and wing leading-edge sweep of 26 degrees Power spectra and rms values of response were obtained for

(1) vertical accelerations at the wing tips, the center of gravity and the pilot's seat,

(2) lateral accelerations at the center of gravity and the pilot's seat,

(3) vertical sheat, bending moment and torsional moment at 4 spanwise locations on the right variable sweep wing panel.

In Phase II the analyses were extended to include maneuvers flown at wing leading-edge sweep values of 50 and 72 5 degrees at subsonic and supersonic speeds and the responses examined were expanded to include vertical shear, bending moment, and hingeline torque of the left and right horizontal tails

This volume emphasizes the results of the Phase II investigations but also contains some Phase I results for comparison purposes Detailed descriptions of the aircraft, the flight instrumentation and the analysis techniques are

given Power spectra, response time histories, variations of rms response with angle of attack and effects of wing sweep and Mach number are presented and discussed

The major conclusions of the investigation are

(1) The structural response to buffet during moderate to high-g maneuvers is very complex Many symmetric and antisymmetric natural vibration modes (and perhaps asymmetric modes) can be excited to significant levels of response.

(2) An array of different types of sensors and locations of the sensors is needed to adequately describe the structural response during buffet investigations

(3) The modal content of the response varies with sensor type and location and also can vary with angle of attack, wing sweep and Mach number. The variations in modal content are attrituted to the variations in the spatial extent and phase relationships of the separated flows.

(4) At low wing sweep there are significant differences in the variations of rms response with angle of attack for different Mach numbers The largest magnitudes of response were measured during flight

conditions where shock induced flow separations were present.

(5) In general, the rise in rms response with angle of attack becomes smaller as wing leading edge sweep is increased

(6) The buffeting loads on the wing are small relative to the maneuver loads at the most inboard measuring station but become larger near the wing tip The larger relative rms values of response near the tip are attributed to higher frequency modes and thus should be considered important from a fatigue standpoint with respect to secondary structure.

The data obtained in this investigation were used to help formulate and evaluate a method of predicting buffeting response which uses wind tunnel measurements of the fluctuating pressures on a "rigid" wing as the input forcing function

The entire investigation is documented in eight reports which are listed below

Benepe, D. B , Cunningham, A. M , Jr , and Dunmyer, W. D An Investigation of Wing Buffeting Response at Subsonic and Transonic Speeds Phase I F-111A Flight Data Analysis

Volume I - Summary of Technical Approach, Results and Conclusions, NASA CR-152109.

Volume II - Plotted Power Spectra, NASA CR-152110

Volume III - Tabulated Power Spectra, NASA CR-152111

Benepe, D B , Cunnıngham, A. M , Jr , Traylor, S., Jr , and Dunmyer, W D. An Investigation of Wıng Buffeting Response at Subsonic and Transonıc Speeds· Phase II F-111A Flıght Data Analysis.

Volume I - Summary of Technical Approach, Results and Conclusıons, NASA CR-152112

Volume II - Plotted Power Spectra, NASA CR-152113

Volume III - Tabulated Power Spectra, NASA CR-152114

Cunnıngham, A. M , Jr , Benepe, D B , Watts, D , and Waner, P G · A Method for Predictıng Full Scale Buffet Response wıth Rigid Wind Tunnel Model Fluctuating Pressure Data.

Volume I - Prediction Method Development and Assessment, NASA CR- 3035.

Volume II - Power Spectral Densitıes for Method Assessment, NASA CR- 3036.

SYMBOLS

Note: Quantities are presented in the International System of Units (U.S. customary units in parenthesis). The work was performed using U.S. customary units.

b	wing span - m, (ft)
$B.M._{DES}$	design value of wing bending moment, N-m, (in - lb)
c.g.,C.G.	"center of gravity"
f	frequency, hertz
f_o	spectral base frequency or analysis bandwidth, hertz
F_Z	wing vertical shear as measured by strain gages - N, (lb)
g	gravitational acceleration
M	Mach number
M_X	Wing Bending Moment as measured by strain gages N-m, (in - lb)
M_Y	Wing torsional moment - N-m, (in - lb)
n_{max}	maximum maneuver load factor - g's
S	theoretical wing area (leading and trailing edges of swept panel extended to airplane centerline m^2, (ft^2)
T	length of input frame in spectral analysis - seconds
T_1	start time of interval for spectral analysis - seconds
T_2	stop time of interval for spectral analysis - seconds
ΔT	time interval used for spectral analysis = T_2-T_1,sec
V_{DES}	design value of wing vertical shear, N, (lb)
y	lateral acceleration g's
z	vertical acceleration g's

SYMBOLS (Continued)

α	indicated angle of attack referenced to wing manufacturing chord plane
α_{max}	maximum indicated angle of attack - deg.
α_{nom}	nominal angle of attack representing time interval ΔT
α_1	indicated angle of attack at time T_1, deg
$\Delta\alpha$	increment in indicated angle of attack during time interval ΔT, deg
β'	indicated sideslip angle, deg
σ_a	rms value of acceleration fluctuations - g, rms
$\sigma_{V_{max}}$	maximum rms value of wing vertical shear fluctuations - N, rms, (lb, rms)
$\sigma_{BM_{max}}$	maximum rms value of wing bending moment fluctuations - N-m, rms, (in - lb, rms)
Ψ_T	average rms value determined from power spectral analysis

ABBREVIATIONS

Alt	altitude
Asym	antisymmetric
B.M.	bending moment
Cross-PSD,XPSD	Cross power spectral density
dB	decibel
Dyn Press	dynamic pressure
FM	frequency modulation
H_z	hertz
hor,hori	horizontal
in-lb, IN-LB	inch-pound
inb'd	inboard
L	left
lb,LB	pound
L/H	left hand
LWT	left wing tip
m	meter
N	newton
N-m,N-M	newton-meter
outbd	outboard
P.S.	pilot seat
PSD	power spectral density
R	right
R/H	right hand

ABBREVIATIONS, (Continued)

rms	root-mean-square
RWT	right wing tip
Sym	symmetric
TOR	torsion
W.S.	Wing Station for strain gage measurements

SECTION 1

INTRODUCTION

A detailed investigation of the structural response of an F-111A aircraft to buffet during moderate to high-g maneuvers was accomplished in two phases. In Phase I (References 1, 2, 3) the response characteristics with the variable sweep wings set at a nominal leading-edge sweep of 26 degrees were examined for the seven maneuvers described in Table 1.

Power spectra and rms values of response were determined for 19 different measurement items consisting of vertical accelerations at the wing tips, the center of gravity and the pilot's seat, lateral accelerations at the center of gravity and the pilot's seat and vertical shear, spanwise bending moment, and torsional moment at 4 different spanwise stations on the right wing.

The conclusions reached from the Phase I Study were:

(1) The structural response during buffet is very complex. Many natural vibration modes both symmetric and antisymmetric can be excited during a maneuver in which flow separation occurs on the wings.

(2) The spectral content of the response varies with the type of sensor, the location of the sensor and in some cases with angle of attack

Table 1

PHASE I FLIGHT MANEUVERS

FLT	RUN	MANEUVER	WING SWEEP DEG	NOMINAL FLIGHT CONDITIONS		
				MACH	ALTITUDE	GROSS WEIGHT
48	6	Windup Turn	26.6	70	7,559 m (24,800 ft)	294,472 N (66,200 lb)
77	S&C-R	Windup Turn	25 6	.80	6,035 m (19,800 ft)	266,004 N (59,800 lb)
78	5	Pullup	26 2	.80	3,780 m (12,400 ft)	327,389 N (73,600 lb)
79	9R	Pullup	26 7	.80	1,494 m (4,900 ft)	323,386 N (72,700 lb)
60	10	Roller Coaster	26 6	.87	8,382 m (27,500 ft)	307,817 N (69,200 lb)
78	4	Pullup	26 3	87	3,688 m (12,100 ft)	330,503 N (74,300 lb)
70	2	Pullup	26 8	86	1,494 m (4,900 ft)	328,800 N (73,800 lb)

(3) The variations of rms values of response with angle of attack can be quite different for different values of Mach number. The largest measured responses occurred under conditions where shock-induced flow separations occurred on the wing. In particular the torsional response was significantly higher than anticipated on the basis of previous buffet studies.

(4) The magnitudes of the wing bending and wing shear responses at the most inboard measurement station are small relative to the maneuver loads. Near the wing tip the buffet loads are a much larger percentage of the maneuver loads.

(5) Horizontal tail vibration modes appear to make significant contributions to the fuselage responses.

In Phase II the structural responses at nominal wing leading-edge sweeps of 50 and 72.5 degrees were analyzed. Vertical shear, bending moment and hingeline torque at the root of the left and right horizontal tails were analyzed in addition to the 19 measurement items examined in Phase I. All 25 items were studied for six maneuvers listed in Table 2 In addition the horizontal tail responses were analyzed for two wind up turn maneuvers from the Phase I Study as listed in Table 2

This Volume (NASA CR-152112) summarizes the Phase II investigation. Some data from the Phase I investigation are included in comparisons for the effects of wing leading-edge sweep angle. In the body of the report descriptions are given of the test aircraft, the airborne instrumentation pertinent to this work, and the data analysis techniques. The results of the study including

Table 2

PHASE II FLIGHT MANEUVERS

Flight	Run	Maneuver	Wing Sweep	Nominal Flight Conditions		
				Mach	Altitude	Gross Weight
61	R227	Windup Turn	49 1	80	8,382 m (27,500 ft)	330,948 N (74,400 lbs)
51	S38/150	Slowdown Turn	49 5	1 25 - 1.13	10,912 m (35,800 ft)	278,903 N (62,700 lbs)
48	4	Windup Turn	49 8	1.20	9,053 m (29,700 ft)	261,111 N (58,700 lbs)
48	7R1	Windup Turn	72 2	.89	7,559 m (24,800 ft)	265,559 N (59,700 lbs)
48	5	Windup Turn	72 2	1 20	9,083 m (29,800 ft)	274,455 N (61,700 lbs)
59	S132R	Slowdown Turn	72 2	1.31 - 0 96	8,382 m (27,500 ft)	274,900 N (61,800 lbs)
77	S&CR*	Windup Turn	25 6	80	6,035 m (19,800 ft)	266,004 N (59,800 lbs)
48	6*	Windup Turn	26 6	.70	7,559 m (24,800 ft)	294,472 N (66,200 lbs)

*Phase I Selections

plots of the rms values of response and typical power spectra are presented for each of the maneuvers and discussed Comparisons are made showing the effects of wing sweep and Mach number. A brief discussion is given of an attempt to derive damping coefficients for the primary wing vibration modes. Finally the conclusions drawn from the investigation are presented.

The complete results of the stochastic analyses are documented in the forms of plotted and tabulated power spectra in Volumes II and III, NASA CR-152113 and NASA CR-152114 respectively for each response item by maneuver and time segment within each maneuver.

SECTION 2

AIRCRAFT DESCRIPTION

The test aircraft was F-111A Number 13. A drawing showing the general features of the aircraft is presented in Figure 1 Detailed geometry associated with the aircraft and its components appears in Table 3. The aircraft has a variable sweep wing and a convention was adopted early in the development program that all aerodynamic coefficients would be referenced to geometric characteristics at a specific wing sweep, namely, Λ_{LE} = 16 degrees. The variations of some key geometric characteristics of the wing with wing leading-edge sweep angle are presented in Figure 2

Although the aircraft is fitted with a high-lift system consisting of multisegment leading-edge slats and multisegment double-slotted trailing-edge flaps, these devices were in their retracted positions for all maneuvers analyzed in this study

Two-segment upper surface spoilers on each wing are used at low wing sweeps in addition to differentially controlled all-movable horizontal tails to achieve roll control

The aircraft has a three-axis stability augmentation system which was operational on all maneuvers analyzed in this investigation.

Figure 1 F-111A THREE-VIEW

ORIGINAL PAGE IS
OF POOR QUALITY

Table 3

PHYSICAL CHARACTERISTICS OF THE
F-111A AIRPLANE (NUMBER 13)

Wing –	
Airfoil section, at pivot	NACA 64A210 7 (modified)*
Airfoil section, tip	NACA 64A209 8 (modified)*
Sweep deg (leading edge)	16 to 71 5
Incidence, deg	1
Dihedral deg	1
Span, area, mean aerodynamic chord	(See fig 2)
Leading-edge slats	
Area (planform projected), $ft^2(m^2)$	60 7(5 64)
Span percent of exposed wing-panel span	96 5
Deflection, maximum, deg	45
Trailing-edge flaps	
Type	Double Slotted Fowler
Area (aft of hinge line), $ft^2(m^2)$	117 8(10 94)
Span, percent of exposed wing-panel span	
Deflection, maximum, deg	37 5
Spoilers	
Area (planform projected), $ft^2(m^2)$	28 6(2 66)
Span, ft(m)	11 8(3 6)
Deflection, maximum, deg	45
Wing pivot	
Distance from airplane nose, ft(m)	40 18(12 25)
Distance from airplane centerline, ft(m)	5 86(1 79)
Horizontal tail (all movable) –	
Airfoil section	BICONVEX
Incidence, deg	1
Dihedral, deg	-1
Sweep at leading edge, deg	57 5
Span, ft(m)	29 3(8 93)
Area (exposed), $ft^2(m^2)$	174 3(15 74)
Area (movable), $ft^2(m^2)$	154 2(13 92)
Aspect ratio	1 42
Mean aerodynamic chord (exposed), in (cm)	137 5(349 3)
Deflection, maximum, deg	
As elevators	
Trailing-edge up	(approx) 25
Trailing-edge down	(approx) 10
As ailerons (total)	(approx) ±15
Surface stops	
Trailing-edge up	(approx) 31
Trailing-edge down	(approx) 16
Vertical tail –	
Airfoil section	BICONVEX
Sweep at leading edge, deg	55
Span, ft(m)	8 9(2 71)
Area $ft^2(m^2)$	111 7(10 09)
Aspect ratio	1 42
Mean aerodynamic chord in (cm)	159 3(404 6)
Rudder	
Span, ft(m)	7 8(2 38)
Area, $ft^2(m^2)$	29 3(2 65)
Deflection, maximum, deg	±30
Speed brake –	
Area $ft^2(m^2)$	26 5(2 39)
Deflection, maximum deg	77
Ventrals –	
Area (total), $ft^2(m^2)$	25(2 26)
Power plants –	
P & W TF30-P-3 engines	2

* $\Lambda_{LE} = 16°$

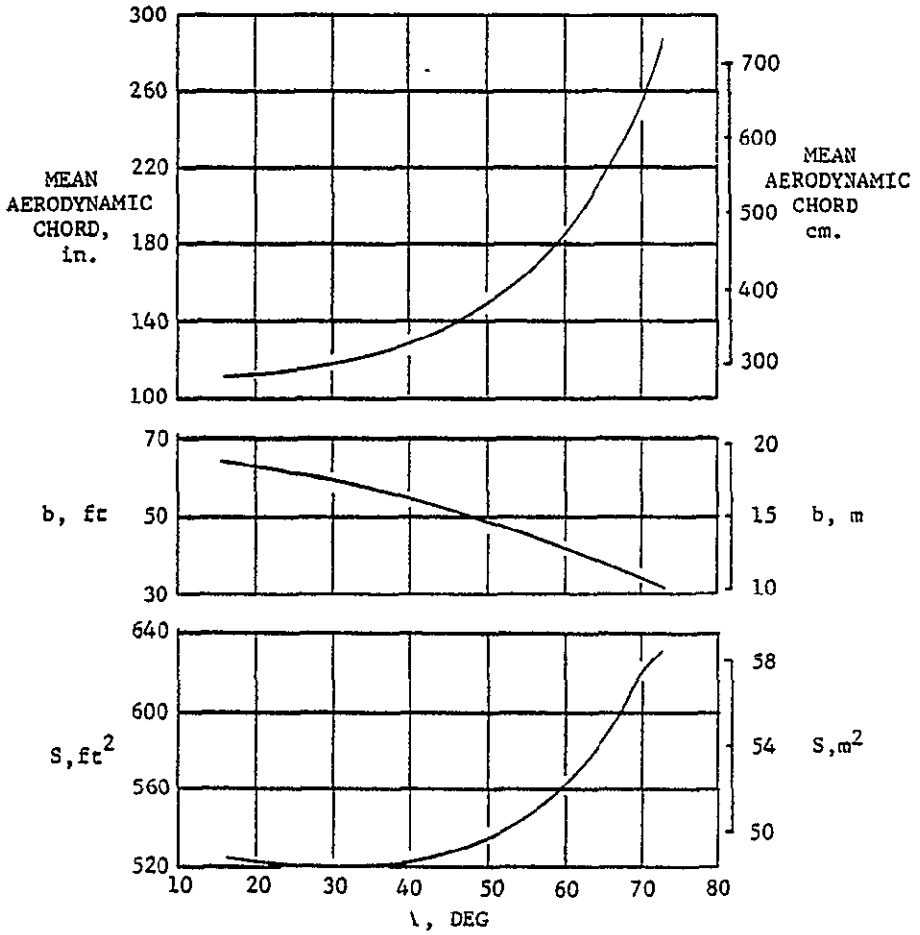

Figure 2 F-111A WING GEOMETRY AS A FUNCTION OF WING-SWEEP ANGLE

SECTION 3

AIRCRAFT INSTRUMENTATION

The instrumentation system installed in the aircraft consisted of two 30 track and one 14 track FM analog magnetic tape recorders and various transducers throughout the airplane. IRIG B time reference signals were recorded on each tape recorder to provide time correlation. The general locations of the accelerometers pertinent to the buffet study are shown in Figure 3. The actual locations in terms of aircraft geometry references are listed in Table 4.

The characteristics of the accelerometers most of which were commercially available units are indicated in Table 5. The accuracies quoted refer to the nominal flat frequency response up to the limit frequency quoted. No calibration data exist above the quoted limit of flat frequency response, however, the natural resonant frequencies are well beyond 100 hertz for all of the accelerometers.

The locations of the wing strain gage sensors pertinent to the buffet study are shown in Figure 4 Shear, bending moment and torque were measured at each of the four indicated wing stations on the right wing.

The locations of the strain gage sensors for the horizontal tail loads measurements are shown in Figure 5. Vertical shear bending moment and hingeline torque were measured at the

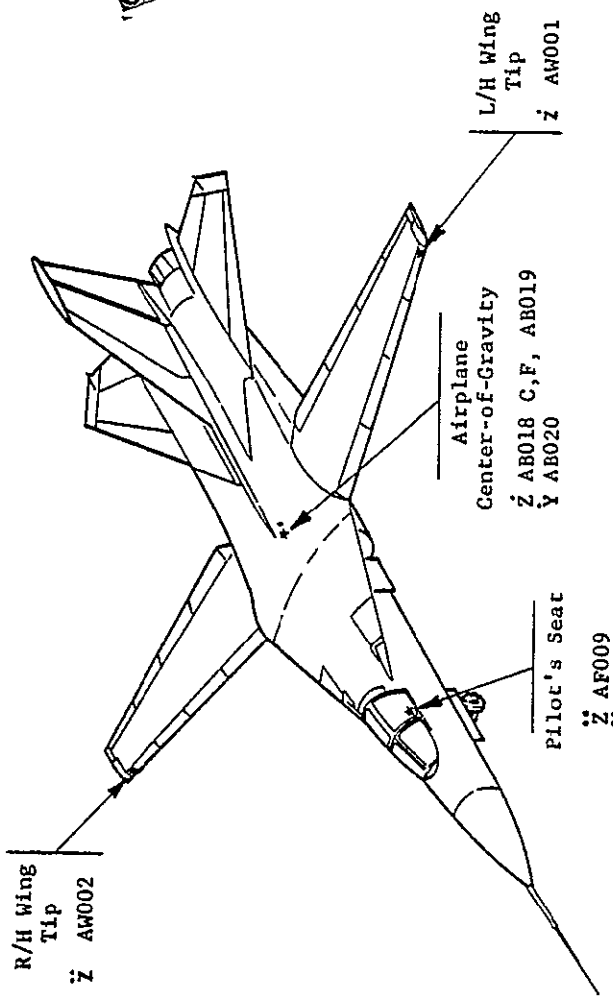

Figure 3. ACCELERATION MEASUREMENTS

Table 4

ACCELEROMETER LOCATIONS

ITEM CODE	MEASUREMENT	LOCATION					
		FUSELAGE STATION		WATERLINE		BUTT LINE	
		METERS	INCHES	METERS	INCHES	METERS	INCHES
AB018	c g vertical	12 996	(511 64)	4 740	(186 62)	0	0
AB019	c g. vertical	12 996	(511.64)	4 740	(186 62)	0	0
AB020	c g. lateral	12.996	(511 64)	4.740	(186 62)	- 023	(- 89)
AF009	Pilot seat vertical	6.462± 127	(254 40±5 0)	4 245± 127	(167 12±5 0)	- 133	(-5 25)
AF010	Pilot seat lateral	6 462± 127	(254 40±5 0)	4 245± 127	(167 12±5 0)	- 133	(-5.25)
AW001	Left wing tip - vertical	Front spar station 9 500 meters (374 inches)					
AW002	Right wing tip - vertical	Wing span station 9.157 meters (360 5 inches) @ Λ_{LE} = 16°					

Table 5

ACCELEROMETER CHARACTERISTICS

ITEM CODE	MEASUREMENT	NOMINAL FULL SCALE RANGE*	SPECIFIED ACCURACY % FULL SCALE**	SPECIFIED FLAT FREQUENCY RESPONSE TO HZ	RESONANT NAT FREQ HZ	FLIGHTS
AB018	C G Vertical	-3.5 to +6 5	±5	25	Not Available	48, 60
AB018	C.G Vertical	±15	±3	42	530	70, 77, 78, 79
AB019	C G Vertical	±10	±5	325	--	ALL
AB020	C G Lateral	±7 5	±5	275	--	ALL
AF009	Pilot Seat Vertical	±10	±3	32	400	ALL
AF010	Pilot Seat Lateral	±7 5	±5	275	--	ALL
AW001	Left Wing Tip Vertical	±25	±5	500	--	ALL
AW002	Right Wing Tip Vertical	±25	±5	500	--	ALL

*The actual range calibrated varied from these nominal values.
**Over range of flatfrequency response and at all temperatures between -70° and +250°F

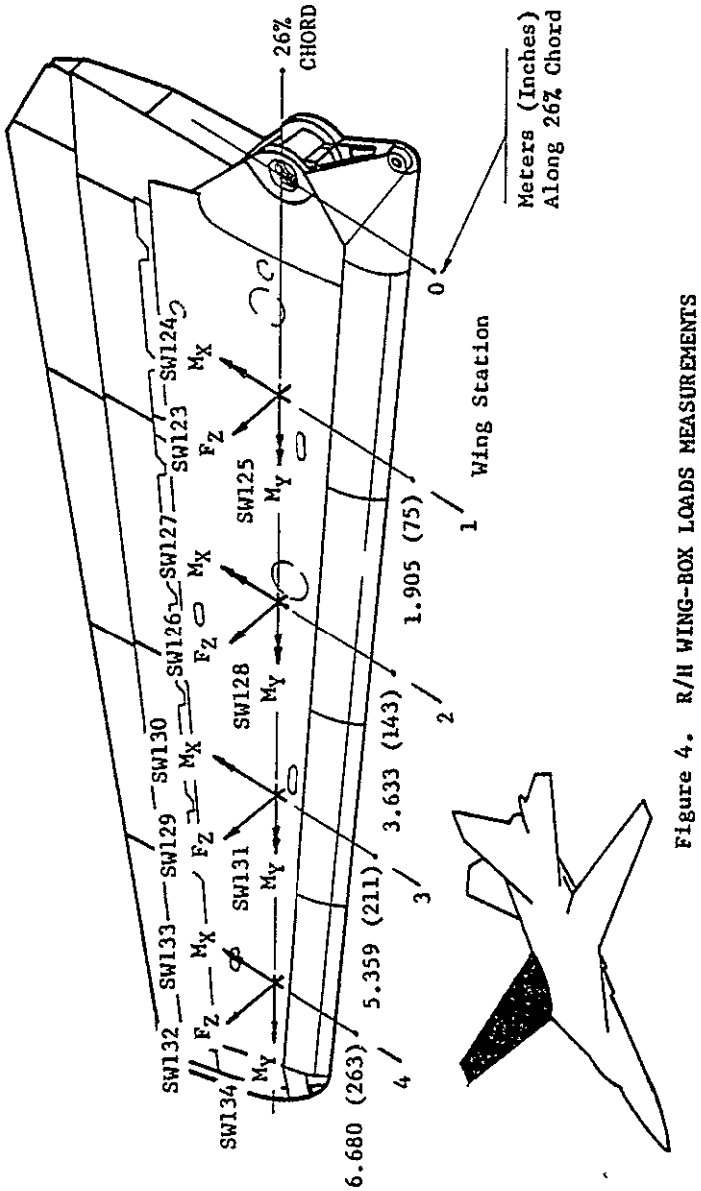

Figure 4. R/H WING-BOX LOADS MEASUREMENTS

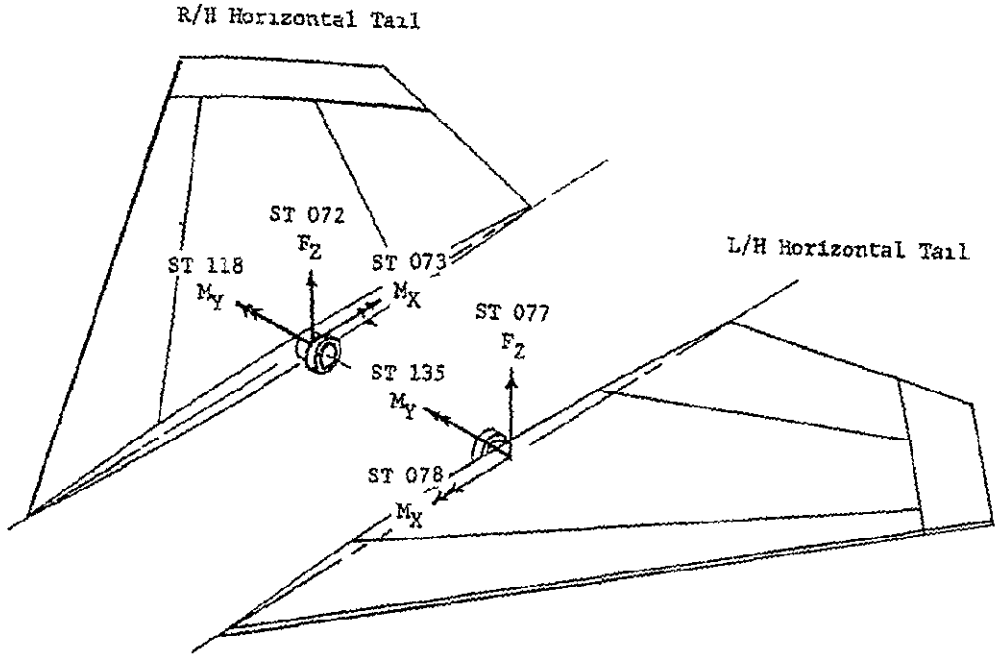

Figure 5. HORIZONTAL TAIL LOADS MEASUREMENTS

root of both the left and right horizontal tails The sensitivities of the wing and tail loads measurements were goverened by the fact that the loads were to be measured during maneuvers at load factors up to the maximum capability of the aircraft. As a consequence the signal-to-noise ratios for the present buffet studies were lower than is desirable. The calibration slopes for each channel of information are shown in Table 6

In several cases the frequency response upper limit for the measurements was set by the subchannel characteristics of the flight recording system. Table 7 lists the appropriate nominal limit frequency of subchannel arrangements for each flight selected for detailed analysis.

Other pertinent measurements such as angle of attack, Mach number, altitude, fuel remaining, horizontal tail position and spoiler position were also recorded on the FM tapes.

TABLE 6

CALIBRATION SLOPES – UNITS/PERCENT OF BANDWIDTH

ITEM	MEASUREMENT	S I UNITS	U S CUST UNITS	FLT 48 S I	FLT 48 CUST	FLT 59-61 S I	FLT 59-61 CUST	FLT 70 S I	FLT 70 CUST	FLTS 77, 78 S I	FLTS 77, 78 CUST	FLT 79 S I	FLT 79 CUST
AW001	LWT-Vert	g's	g's		50304		50304		33578		33578		33578
AW002	RWT-Vert	g's	g's		50232		50232		33322		33322		33322
AB018C	CG-Vert	g's	g's		130		130		10690		10313		18339
AB018F	CG-Vert	g's	g's		010		010		---		---		---
AB019	CG-Vert	g's	g's		20142		20142		20172		20172		20172
AB020	CG-Vert	g's	g's		05129		05129		05052		05052		05052
AF009	P S -Vert	g's	g's		15306		15306		29280		29280		29280
AF010	P S -Lat	g's	g's		10232		10232		10128		10128		10128
AB015	Ang Roll	rad/sec^2	rad/sec^2		53569		53569		3012		3012		3012
AB016	Ang. Pitch	rad/sec^2	rad/sec^2		32175		32175		0998		0998		0998
SW123	Shear-W S 1	N	lbs	8011	1801	8011	1801	11770	2464	11770	2464	11926	2681
SW124	B M -W S 1	m-N	in-lbs	22517	202896	22517	202896	37110	334383	37110	334383	37393	336937
SW125	TOR -W S 1	m-N	in-lbs	4136	37264	4136	37264	3913	35263	3913	35263	3969	35767
SW126	Shear-W S.2	N	lbs	5124	1152	5124	1152	9475	2130	9475	2130	9608	2160
SW127	B M -W S 2	m-N	in-lbs	9981	89935	9981	89935	9828	88557	9828	88557	9897	89181
SW128	TOR -W S 2	m-N	in-lbs	1251	11268	2501	22535	2798	25215	2798	25215	2834	25539
SW129	Shear-W S 3	N	lbs	2358	530	2358	530	3479	782	3479	782	3523	792
SW130	B M -W S 3	m-N	in-lbs	2800	25228	2800	25228	4160	37481	4160	37481	4197	37821
SW131	TOR -W S 3	m-N	in-lbs	1008	9084	1008	9804	964	8690	964	8690	982	8847
SW132	Shear-W S 4	N	lbs	801	180	801	180	1561	351	1561	351	1588	357
SW133	B M -W S 4	m-N	in-lbs	393	3541	393	3541	758	6835	758	6835	765	6896
SW134	TOR -W S 4	m-N	in-lbs	188	1694	188	1694	344	3100	344	3100	349	3142
DH001C	α	deg	deg		875		875		875		875		875
DH001F	α	deg	deg		080		080		080		080		080
DH002F	β	deg	deg		080		080		080		080		080
DW001	L Inbd Spoil	deg	deg		60		60		60		60		60
DW002	R Inbd Spoil	deg	deg		60		60		60		60		60
DW003	L Outb Spoil	deg	deg		60		60		60		60		60
DW001	R Outb Spoil	deg	deg		60		60		60		60		60
DT003C	L Hor T	deg	deg		88		88		88		88		88
DT004C	R Hor T	deg	deg		88		88		88		88		88
PD016F	Mach	---	---		0034		0034		0034		0034		0034
PD004F	Alt	m	Ft	15 24	50	15 24	50	---	---		---		---
PH022F	Alt	m	Ft	---	---	---	---	12 192	40	12 192	40	12 192	40

Table 6 (Concluded)

ITEM	MEASUREMENT	S I UNITS	U S CUST. UNITS	FLT 48 S I	FLT 48 CUST	FLTS 59,60,61 S I	FLTS 59,60,61 CUST.	FLT 70 S I.	FLT 70 CUST	FLTS 77,78 S I	FLTS 77,78 CUST	FLT 79 S I	FLT 79 CUST
ST072	R/H H.T SHEAR	N	lbs	5249	1180	5249	1180	8051	1810	8051	1810	8051	1810
ST073	R/H H T BEND. MOM.	M-N	in-lbs	5512	49663	5512	49663	6978	62874	6978	62874	-	-
ST073S	R/H H T BEND MOM.	M-N	in-lbs	-	-	-	-	-	-	-	-	5256	47363
ST0118	R/H H T TORQUE	M-N	in-lbs	2377	21416	2377	21416	2443	22014	2443	22014	2458	22151
ST077	L/H H.T SHEAR	N	lbs	4466	1004	4466	1004	4466	1004	4466	1004	4497	1011
ST078	L/H H T BEND MOM.	M-N	in-lbs	3485	31402	3485	31402	6970	62804	6970	62804	4860	42185
ST135	L/H H.T TORQUE	M-N	in-lbs	2134	19233	2134	19233	2134	19233	2134	19233	2148	19357

Table 7

FLIGHT RECORDER FREQUENCY RESPONSE CHARACTERISTICS

ITEM CODE	FLIGHTS 48-61		FLIGHTS 70-79	
	IRIG CHANNEL	FILTER FREQ. - HZ	IRIG CHANNEL	FILTER FREQ. - HZ
AW001	8	45	11	110
AW002	12	160	12	160
AB018	14	330	11	110
AB019	9	59	8	45
AB020	14	330	9	59
AF009	11	110	12	160
AF010	12	160	10	81
SW123	10	81	7	35
SW124	11	110	8	45
SW125	12	160	9	59
SW126	13	220	10	81
SW127	8	45	11	110
SW128	9	59	12	160
SW129	10	81	13	220
SW130	11	110	6	25
SW131	12	160	7	35
SW132	13	220	8	45
SW133	8	45	9	59
SW134	9	59	10	81
ST072	11	110	11	110
ST073	12	160	13	220
ST118	13	220	10	81
ST077	8	45	12	160
ST078	9	59	11	110
ST135	8	45	9	59

SECTION 4

BASIC DATA PROCESSING METHODS

During the Loads Demonstration Flight Program, the FM analog magnetic tapes containing raw flight test data were processed by automated processing techniques The data were first played out on strip chart recorders for instrumentation verification. Next, the data were digitized at sample rates of up to 20 samples per second under computer control. Either 10 or 20 samples per second were used for the data pertinent to this study. The digitized data were then scaled, calibrated and output in computer listings and computer tapes for additional processing on an IBM System/360. Second generation computer runs were made to obtain corrected flight condition data such as gross weight, Mach number, altitude, dynamic pressure and fuel distribution at 1-second intervals.

Microfilm records of the computer listings from the original flight program data reduction were used in the present program to make plots of angle of attack, normal load factor, Mach number and dynamic pressure as functions of flight time and to identify the gross weights and altitudes for the selected flight maneuvers. The Mach number, altitude and dynamic pressure data include corrections for position error The angles of attack from the basic reduction are indicated angles and do not include the effect of

upwash at the nose boom. A correction formula to account for the upwash is

$$\alpha_T = 0\ 318 + 0.931\ \alpha \text{ (degrees)}.$$

It was not considered fruitful to apply this correction in the various plots presented in this report because corrections to the wing angle of attack due to structural flexibility are much larger in magnitude and can only be approximated. Both corrections were considered in selecting the time intervals for the stochastic analysis in Phase II in order to obtain agreement with existing wind tunnel model data insofar as possible.

Time histories were made of about 30 items of instrumentation measurements which were considered pertinent to the buffet study Examples of each of the strip chart records have been previously presented in the Phase I report (Reference 1) These records were used to aid in the process of selecting the maneuvers for the Phase II Study. The records for the Phase II Study maneuvers were in general too large to be legibly reproduced on an unfolded page

SECTION 5

FLIGHT CONDITIONS FOR DETAILED ANALYSIS

In the Phase II Study the major criterion for selecting the particular flight maneuvers was matching insofar as possible conditions of wing sweep, Mach number and angle of attack for which wind tunnel data already existed. It was considered important to use maneuvers for at least two additional wing sweeps and at both subsonic and supersonic speeds The four wind up turn maneuvers listed in Table 2 were selected on that basis.

A question had arisen in the Phase I Study with respect to the character of the structural responses as deduced from relatively short time samples The two slowdown turn maneuvers listed in Table 2 were chosen to examine whether or not short time samples and longer time samples gave consistent results.

Variations of angle of attack, load factor Mach number and dynamic pressure with flight time are presented in Figure for each of the selected maneuvers.

Table 8 lists the segments of each maneuver selected for detailed analysis In most cases the time duration of the records (ΔT) is one second, but some longer records were used. The table also lists the indicated angle of attack at the start

a) FLIGHT 61, R227, WINDUP TURN

Figure 6 FLIGHT CONDITIONS FOR SELECTED MANEUVERS

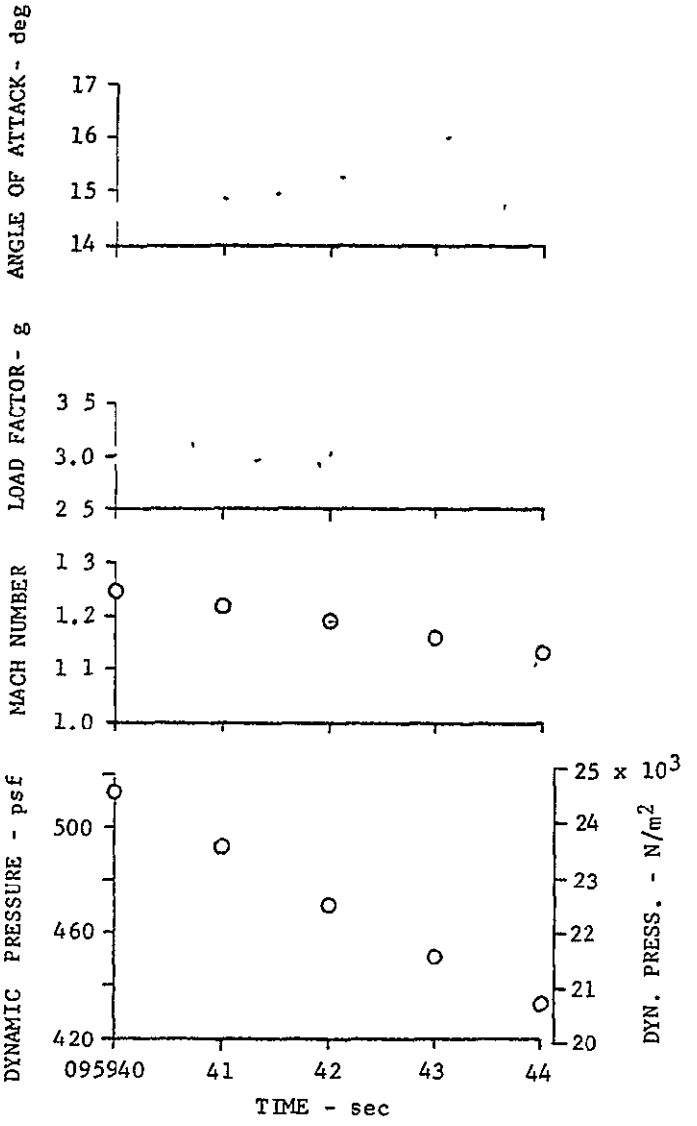

b) FLIGHT 51, S38/150, SLOW DOWN TURN

Figure 6 Continued

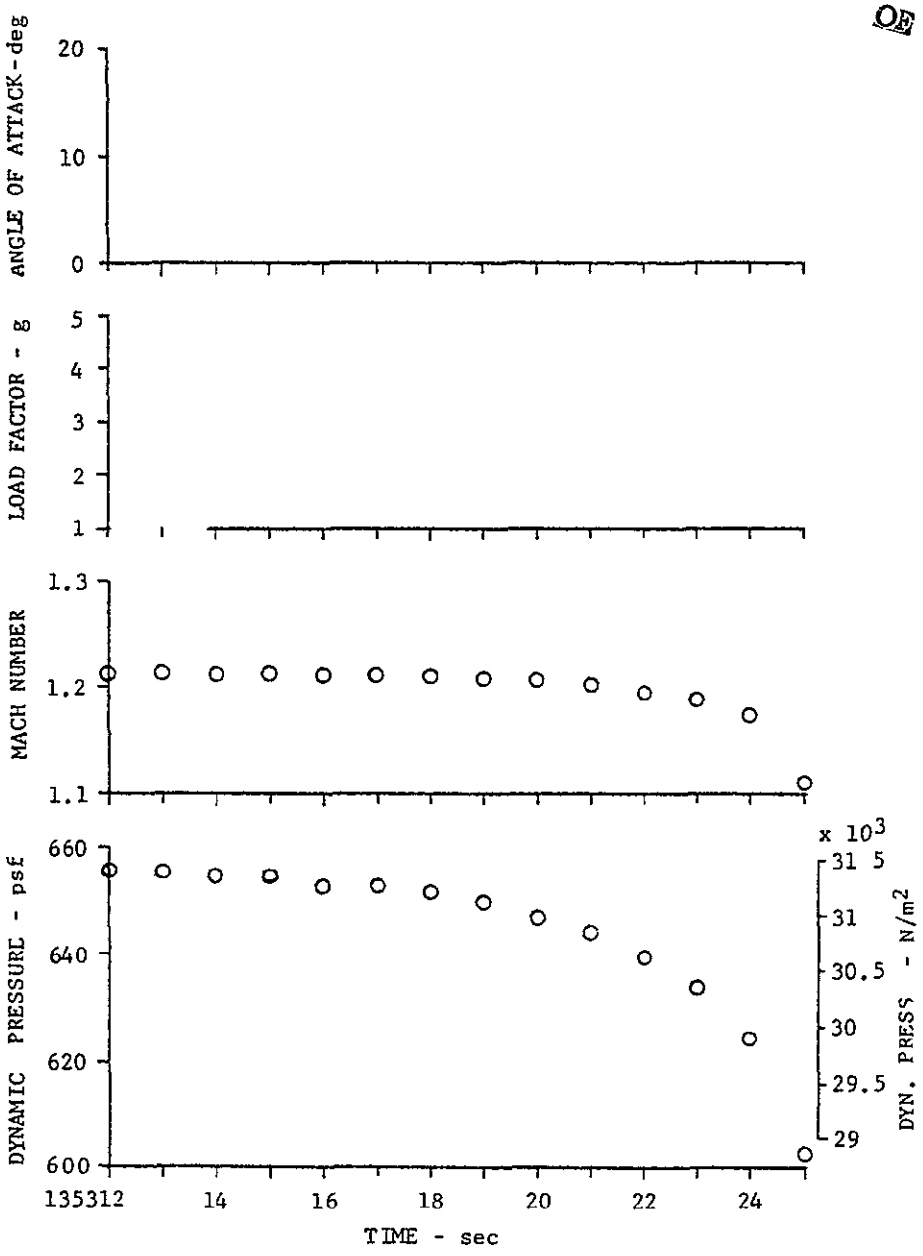

c) FLIGHT 48, Run 4, WINDUP TURN

Figure 6 Continued

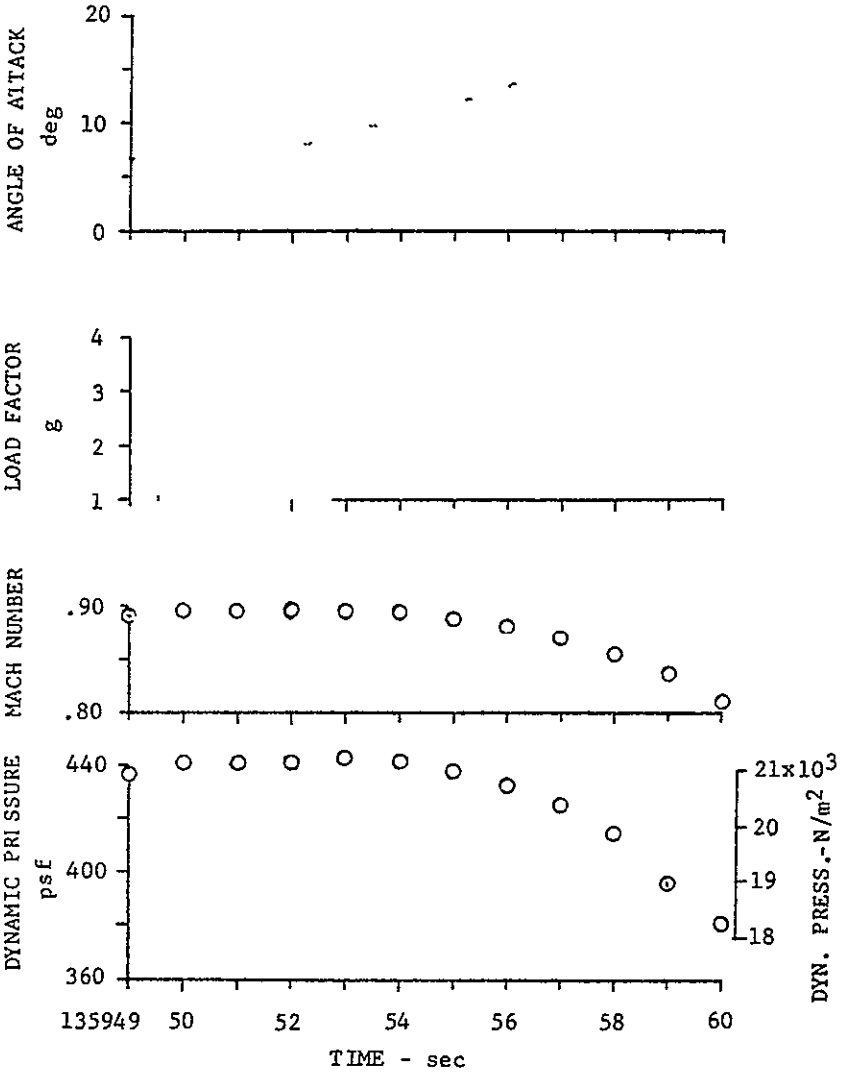

d) FLIGHT 48, RUN 7R1, WINDUP TURN

Figure 6. Continued

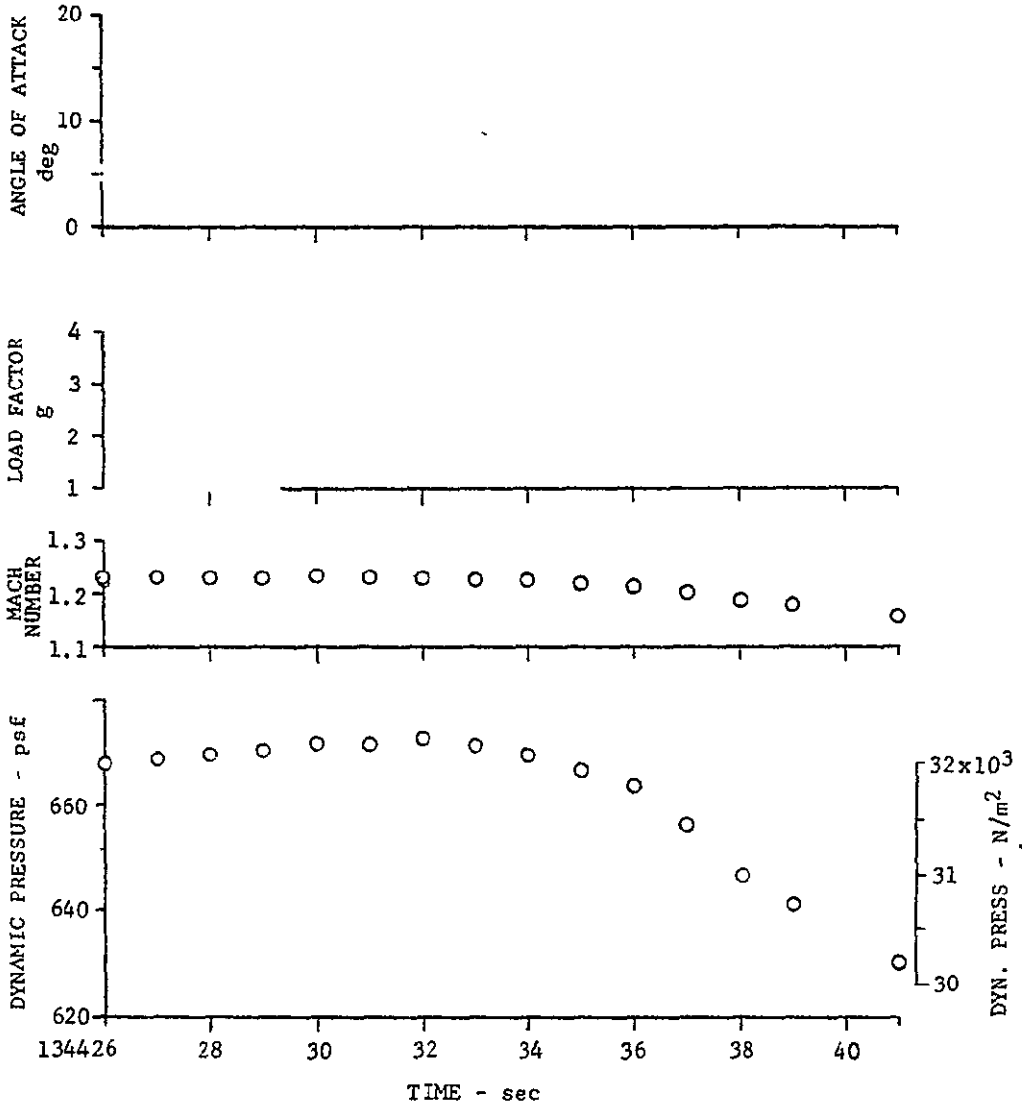

e) FLIGHT 48, Run 5, WINDUP TURN

Figure 6 Continued

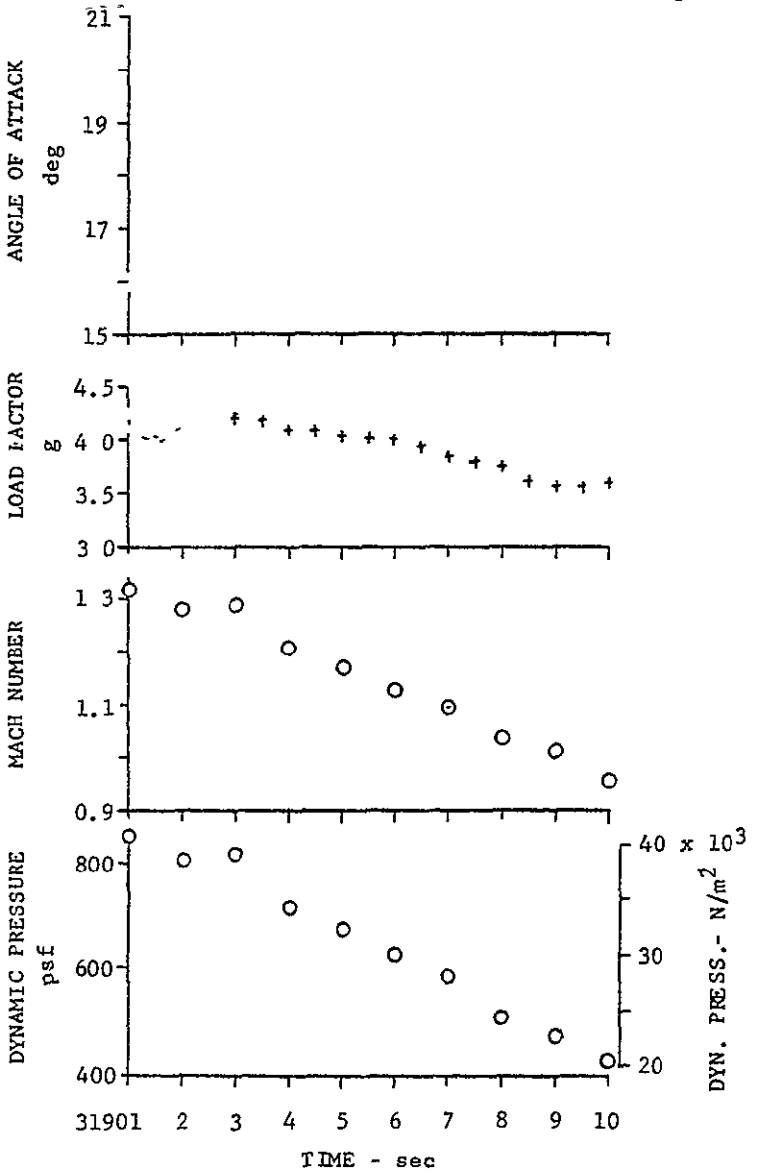

f) FLIGHT 59, Run S132R, SLOW DOWN TURN

Figure 6. Continued

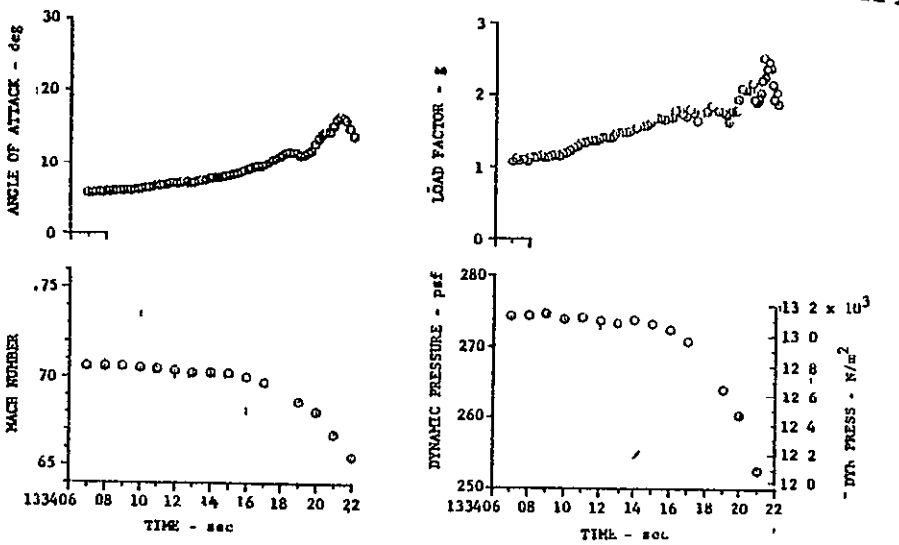

(g) FLIGHT 48, RUN 6, WINDUP TURN

Figure 6. Continued

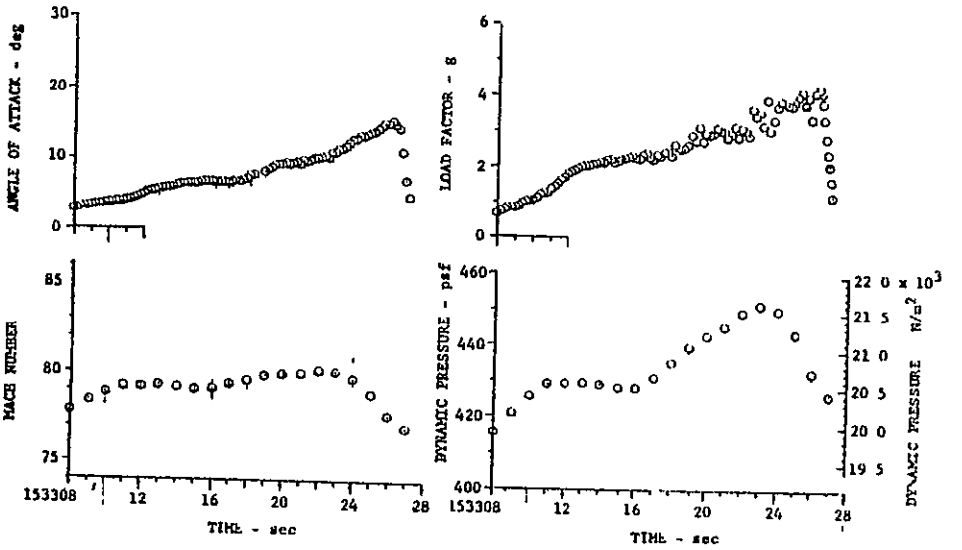

(h) FLIGHT 77, RUN S6C-R, WINDUP TURN

Figure 6. Concluded

Table 8

FLIGHT POINTS SELECTED FOR STOCHASTIC ANALYSIS

Flight	Run	Point	Start Time T_1	Stop Time T_2	ΔT (SEC)	α_1 (DEG)	α_2 (DEG)	α_{max} (DEG)	α_{now} (DEG)	$\Delta\alpha$ (DEG)
61	R227	1	110107 9	110108 9	1	7 10	9 25	--	8 05	2 15
		2	110108 4	110109 4	1	8 05	10 10	--	9 25	2 05
		3	110109 7	110110 7	1	10 10	10 80	--	10 42	0 70
		4	110110 6	110111 6	1	10 60	12 70	--	11 65	2 10
		5	110112 0	110113 0	1	12 90	14 60	14 60	13 75	1 70
51	S38/150	1	95940 0	95942 0	2	14 55	15 12	--	14 85	0 75
		2	95943 0	95944 0	1	15 95	16 45	--	16 25	0 50
		3	95940 0	95944 0	4	14 55	16 45	--	15 12	1 90
48	4	1	135315 7	135316 7	1	4 70	5 50	--	4 95	0 80
		2	135320 7	135321 7	1	8 20	9 80	--	8 90	1 60
		3	135322 8	135323 8	1	12 10	13 70	--	12 95	1 70
		4	135323 9	135324 9	1	13 70	13 90	15 0	14 3	1 30
48	7R1	1	135951 7	135952 7	1	7 15	8 65	--	8 00	1 50
		2	135952 7	135953 7	1	8 65	10 00	--	9 40	1 35
		3	135954 3	135955 3	1	10 75	12 20	--	11 62	1 45
		4	135956 8	135957 8	1	14 15	16 15	--	15 15	2 00
		5	135958 55	135959 55	1	17 90	18 90	19 35	18 70	1 45
48	5	1	134426 2	134427 2	1	4 80	4 80	--	4 80	$\pm$0 1
		2	134432 3	134433 3	1	8 00	8 80	--	8 41	0 80
		3	134436 2	134437 2	1	11 30	12 70	--	12 10	1 40
		4	134439 65	134440 65	1	14 95	16 75	--	15 95	1 80
59	S132R	1	31901 0	31903 0	2	15 95	17 55	--	16 75	1 60
		2	31903 0	31905 0	2	17 55	18 13	--	17 75	0 63
		3	31907 0	31909 0	2	19 55	19 60	20 00	19 80	0 45
48	6*	3	133415 0	133416 0	1	8 72	9 55	--	9 1	0 83
		4	133416 7	133417 7	1	9 70	10 75	--	10 2	1 05
		5	133417 3	133418 3	1	10 30	11 75	--	11 1	1 45
		6	133419 0	133420 0	1	11 15	13 55	--	12 3	2 40
		7	133420 3	133421 3	1	14 25	16 60	--	15 3	2 35
77	S&C-R*	7	153311 0	153313 0	2	4 22	5 98	--	5 1	1 76
		8	153315 5	153317 5	2	7 00	7 32	--	7 1	0 32
		9	153318 5	153320 5	2	8 45	9 65	--	9 2	1 24
		10	153322 35	153324 35	2	10 85	13 40	--	12 2	2 55
		11	153324 35	153326 35	2	13 40	15 35	15 55	14 8	2 15

* Phase I selections used in Phase II for consistency

of each record (α_1), at the end of each record (α_2) and in a few cases the maximum angle of attack occurring during the record (α_{max}). A nominal angle of attack (α_{nom}) has been assigned to each data segment which is used later to plot trends in the variations of instrument responses with angle of attack.

SECTION 6

STOCHASTIC ANALYSIS TECHNIQUES

The analysis techniques used in this study are compatible with American National Standard (ANS S2.10-1971) recommended methods for analysis and presentation of shock and vibration data A quick-look examination was performed on each time-history measurement to determine the data classification, degree of stationarity, record length and recoverability

Measurements

Data reduction was performed on the following data:

1. Shear, bending moment and torsion at four wing stations, (12 measurements).

2 Shear, bending moment and hingeline torque at the root of both left and righ horizontal tails (6 measurements)

3. Two wing tip accelerometers (verticals)

4. Two c.g. vertical and one c.g. lateral accelerometers.

5 Pilot's seat vertical and lateral accelerometer.

The stochastic analysis performed on these items was limited to power spectral densities (PSD) and average rms values for each data sample. A total of 660 PSD's were processed in Phase II

In addition a few narrow band time histories were made for selected wing instrumentation items.

Special-Purpose Processing

A block diagram of the special-purpose stochastic equipment is shown in Figure 7. The FM signal is discriminated to recover the analog signal Band-pass filters at 3 H_z and 100 H_z (48 dB per octave) were used to reject unwanted frequencies and to minimize aliasing effects on the sampled data. The data is calibrated at this point The T/D 100 analyzer was used to compute the PSD's The stochastic algorithm utilized by the T/D 100 to perform this function is discussed below

Prior to the Phase II Study the equipment was modified to achieve a direct interface with an SEL-810A mini-computer which then permitted direct recording of the output of the T/D-100 on magnetic tape. The tapes were then used as input to a plotting routine

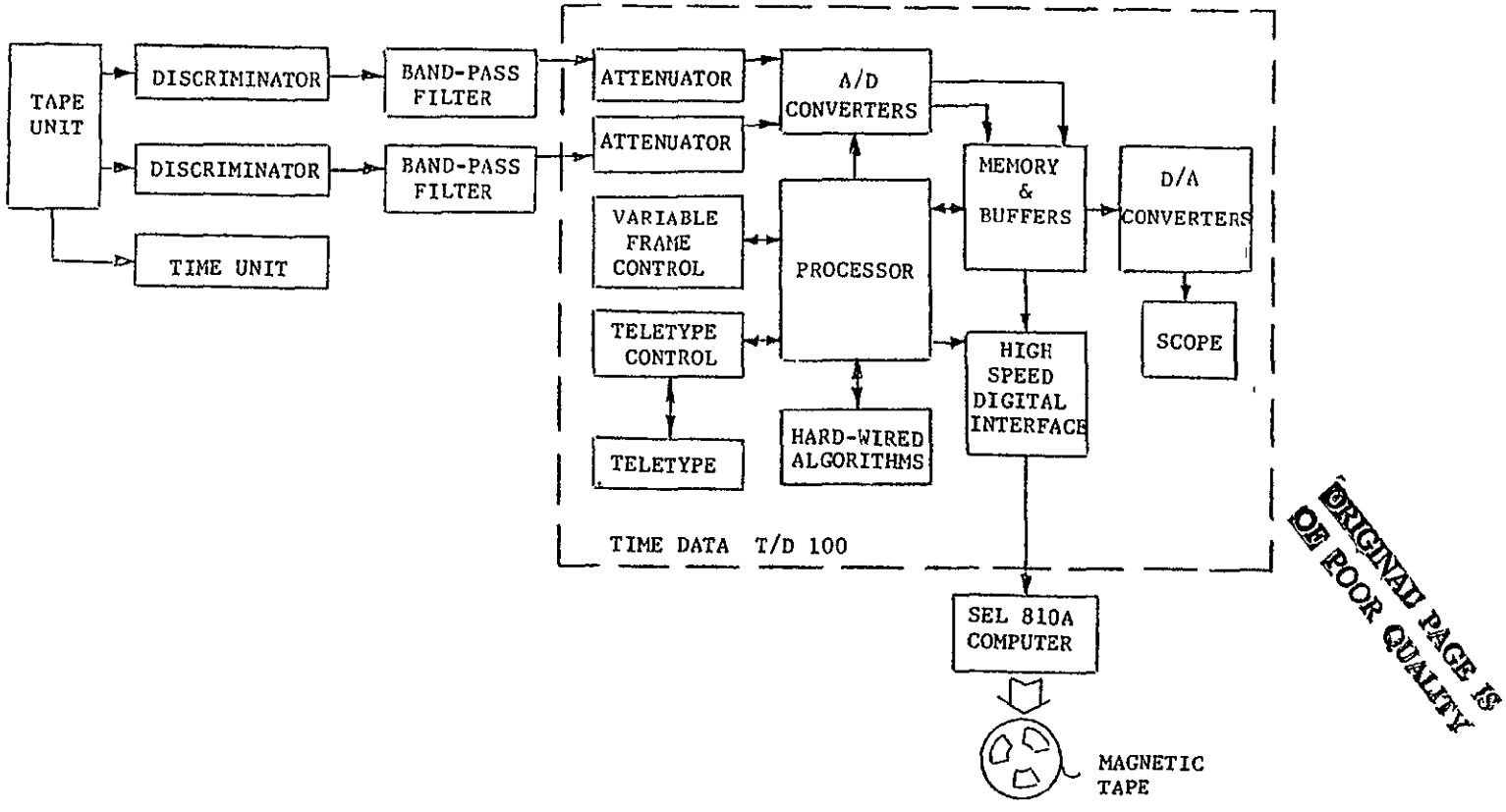

Figure 7. STOCHASTIC SPECIAL-PURPOSE EQUIPMENT

Auto-Spectral Density (PSD)

The T/D 100 computes the PSD coefficients by first approximating the complex Fourier transform of the input signal. The Fourier transform of the time-domain input function x(t) is given by:

$$G(jf) = \int_{-}^{+} x(t)(\cos 2\pi ft - j \sin 2\pi ft)\, dt \qquad (1)$$

where $j = \sqrt{-1}$. Since the time-domain input is sampled and quantitized in the analyzer, and only a finite number of samples are available, the finite transform is used, and separated into its real P(f) and imaginary Q(f) components can be written as follows:

$$P_T(f) = \int_{-T/2}^{T/2} x(t) \cos 2\pi ft \; dt \qquad (2)$$

$$Q_T(f) = \int_{-T/2}^{T/2} x(t) \sin 2\pi ft \; dt \qquad (3)$$

where T is the length of the input frame, which is assumed to be centered about time t=0.

Replacing the continuous input, x(t), with a set of 2N+1 discrete samples at intervals of $t_o = \frac{1}{2N}$, and replacing the sinusoidal functions by corresponding values, the continuous integrals may be expressed as the sum of products:

$$P(kf_o) = \sum_{n=-N}^{+N} x(nt_o) \cos \left[2 \quad kf_o(nt_o) \right] \tag{4}$$

$$Q(kf_o) = -\sum_{n=-N}^{+N} x(nt_o) \sin \left[2 \quad kf_o(nt_o) \right] \tag{5}$$

where k is a series of 2N integers and f_o is the base frequency which is equal to $\frac{1}{2T}$.

The PSD coefficients $\left[S(kf_o) \right]$ are then computed from (4) and (5) by the equation:

$$S(kf_o) = \left| P(kf_o) \right|^2 + \left| Q(kf_o) \right|^2 \tag{6}$$

Average rms (Ψ_T)

The average rms of the input signal is calculated from the PSD coefficients $\left[S(kf_o) \right]$ by the following equation:

$$\Psi_T = \sqrt{f_o \sum_{k=0}^{2N} S(kf_o)}$$

where $f_o = \frac{1}{2NT}$ is the base frequency or analysis bandwidth.

Narrow Band Time Histories

Narrow band time histories were prepared for a few selected items of wing instrumentation and frequency bands as listed in Table 9. The particular frequency bands used were selected such that motion damping in particular modes of vibration might

be analyzed. The modes examined included first symmetric and first antisymmetric wing bending, second symmetric and antisymmetric wing bending and first symmetric and antisymmetric wing torsion and second symmetric wing torsion.

The narrow band time histories were recorded at various paper speeds from 5 to 200 mm/sec to allow the decay of amplitude

TABLE 9

NARROW BAND TIME HISTORIES FREQUENCY BANDS (H_Z)

		ITEM					
Flight	Run	AW002	SW124	SW127	SW133	SW125	SW134
61	R227	4-6 6-8	4-6 6-8	15-17	4-6 15-17 28-30	23-25 25-27 28-30	23-25 25-27 38-40
48	7R1	4-6 6-8	4-6 6-8	15-17	4-6 15-17 28-30	23-25 25-27 28-30	23-25 25-27 28-30
77	S&C-R	4-6 6-8	4-6 6-8	16-18	23-25 25-27 28-30	23-25 25-27 28-30	23-25 25-27 28-30
48	6	4-6 6-8	4-6 6-8	16-18	23-25 25-27 28-30	23-25 25-27 28-30	23-25 25-27 28-30

with time and the vibration frequencies to be analyzed Since only the relative amplitudes were needed for this analysis, the gains for each channel were adjusted to obtain approximately full bandwidth on the record for the maximum output signal during a maneuver.

SECTION 7

DISCUSSION OF RESULTS

The Phase II flight data analysis were aimed primarily at providing additional data for verification of a prediction method. The rms magnitudes and the spectral content of the structural responses were determined for each of the flight points listed in Table 8. The presentation of results in this report emphasizes the variations of rms magnitudes of response with angle of attack for each of the maneuvers. Some typical comparisons are made to show the effects of wing sweep and Mach number. The presentation of spectral data in the body of the report is limited to a few typical power spectra which illustrate the salient effects of wing sweep, and sensor location. The spectral data are presented in plotted form in NASA CR-152113. Tabulations of all the spectral data are contained in NASA CR-152114.

MAGNITUDES OF THE STRUCTURAL RESPONSES

The complexity of the modal responses makes it difficult to comprehend the variations in magnitude of the structural responses if compared mode by mode. Consequently, the root-mean square value concept is used for making comparisons. The rms values were derived from the power spectra by summing

the spectral values over a range of frequencies and then taking the square root of the sum.

In the following discussion the rms values are evaluated over the frequency ranges from 1 to 50 hertz, or from .1 to the frequency limit of the recorder response if less than 50 hertz. If rms values over a different frequency range are desired they can be calculated using the tabulated PSD data presented in Volume III (NASA CR-152114).

One purpose of the rms analysis was to investigate effects of wing sweep and Mach number. The order of data presentation is as follows:

(1) Horizontal tail responses for $\Lambda_{LE} = 26^{o}$

(2) All measured responses for $\Lambda_{LE} = 50^{o}$ M = 0.81

(3) All measured responses for $\Lambda_{LE} = 50^{o}$ M = 1.20

(4) All measured responses for $\Lambda_{LE} = 72.5^{o}$ M = 0.89

(5) All measured responses for $\Lambda_{LE} = 72.5^{o}$ M = 1.20

Discussions of the effects of wing sweep at subsonic Mach numbers, comparisons of responses at subsonic and supersonic Mach numbers and evaluation of normalized wing buffet loads follow the basic data presentation.

Horizontal Tail Responses at $\Lambda_{LE} = 26^{o}$

During the prediction method development effort conducted in Phase I, it was found that consideration of the buffet

forcing function acting on the wing only did not adequately predict the rms values or spectral content of the fuselage responses. Significant contributions at frequencies associated with horizontal tail vibration modes were evident in the power spectra for the center of gravity and pilot's seat accelerometers. Buffet pressures on the horizontal tail were not measured during the wind tunnel tests and analysis of flight test data for the horizontal tail had not been accomplished in Phase I.

One of the first flight test data analysis tasks during Phase II was to obtain horizontal tail buffet loads for two of the maneuvers previously selected for the Phase I wing-fuselage analysis. The rms values of vertical shear, bending moment and hingeline torque on both the left and right vertical tails are presented in Figures 8 and 9 for those two Phase I maneuvers. The dynamic loads are plotted as functions of the nominal angle of attack assigned in Table 8 to each time segment analyzed. Scales are presented for both the International System and U.S. Customary System of units.

The variations of dynamic loads with angle of attack shown in Figure 8 for the M = 0.80 case are quite consistent with the wing and fuselage responses presented in Reference 1 for this case. The slight difference between the data for the left and right tails is likely caused by differential tail

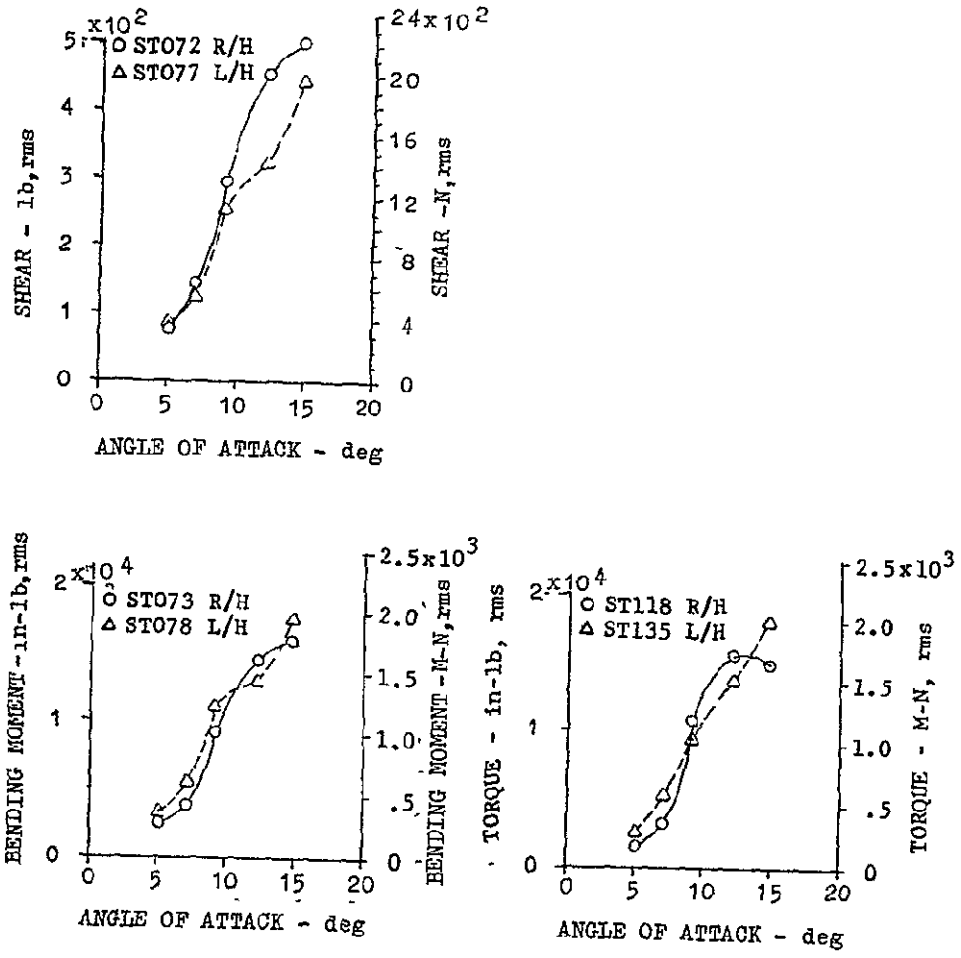

Figure 8. HORIZONTAL TAIL RESPONSE, FLIGHT 77, RUN S&CR
WINDUP TURN Λ_{LE} = 26°, M = 0.80 , h = 19,800 ft

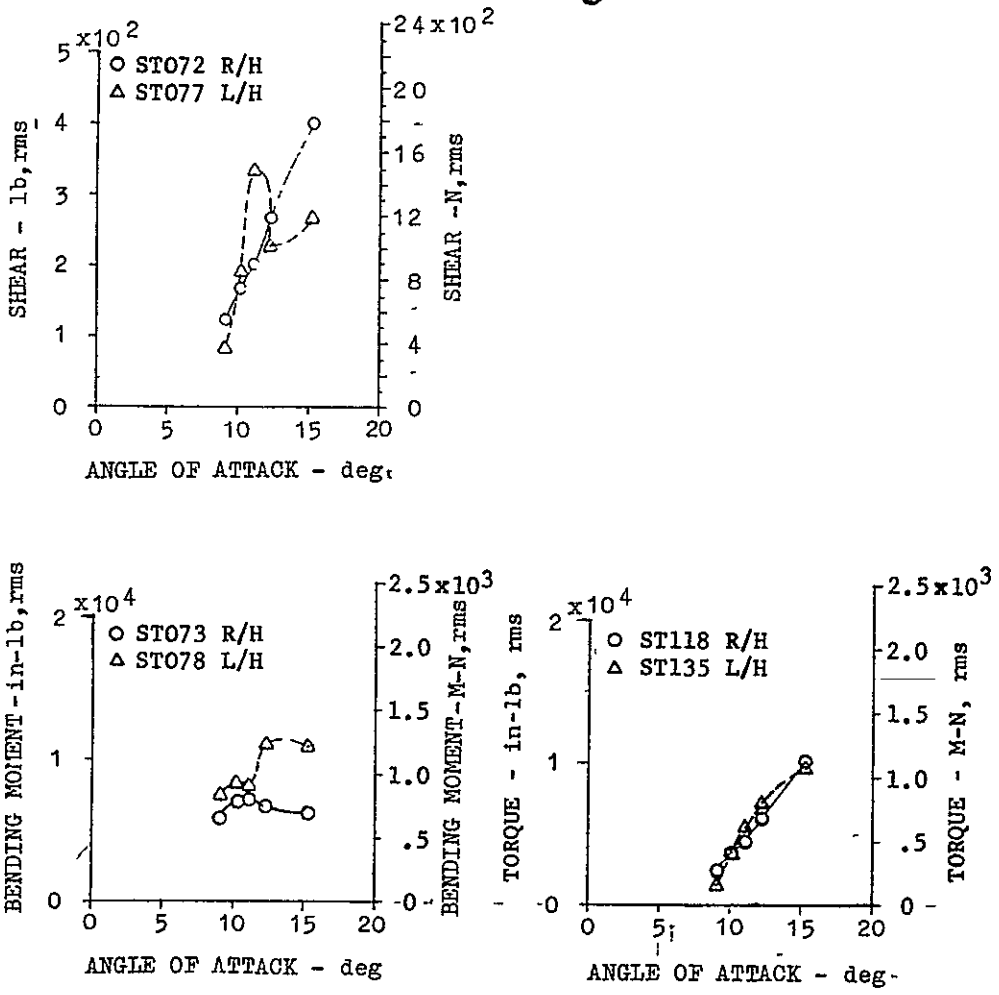

Figure 9. HORIZONTAL TAIL RESPONSE, FLIGHT 48, RUN 6, WINDUP TURN Λ_{LE} = 26°, M = 0.70, h = 24,800 ft

movement during the maneuver. The variations of tail buffet loads with angle of attack for the M = 0.70 $\Lambda_{LE} = 26^{o}$ case presented in Figure 9 are not consistent in general with the variations of the wing and fuselage responses. Only the shear measurement on the left horizontal tail exhibits the definite peak at 11 degrees which characterized the wing and fuselage responses presented in Reference 1. Apparently the horizontal tail roll control function causes significant differences in the variations of responses for left and right horizontal tails.

Note also that the maximum rms values for shear at M = 0.70 are only slightly lower than those at M = 0.80 while the maximum values of bending moment and torque response are much lower. No obvious explanation exists for this fact.

Responses for $\Lambda_{LE} = 50^{o}$ at Subsonic Mach Number

The measured dynamic responses for the $\Lambda_{LE} = 50^{o}$, M = 0.80 h = 27,500 ft case are presented in Figures 10 through 12. The accelerometer data are discussed first, then the wing loads data and finally the horizontal tail loads data.

The rms values of vertical accelerations for the right wing tip, the center of gravity and the pilot's seat are presented in Figures 10a through 10d. The variations with

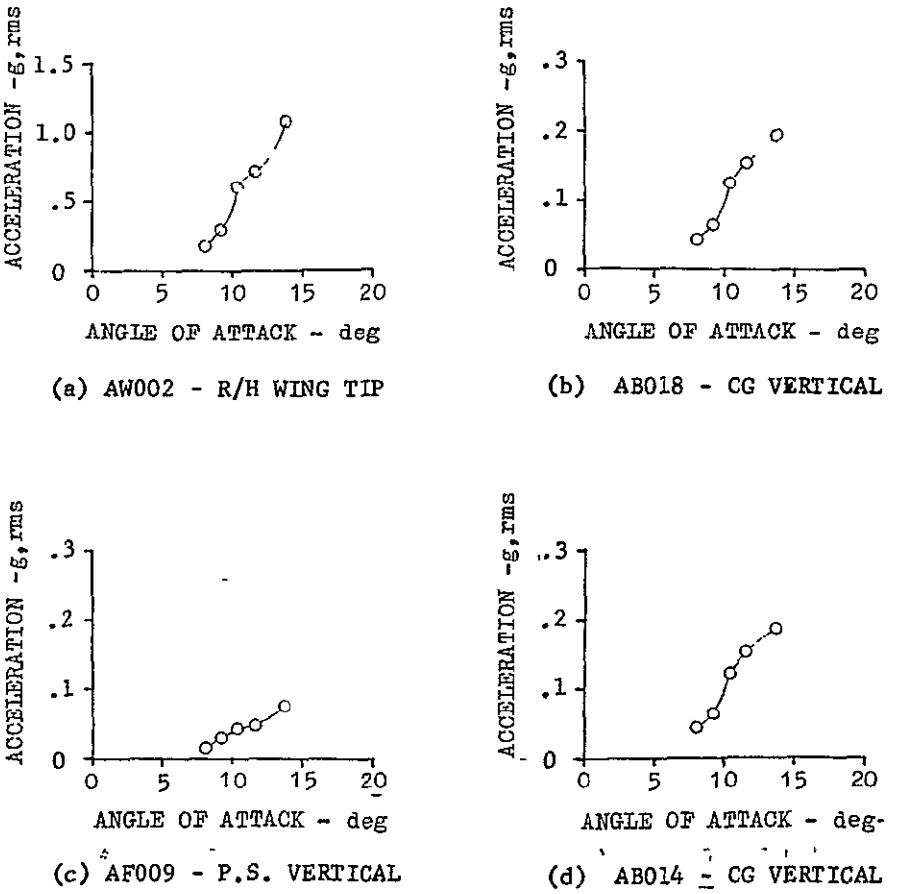

Figure 10. ROOT MEAN SQUARE VALUES OF ACCELERATION, $\Lambda_{LE} = 50^{\circ}$, NOMINAL MACH = 0.80, WINDUP TURN

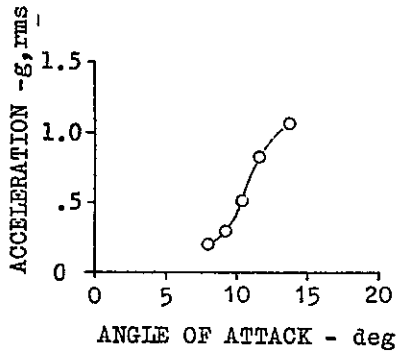

(e) AW001 - L/H Wing Tip

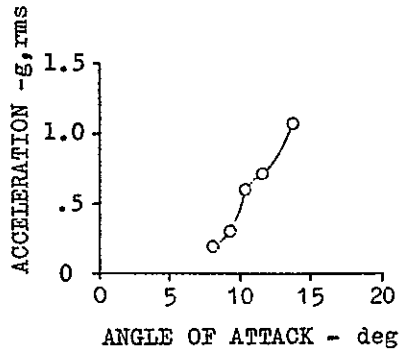

(f) AW002 - R/H Wing Tip

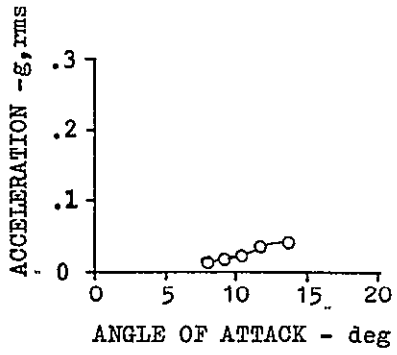

(g) AF010 - P.S. LATERAL

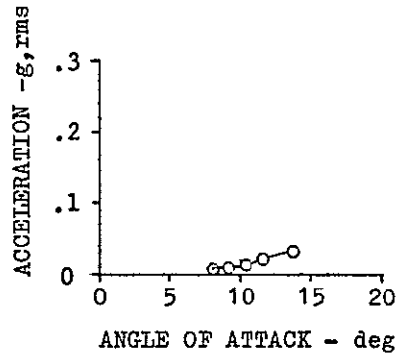

(h) AB020 CG LATERAL

Figure 10. Concluded

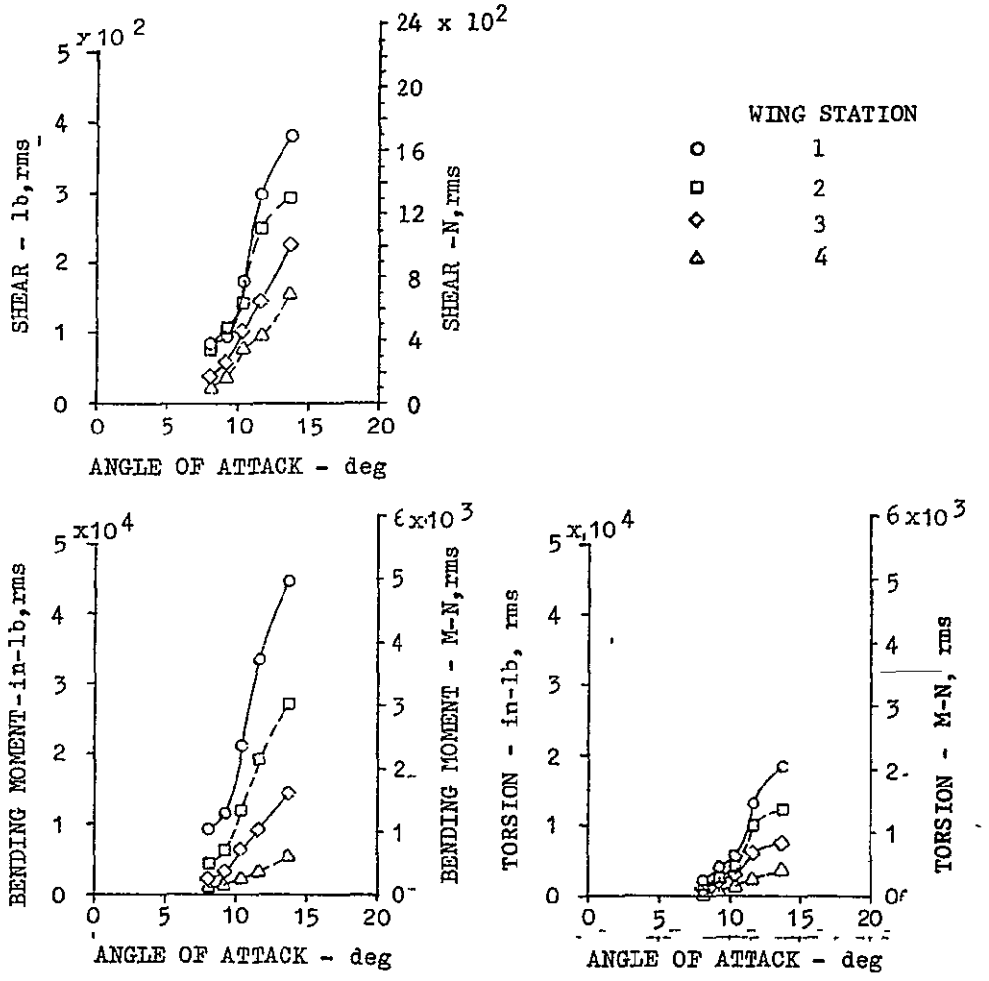

Figure 11. ROOT MEAN SQUARE VALUES OF WING DYNAMIC LOADS
Λ_{LE} = 50°, NOMINAL MACH = 0.80, WINDUP TURN

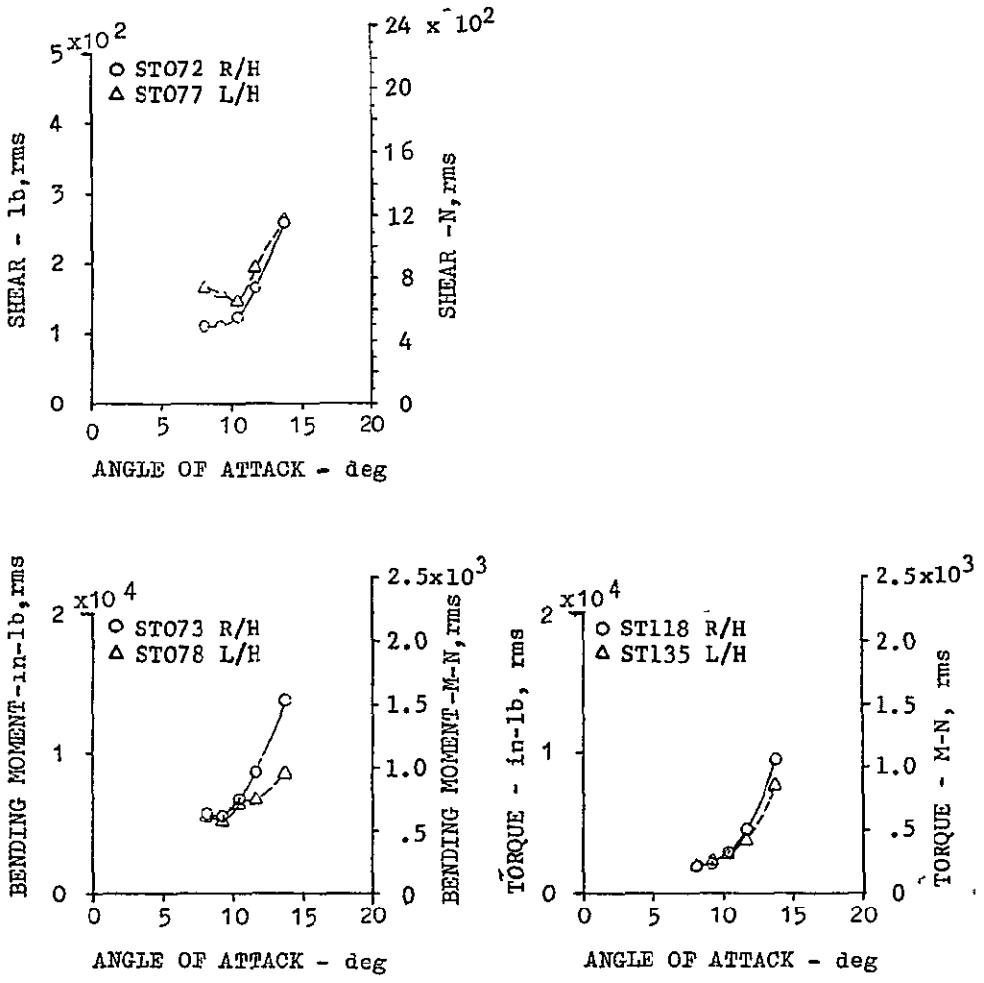

Figure 12. ROOT MEAN SQUARE VALUES OF HORIZONTAL TAIL DYNAMIC LOADS, $\Lambda_{LE} = 50^{\circ}$, NOMINAL MACH = 0.80, WINDUP TURN

angle of attack are all non-linear and show a mild inflection at about 10.4 degrees. The maximum rms values at the pilot's seat are less than half those at the c.g. and less than 0.1 those measured on the right wing tip. The values for the two different c.g. accelerometers are almost identical.

Figures 10e and 10f present vertical accelerations at the left and right wing tips respectively while Figures 10g and 10h show the lateral accelerations at the pilot's seat and center of gravity. Note that for this maneuver the wing tip responses have slightly different variations with angle of attack, but reach almost identical values at the maximum angle of attack. The lateral accelerations are quite small.

The wing dynamic responses at all of the 4 spanwise stations are presented in Figure 11. The magnitudes of response decreases with increasing spanwise distance from the pivot as expected from the Phase I studies at $\Lambda_{LE} = 26^{o}$. The non-linearity with angle of attack is consistent with that shown for the fuselage accelerations shown previously in Figure 10.

The corresponding horizontal tail responses are presented in Figures 12. Once again there are some differences between the responses for the left and right tails which can be attributed to control activity during the maneuver. One point worth mentioning is that a definite change in the slopes of

the variations with angle of attack occurs between 9 and 10 degrees. One can surmize that the wake flow from the wings begins to affect the horizontal tail significantly at 10 degrees angle of attack.

Responses for $\Lambda_{LE} = 50^{o}$ at Supersonic Mach Number

The investigation of buffeting response at supersonic speeds brought a few surprises. It was anticipated on the basis of pilot comment that little if any buffeting response would be present at M = 1.2. The magnitudes of the structural response which were measured during a supersonic wind-up turn and a supersonic slow down turn were higher than anticipated but lower than those for the subsonic turn. Figures 13-15 present the rms responses for the wind-up turn. The variations of accelerometer response with angle of attack shown in Figure 13 indicate that buffet onset might occur at lower angle of attack at M = 1.20 than at M = 0.80. The dynamic wing responses shown in Figure 14 indicate an anomalous high response in bending at wing station 1 at low angle of attack which is not present at the other wing stations. It is possible that the noted response is by residual activity in an antisymmetric mode due to the initial roll into the wind-up turn. Figure 15 shows that the shear response

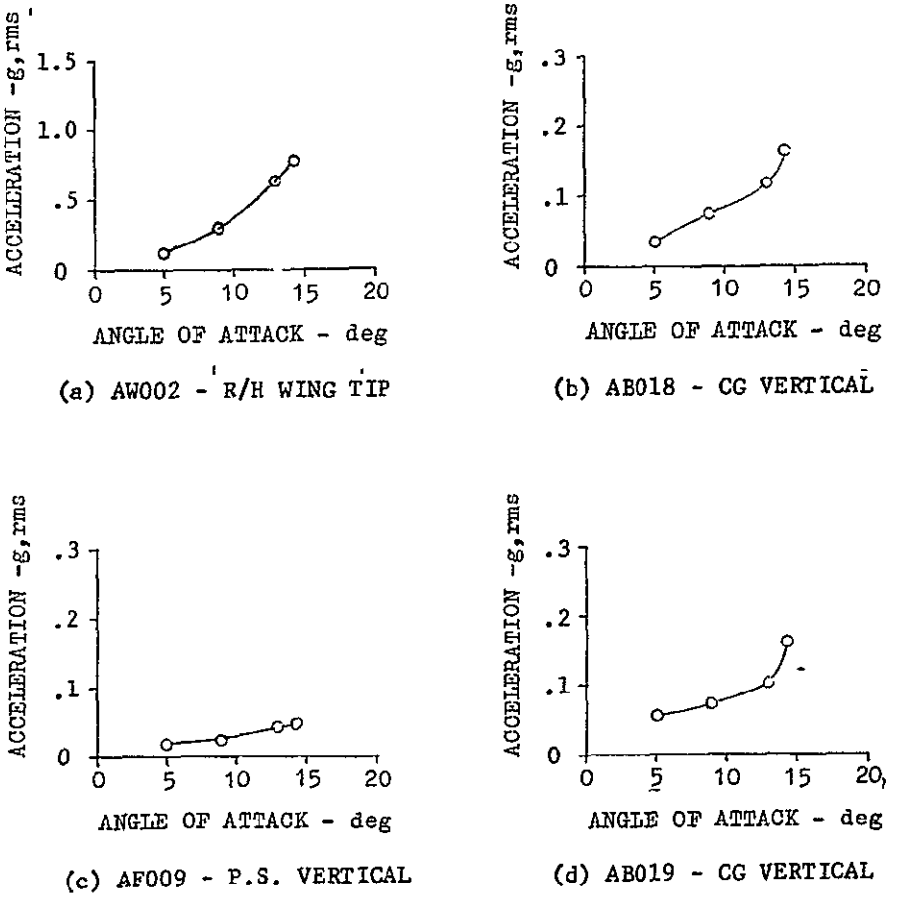

Figure 13. ROOT MEAN SQUARE VALUES OF ACCELERATION, $\Lambda_{LE} = 50^{\circ}$ NOMINAL MACH = 1.20 WINDUP TURN

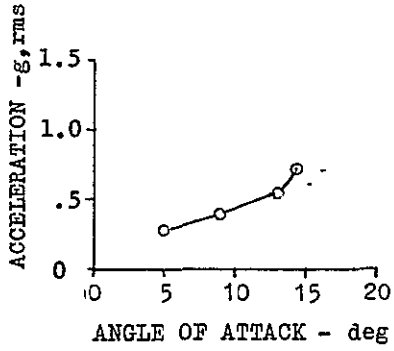

(e) AW001 - L/H WING TIP

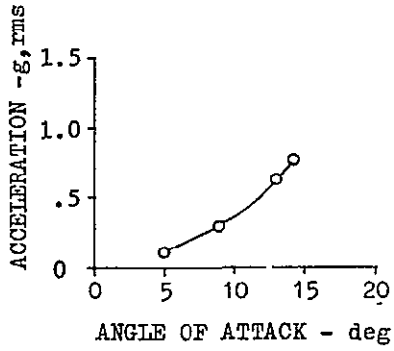

(f) AW002 - R/H WING TIP

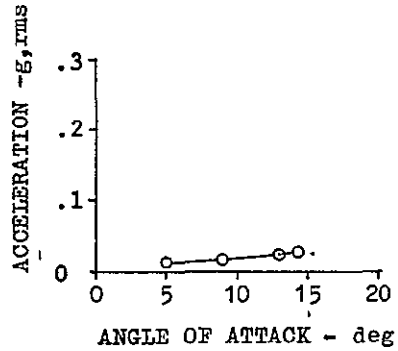

(g) AF010 - P.S. LATERAL

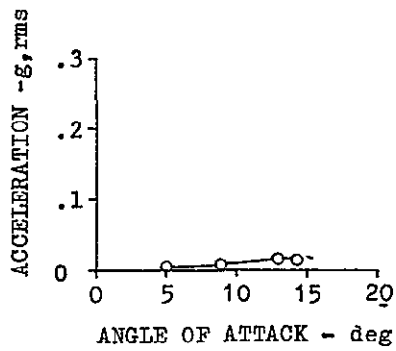

(h) AB020-CG LATERAL

Figure 13. Concluded

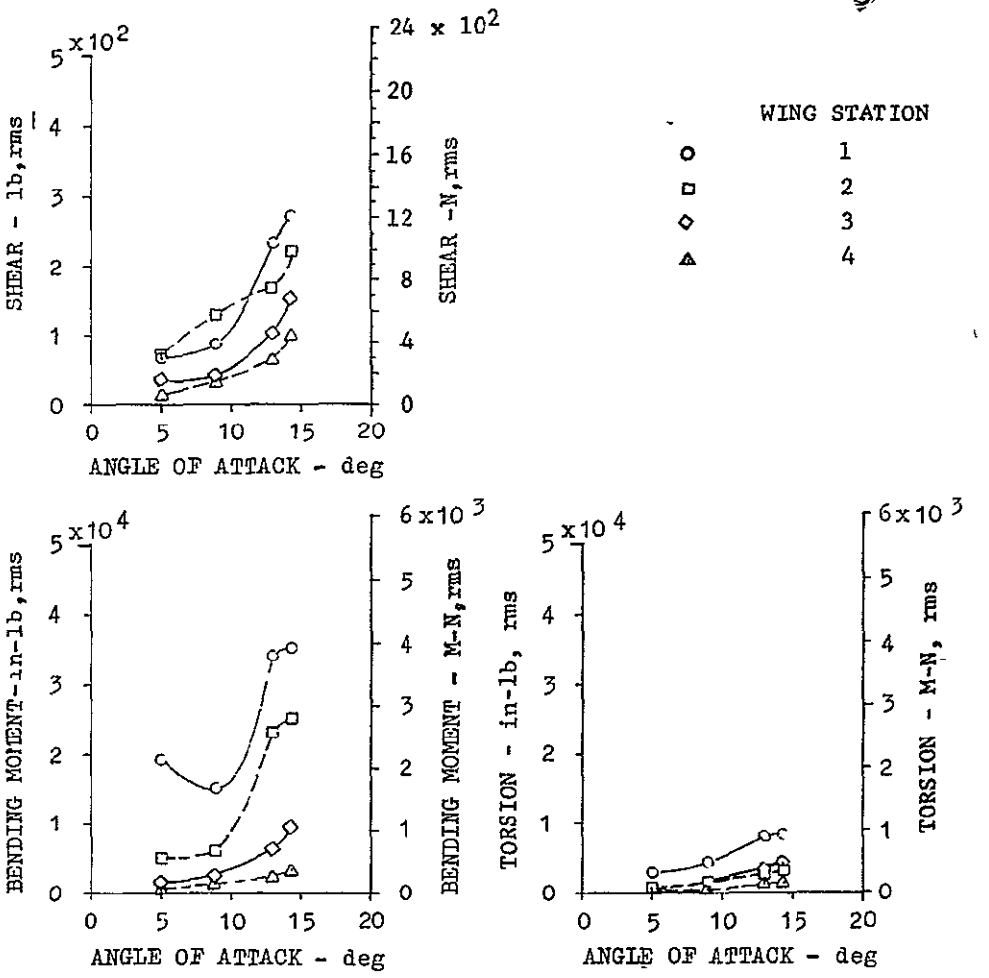

Figure 14. ROOT MEAN SQUARE VALUES OF WING DYNAMIC LOADS, Λ_{LE}= 50°, NOMINAL MACH = 1.20, WINDUP TURN

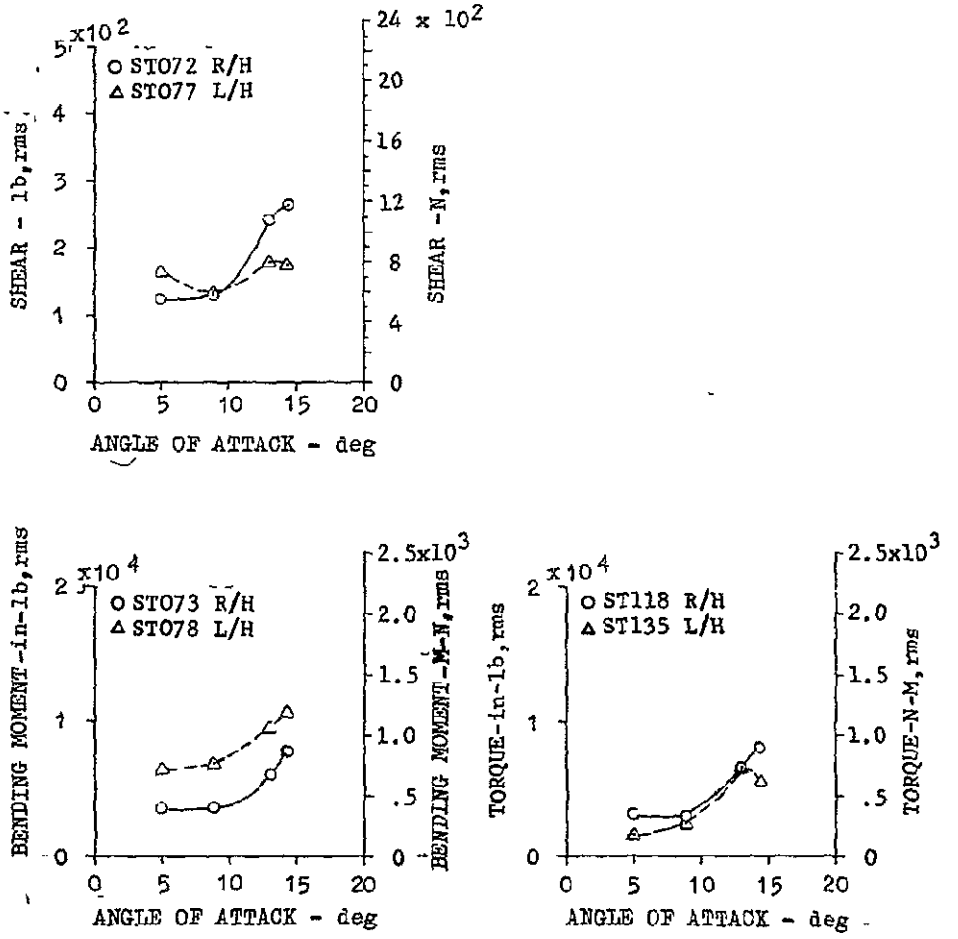

Figure 15. ROOT MEAN SQUARE VALUES OF HORIZONTAL TAIL DYNAMIC LOADS, $\Lambda_{LE} = 50^{\circ}$, NOMINAL MACH = 0.80, WINDUP TURN

for the left horizontal tail is also relatively high at the lowest angle of attack.

Response data from the supersonic slow down turn maneuver are presented in Figures 16, 17 and 18. In this particular analysis the data shown for each point are derived from different data sample durations. The intent of this analysis was to determine if any really significant differences existedbetween data derived from 1 second data samples and longer duration samples. In addition, it was desired to find out if any significant differences occurred between data obtained from the transient wind-up turn maneuver in which the load factor was continuously increasing and data obtained from the slow down turn maneuver in which the load factor was nominally constant. Figures 16, 17 and 18 therefore contain faired lines representing the results for the wind-up turn as previously presented in Figures 13, 14 and 15.

In general there are relatively small differences in the magnitudes of the responses obtained for the different data sample durations that cannot be explained by the slight differences in nominal angles of attack. One exception occurs for the pilot seat vertical accelerometer where the level derived from the 4 second data sample is roughly 60 to 70 percent higher than the values for the 1 second and

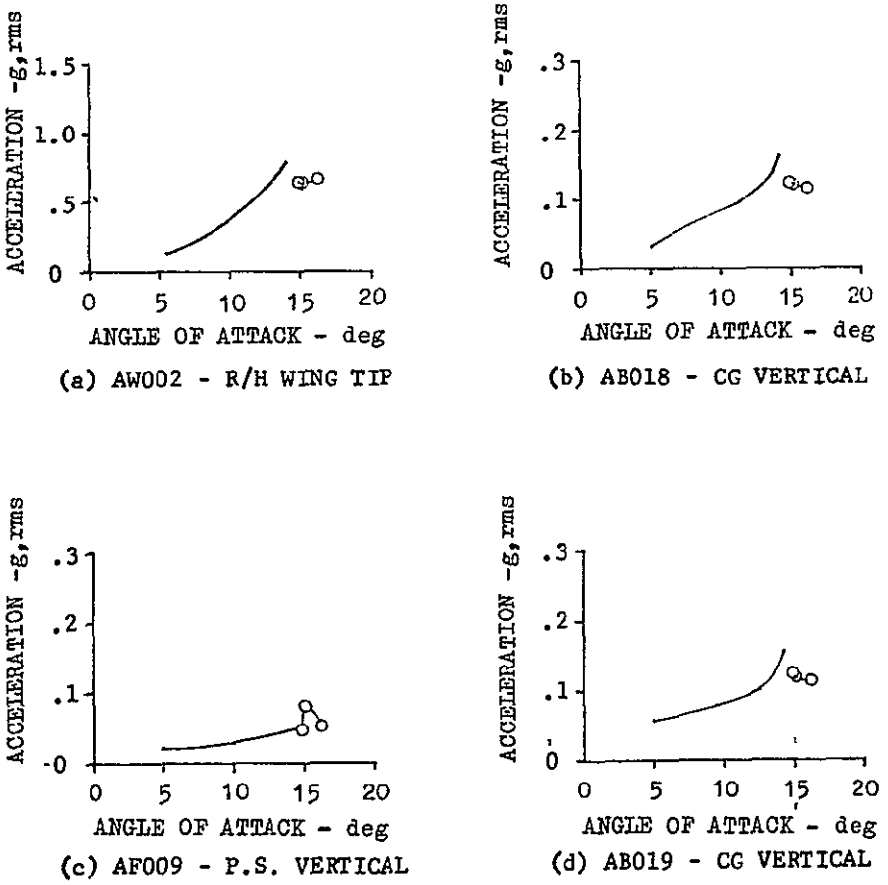

Figure 16. ROOT MEAN SQUARE VALUES OF ACCELERATION, $\Lambda_{LE} = 50^{\circ}$, SUPERSONIC SLOW DOWN TURN

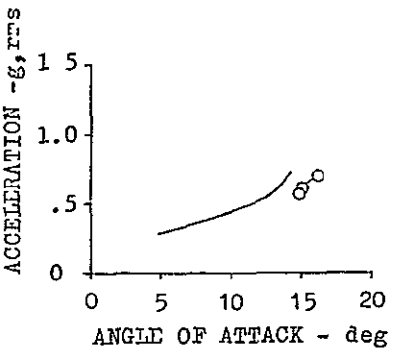

(e) AW001 - L/H WING TIP

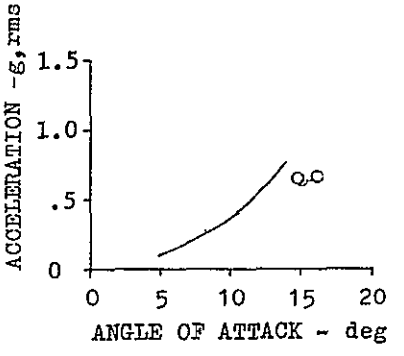

(f) AW002 - R/H WING TIP

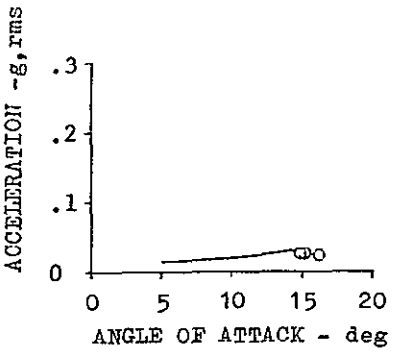

(g) AF010 - P.S. LATERAL

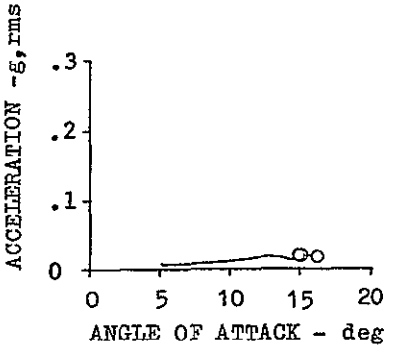

(h) AB020 - CG LATERAL

Figure 16. Concluded

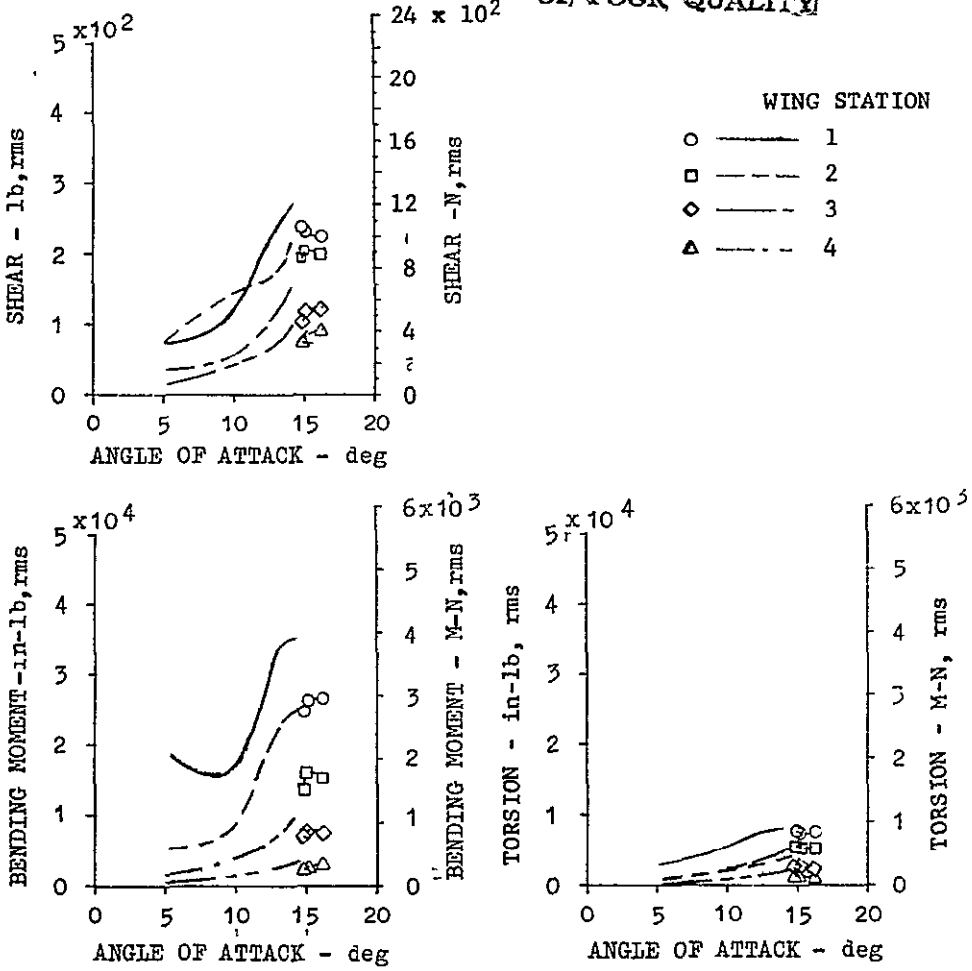

Figure 17. ROOT MEAN SQUARE VALUES OF WING DYNAMICS LOADS
$\Lambda_{LE} = 50^{o}$, SUPERSONIC SLOWDOWN TURN

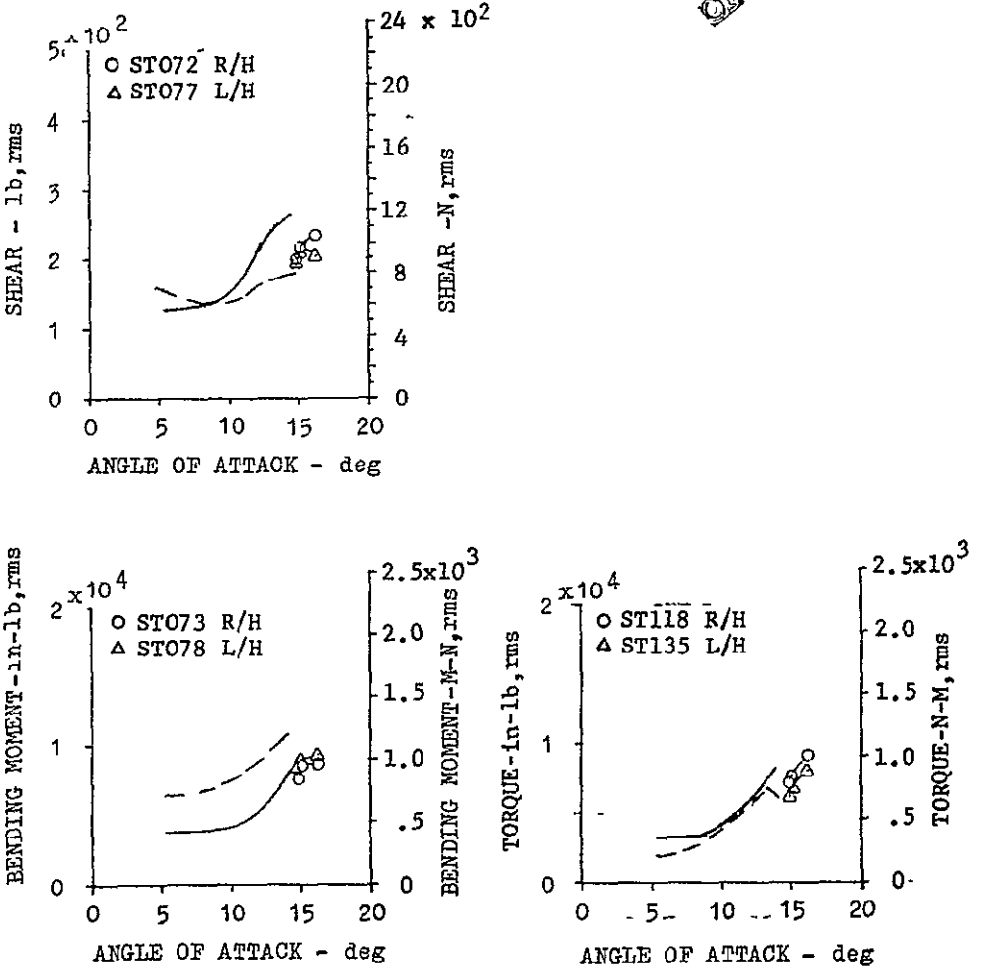

Figure 18. ROOT MEAN SQUARE VALUES OF HORIZONTAL TAIL DYNAMIC LOADS, $\Lambda_{LE} = 50^{\circ}$, SUPERSONIC SLOWDOWN TURN

2 second samples. This anomaly will be discussed in more detail when the power spectra are presented.

The comparisons between the wind-up turn data and the slow down turn data reveal that the vertical acceleration and wing loads are in general lower for the slow down turn than would be obtained by extrapolating the wind-up turn data to the higher angles of attack. It is possible that the differences may be due to the differences in damping effects at the different dynamic pressures.

Responses for $\Lambda_{LE} = 72.5^{o}$ at Subsonic Mach Number

Figures 19, 20 and 21 present the dynamic response data as variations with angle of attack for a subsonic wind-up turn maneuver with the wings set at $\Lambda_{LE} = 72.5$ degrees. In this particular case the first data segment was chosen to be slightly into buffet. The variation of wing tip and cg accelerations and wing bending and shear with angle of attack have a very distinctive early peak followed by a dip in response and then another increase in response. In general the rms values are lower than those experienced at the other sweep angles. In particular wing torsion is much lower which is reflected in much lower vertical acceleration response at the pilot's seat.

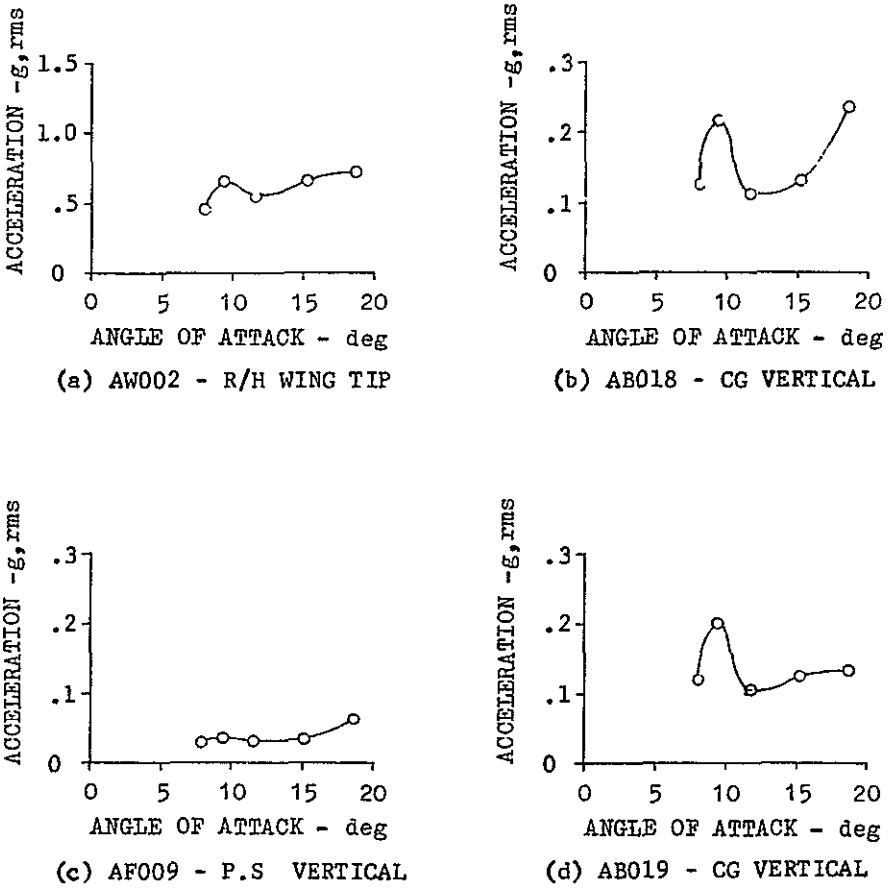

Figure 19. ROOT MEAN SQUARE VALUES OF ACCELERATION, $\Lambda = 72.5^{\circ}$, NOMINAL MACH = 0.89, WINDUP TURN

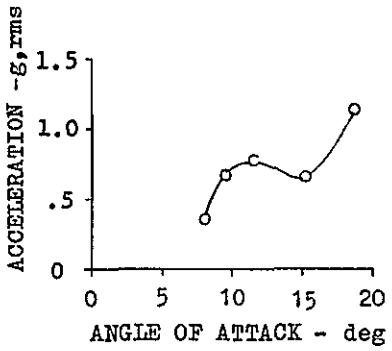

(e) AW001 - L/H WING TIP

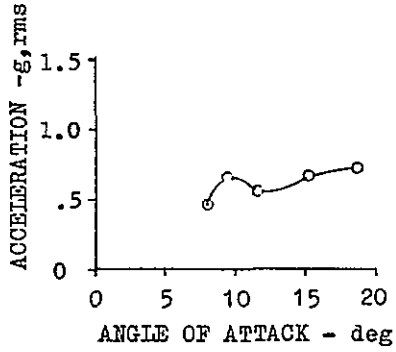

(f) AW002 - R/H WING TIP

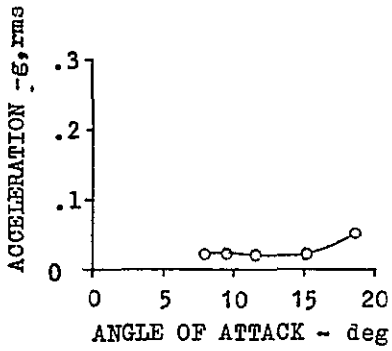

(g) AF010 - P.S. LATERAL

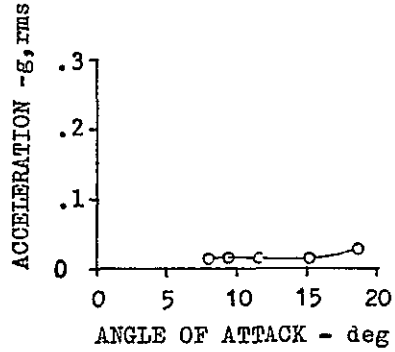

(h) AB020 - CG LATERAL

Figure 19. Concluded.

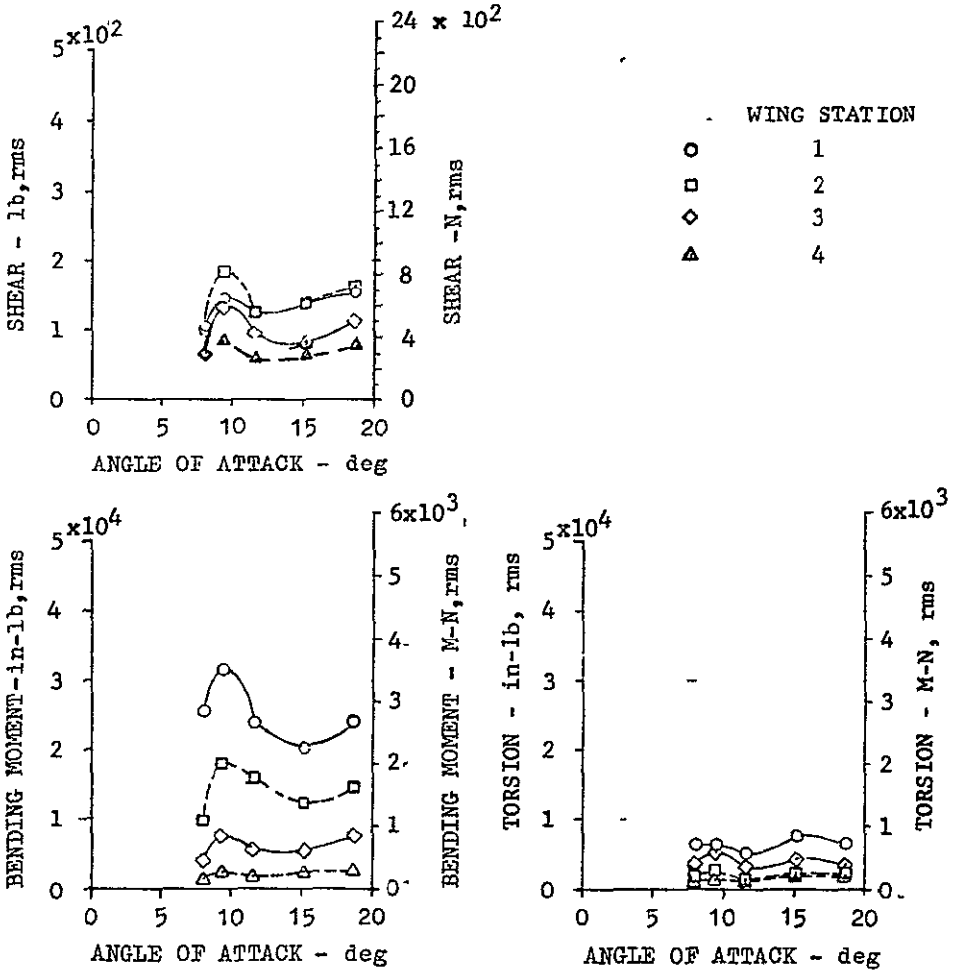

Figure 20. ROOT MEAN SQUARE VALUES OF WING DYNAMIC LOADS, $\Lambda_{LE} = 72.5^{\circ}$, NOMINAL MACH = 0.89, WINDUP TURN

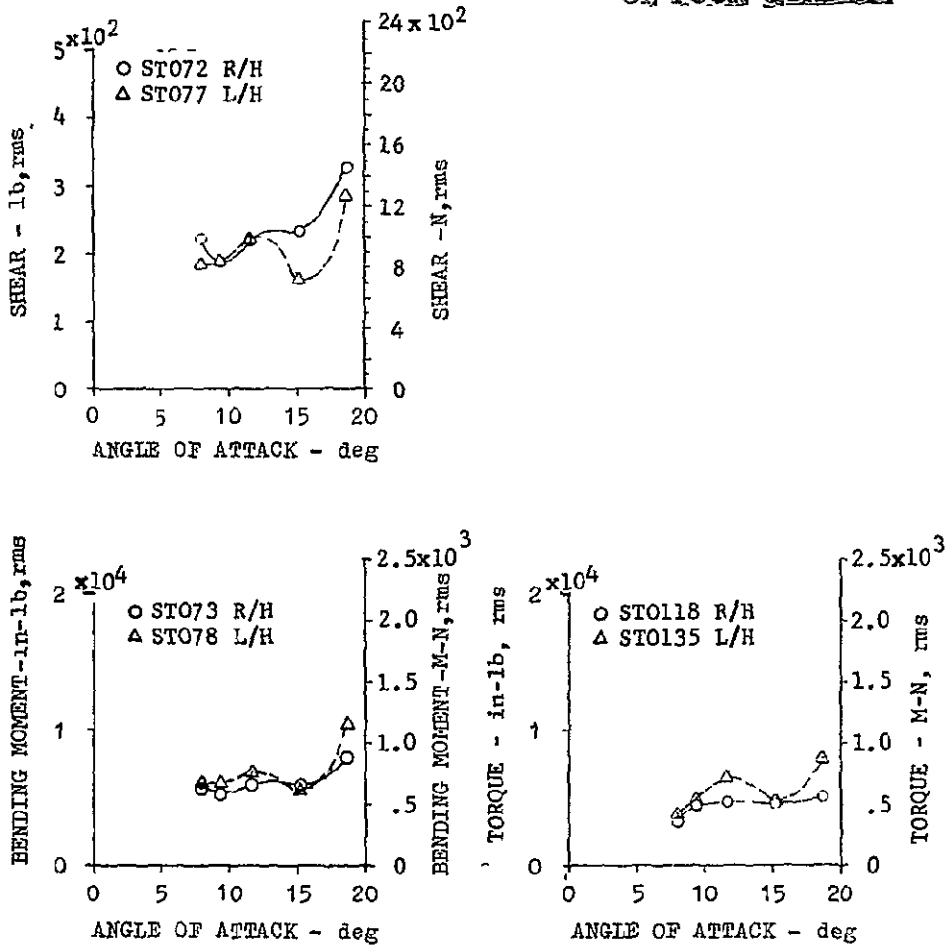

Figure 21. ROOT MEAN SQUARE VALUES OF HORIZONTAL TAIL DYNAMIC LOADS, Λ_{LE} = 72.5°, NOMINAL MACH = 0.89, WINDUP TURN

Responses for $\Lambda_{LE} = 72.5^{o}$ at Supersonic Mach Number

Figures 22, 23 and 24 present the dynamic response data for the supersonic wind-up turn with the wings set at $\Lambda_{LE} = 72.5$ degrees. In general the variations of response with angle of attack are similar to those for the subsonic wind-up turns but the initial peak at low angle of attack is reduced in magnitude. One anomaly occurs in the bending moment at wing station 1 which shows a higher response at the lowest angle of attack than is indicated by the other sensors. This anomaly is similar to the occurrence for the supersonic wind-up turn at $\Lambda_{LE} = 50$ degrees.

Response data from a supersonic slow down turn with $\Lambda_{LE} = 72.5$ degrees were also analyzed and the results are presented in Figures 25, 26 and 27. Also shown are curves representing the data from the wind-up turn for comparison. The data points represent responses over 2 second intervals. It is apparent that the very high peaks associated with the point at 17.5 degrees angle of attack do not correlate well with the data from the wind-up turn. Referring back to the maneuver time histories in Figure 6 it is apparent that a rather abrupt pitch transient occurred during that data sample. Examination of the time histories (not presented) showed that wing rocking also occurred during a brief portion of the data sample (less than one-half second) which was

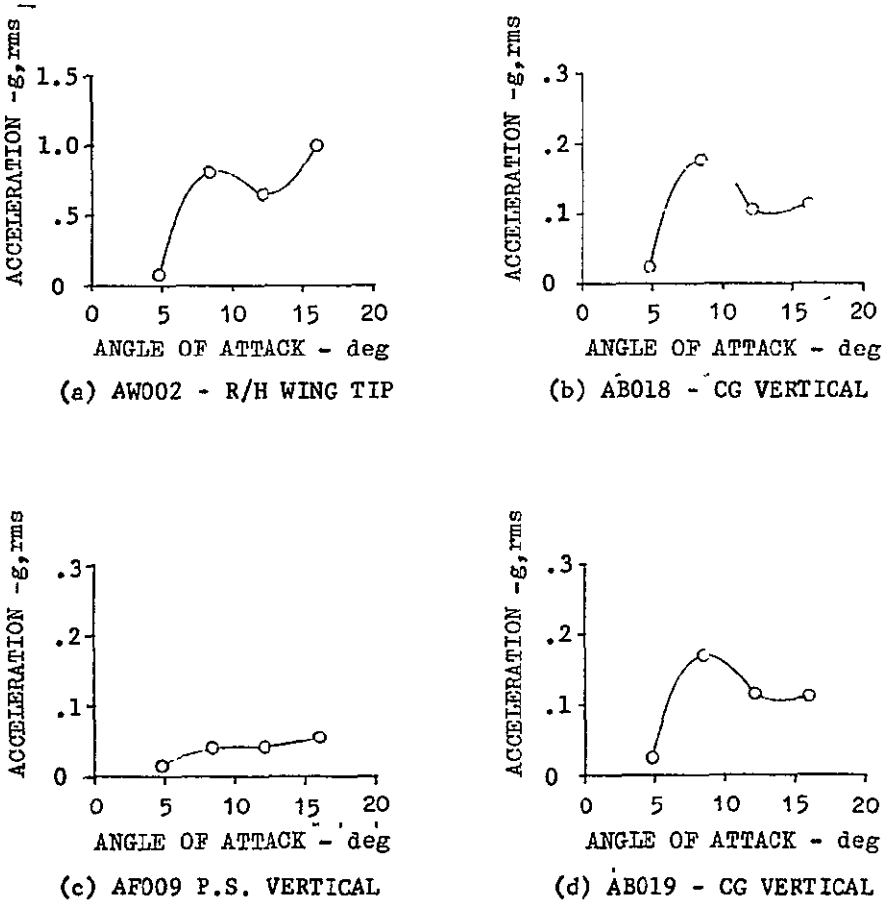

Figure 22. ROOT MEAN SQUARE VALUES OF ACCELERATION, $\Lambda_{LE} = 72.5^{\circ}$, NOMINAL MACH = 1.20 , WINDUP TURN

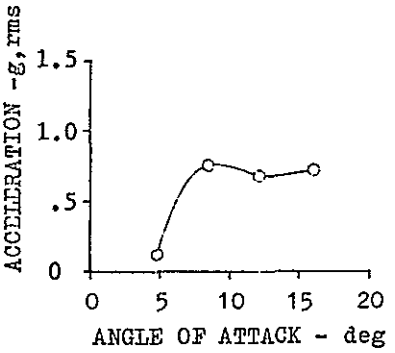

(e) AW001 - L/H Wing Tip

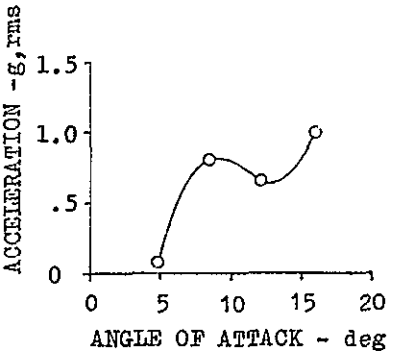

(f) AW002 - R/H Wing Tip

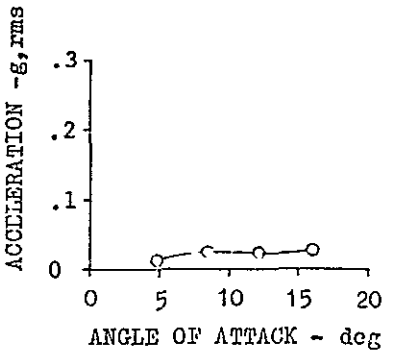

(g) AF010 - P.S. LATERAL

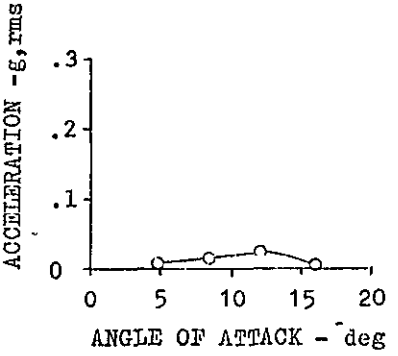

(h) AB020 CG LATERAL

Figure 22. Concluded

ORIGINAL PAGE IS
OF POOR QUALITY

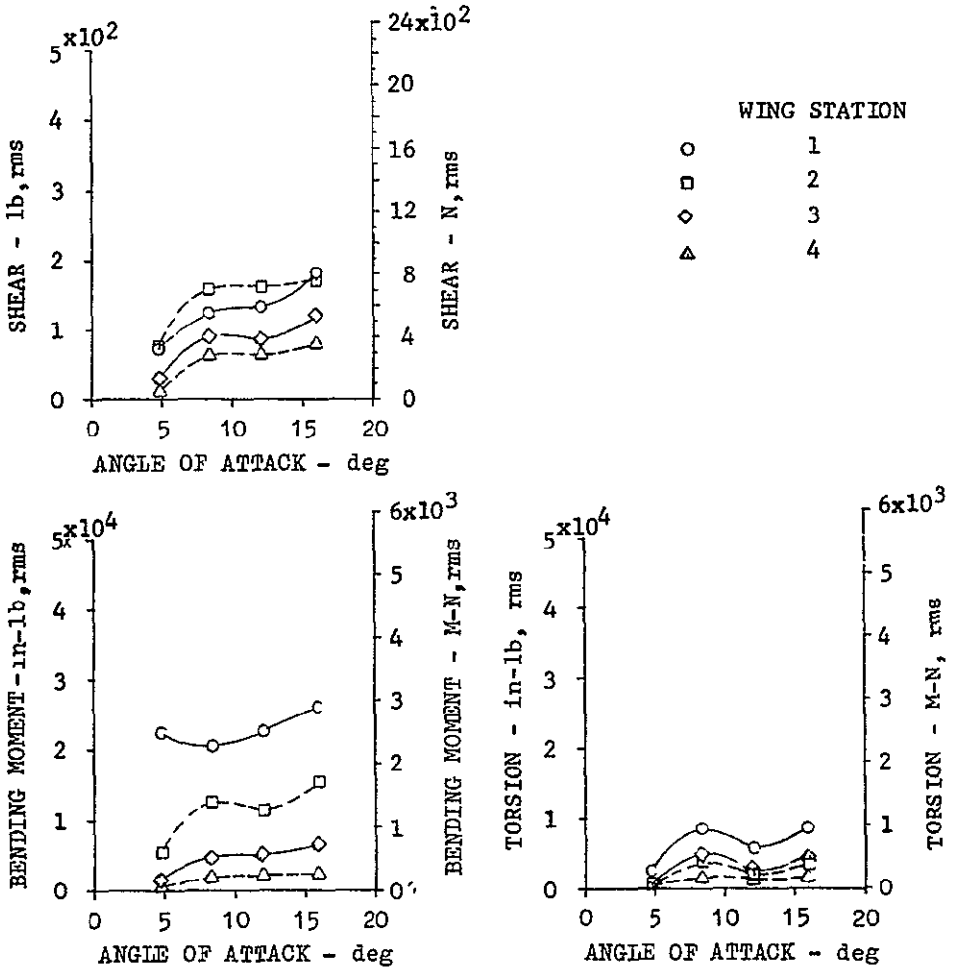

Figure 23 ROOT MEAN SQUARE VALUES OF WING DYNAMIC LOADS, $\Lambda_{LE} = 72.5^{\circ}$, NOMINAL MACH = 1.20, WINDUP TURN

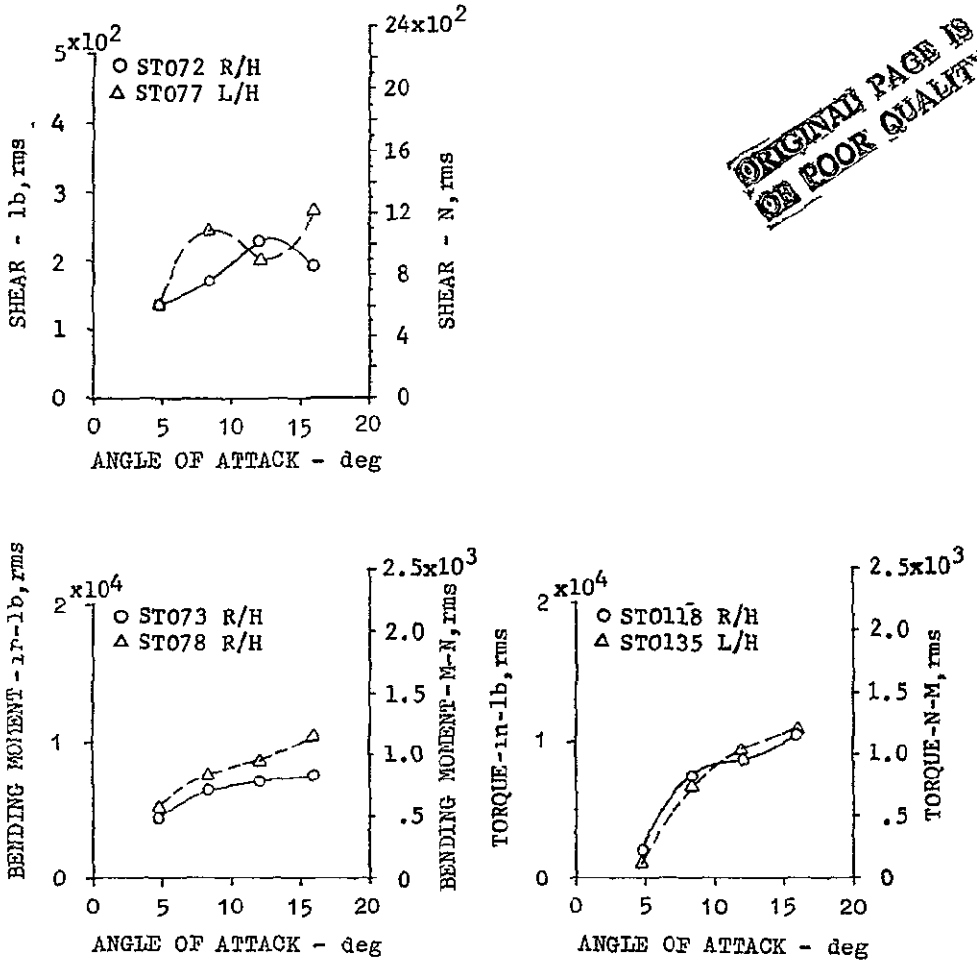

Figure 24. RMS VALUES OF HORIZONTAL TAIL DYNAMIC LOADS
$\Lambda_{LE} = 72.5^{\circ}$, NOMINAL MACH = 1.2, WINDUP TURN

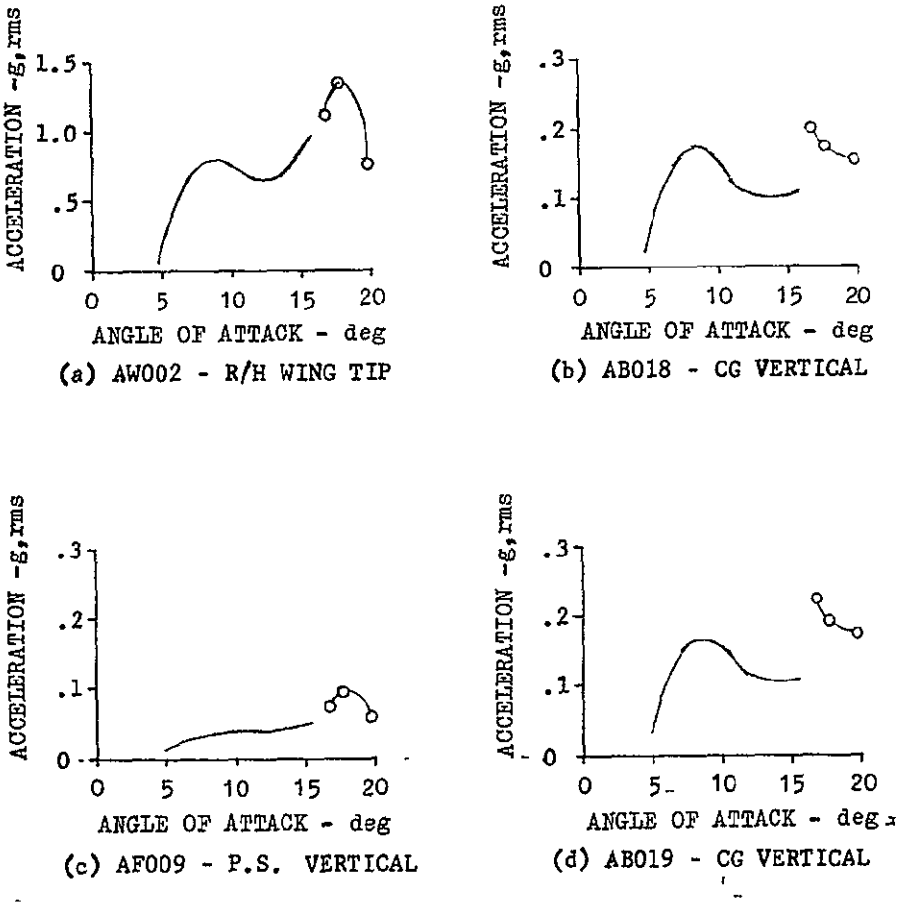

Figure 25. RMS VALUES OF ACCELERATIONS, $\Lambda_{LE} = 72.5^{o}$ SUPERSONIC SLOWDOWN TURN

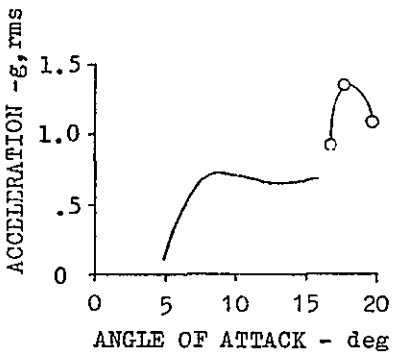

(e) AW001 - L/H WING TIP

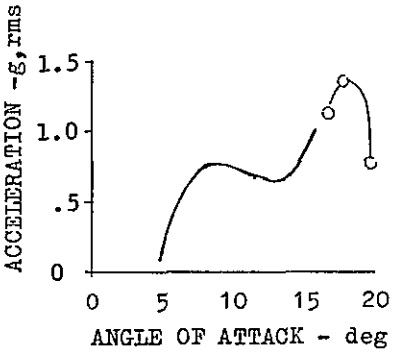

(f) AW002 - R/H WING TIP

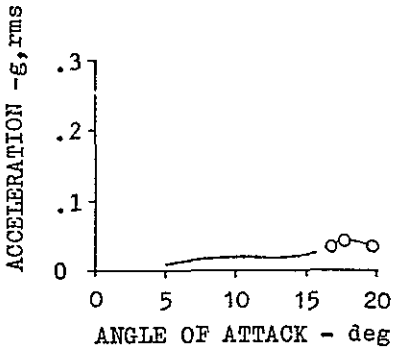

(g) AF010 - P.S LATERAL

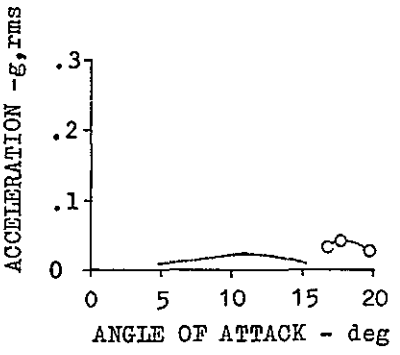

(g) AB020 - CG LATERAL

Figure 25. Concluded.

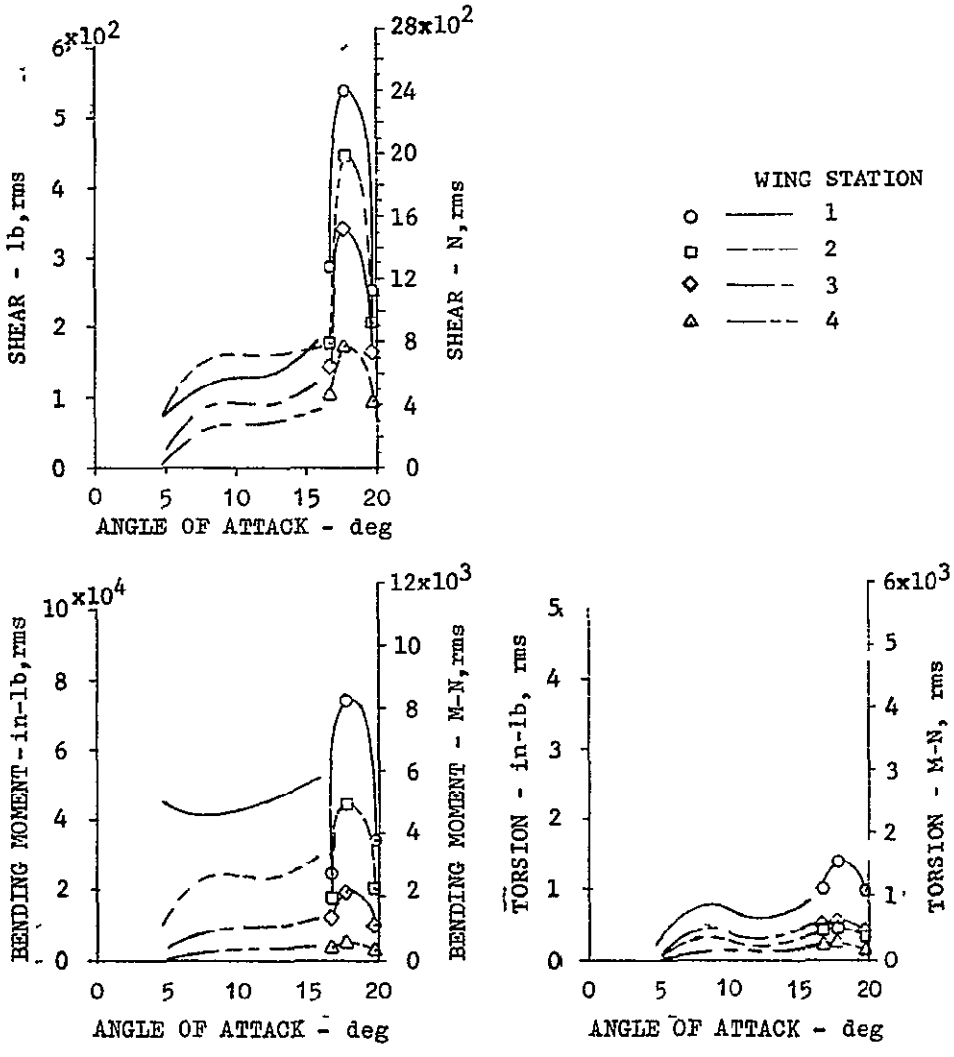

Figure 26. RMS VALUES OF WING DYNAMIC LOADS, $\Lambda_{LE} = 72.5^{\circ}$, SUPERSONIC SLOWDOWN TURN

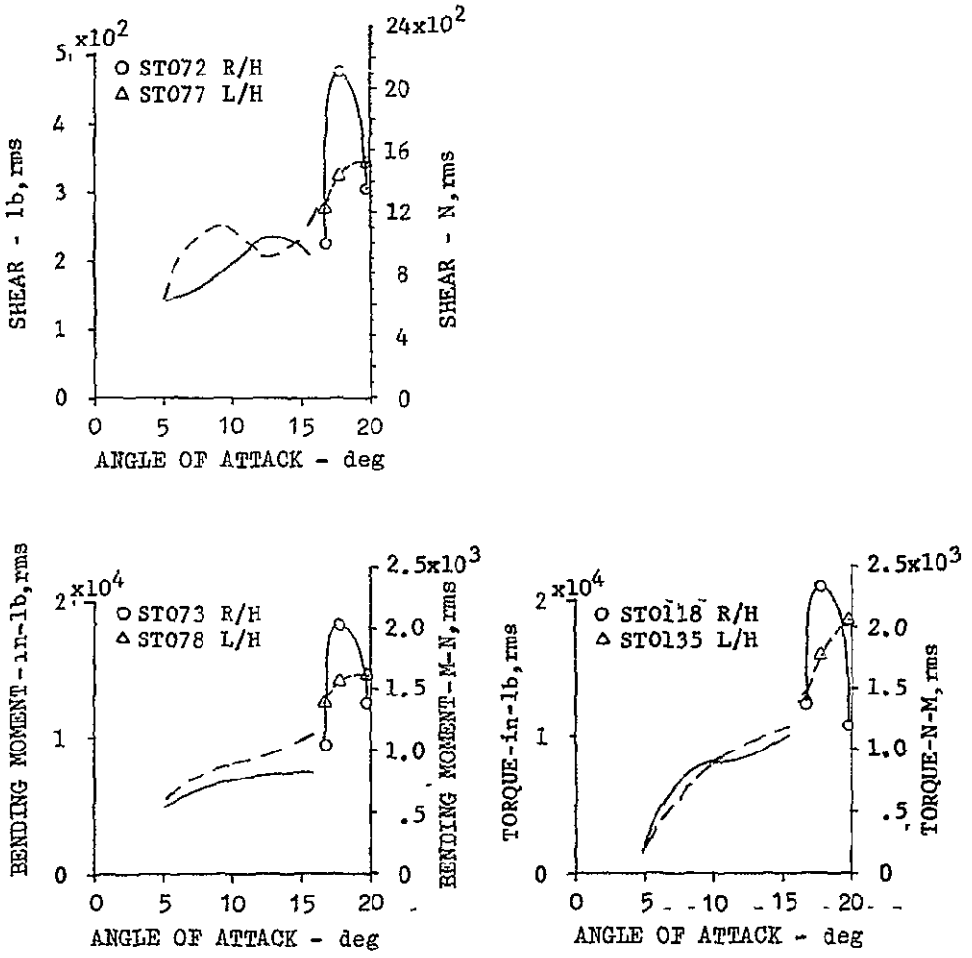

FIGURE 27. RMS VALUES OFHORIZONTAL TAIL DYNAMIC LOADS
$\Lambda_{LE} = 72.5^{o}$, SUPERSONIC SLOWDOWN TURN

not pilot induced. Further examination of earlier attempts at this same maneuver also showed pitch and roll transients at approximately the same time into the maneuver which indicates that some flow phenomenon is occurring. Note in Figure 6f that the Mach number is just passing through 1.20 during the data sample.

Recent wind tunnel force data (Reference 4) show that mild lift-curve and pitching-moment curve breaks occur between 16 and 18 degrees angle of attack at M = 1.20 which is indicative of a change in the wing flow field.

Effects of Wing Sweep on Magnitudes of Response

One of the objectives of the Phase II studies was to determine the effects of wing sweep on the magnitudes and spectral content of the structural response. Figure 28 presents comparisons of nine items of structural response as functions of angle of attack for subsonic wind-up turn maneuvers performed at high altitudes and nominal wing leading-edge sweeps of 26, 50 and 72.5 degrees. The nominal Mach numbers are 0.70, 0.80 and 0.89 respectively; thus each maneuver is essentially at subcritical flow conditions. The nine items are right wing tip, center of gravity and pilot's seat vertical accelerations, vertical shear, bending moment and torque at wing station 1, and vertical shear, bending moment and hingeline torque on the right horizontal tail.

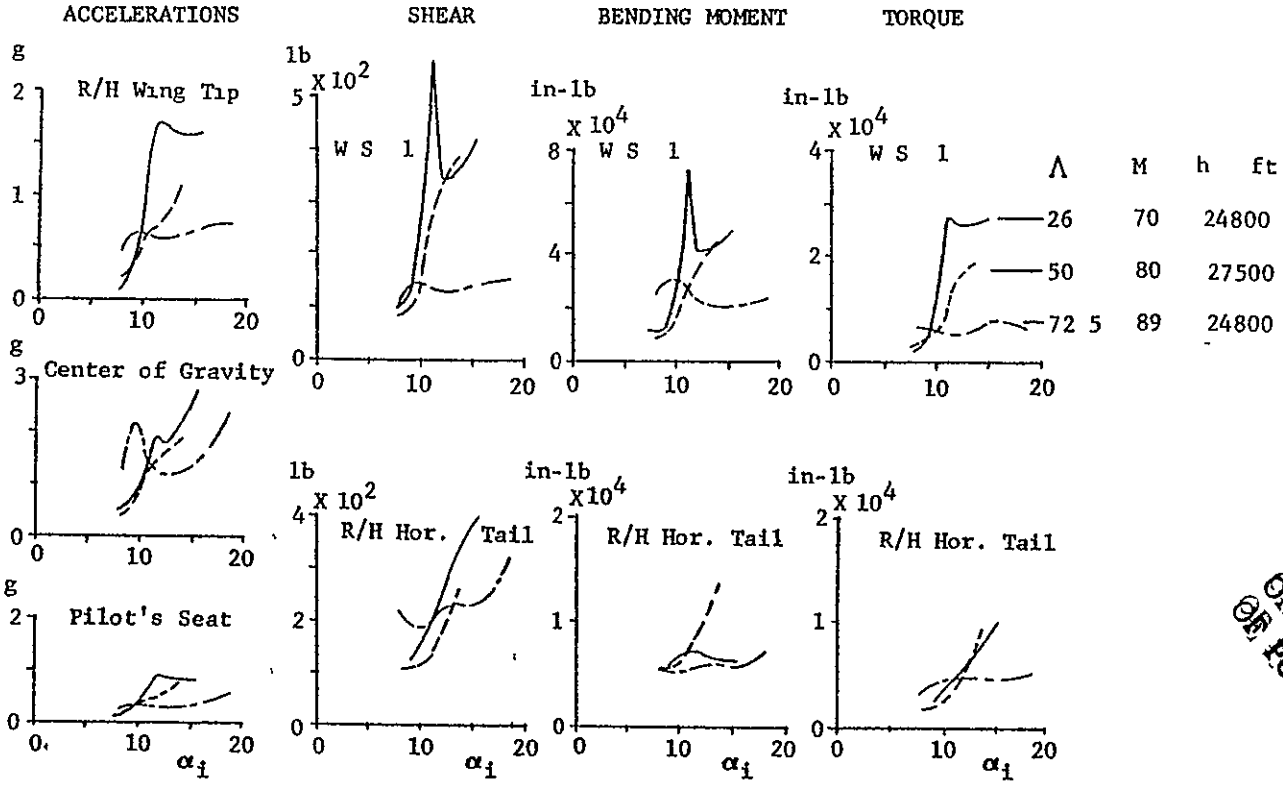

Figure 28 EFFECTS OF WING SWEEP ON RMS VALUES OF RESPONSE

In general the dimensional rms magnitudes of wing and fuselage responses decrease with increasing wing sweep at the higher angles of attack. The responses just above buffet onset are larger for the highest sweep but remain at relatively low values as angle of attack is increased in contrast to the responses at the lower wing sweeps which rise to higher levels. At the center of gravity the buffet accelerations for the highest sweep are quite large. The power spectra to be shown later indicate that the high rms values are caused by response at relatively high frequencies which are not significantly excited at the pilot's seat.

The trends shown for the horizontal tail are somewhat inconsistent with those shown for the wing responses. This inconsistency is most likely caused by the fact that some horizontal tail control activity occurs during the maneuvers both in pitch and roll. It is interesting to note that the horizontal tail shear and torque are relatively high percentages of the corresponding wing responses, particularly at the highest wing sweep. It is probable that the turbulent wake from the wing is the major excitation force on the horizontal tails although some of the response is undoubtedly caused by transmission from the wing through the aircraft structure.

Effects of Mach Number

The investigation of buffeting response at supersonic speeds was primarily aimed at providing data for formulating and verifying the prediction method since past flight experience has indicated little if any significant buffet at supersonic speeds. Figure 29 presents comparisons of selected responses at M = 0.80 and 1.20 for 50 degrees sweep and Figure 30 similar comparisons at M = 0.89 and 1.20 for 72.5 degrees sweep.

At 50 degrees sweep the rms magnitudes of response at M = 1.2 are somewhat smaller at the high angles of attack than at M = 0.8. In particular the wing torsion response is much reduced and this is reflected in a small vertical acceleration at the pilot's seat. This reduction of torsional response is likely the major reason that the buffeting at supersonic speeds is considered minimal by the pilots. There is an anomalous high response in bending at wing station 1 at low angles of attack at M = 1.2 which does not occur at the other wing stations. It is probable that the anomalous response is due to residual response in one or more antisymmetric modes caused by the initial roll into the maneuver. The difference shown in bending response of the right hand horizontal tail is somewhat larger and brackets the M = 0.8 response shown for the right hand tail.

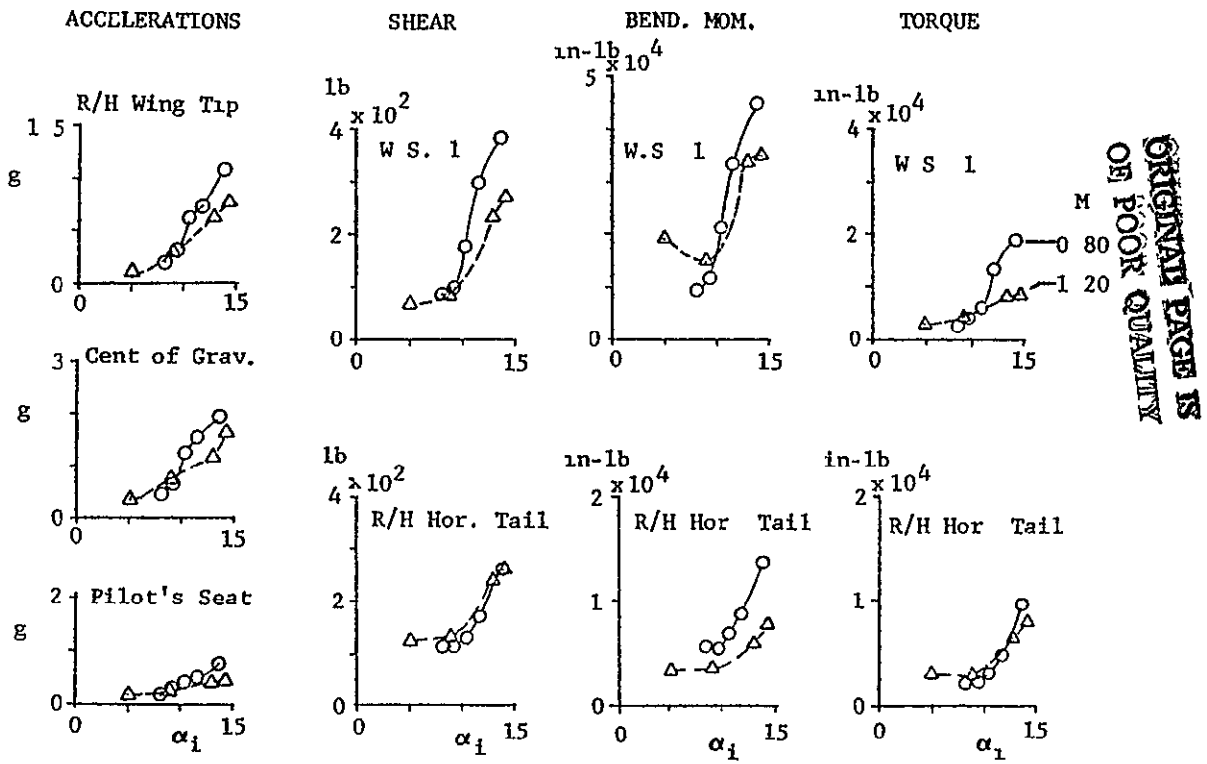

Figure 29 COMPARISON OF SUBSONIC AND SUPERSONIC RMS RESPONSES - $\Lambda = 50^{\circ}$

The magnitudes of response at M = 1.2 at 72.5 degrees shown in Figure 30 are very similar to the subsonic responses with the exception of bending at wing station 1 which again has a relatively high initial value at low angle of attack and probably for the same reason as the 50 degree sweep case. The increase in horizontal tail torque response at M = 1.2 over that at M = 0.89 may be significant from an academic point of view (i.e.,can it be predicted?) but the buffet loads are still small.

Summary Analyses

In order to gain a perspective of the relative magnitudes of the buffet accelerations and loads two summary figures were prepared which are presented in Figures 31 and 32. In Figure 31 the maximum buffet acceleration measured during each maneuver analyzed in both phases of the investigation has been normalized by the maximum normal load factor obtained. The curves represent data obtained in Phase I for 26 degrees sweep. The discrete data points represent the results obtained in Phase II from the wind-up turn maneuvers. The left side of Figure 31 shows the effect of altitude on the relative responses for 26 degrees sweep. There is a definite reduction in the relative responses with decreasing altitude which is expected since the aircraft must penetrate farther above buffet onset at high altitude to produce a given load

Figure 30 COMPARISON OF SUBSONIC AND SUPERSONIC RMS RESPONSES - $\Lambda = 72.5^{o}$

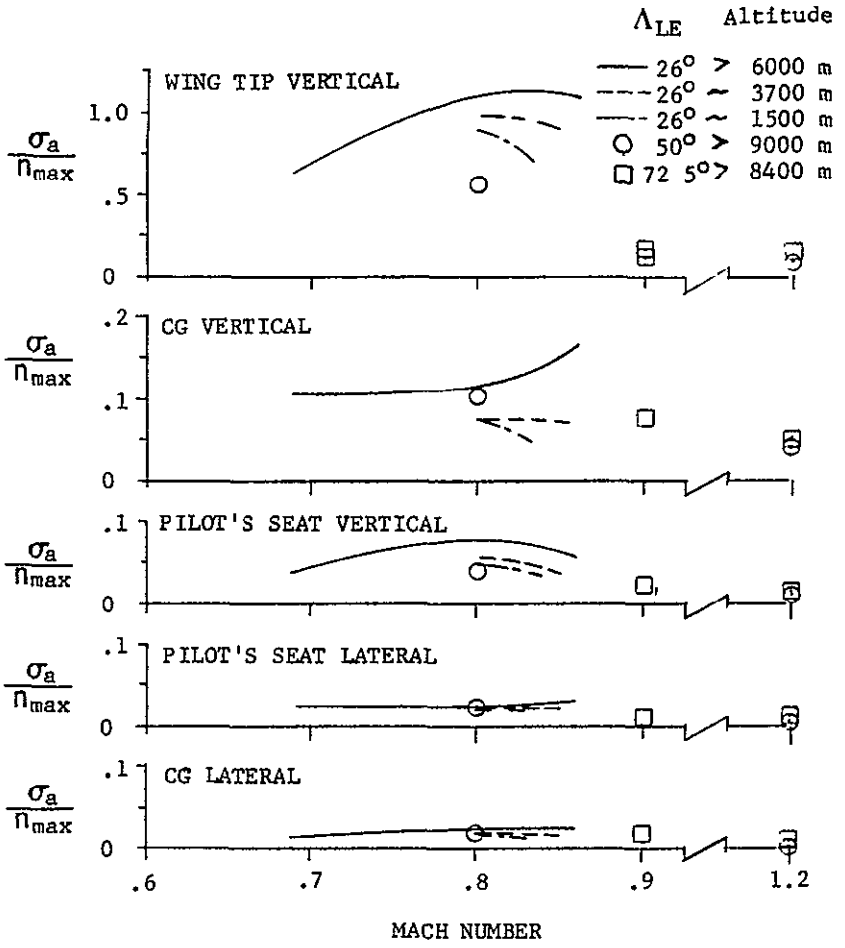

Figure 31. PEAK ACCELEROMETER RESPONSES NORMALIZED BY MANEUVER MAXIMUM LOAD FACTOR

Figure 32 SUMMARY OF NORMALIZED BUFFET LOADS

factor turn than at low altitude. The right side of Figure 31 shows that the relative responses are generally lower for the higher wing sweeps. Qualitatively, the levels of response for $\Lambda_{LE} = 26^{o}$ at high altitude and the higher Mach numbers represent a rather rough ride for the crew.

The normalized wing shear and bending moment loads due to buffet are summarized in Figure 32. In this figure the normalizing quantity is the maximum "steady" or mean load developed at each wing station during each maneuver. The left hand and center plots of Figure 32 are for maneuvers performed at 3 altitudes and for M = 0.80 and 0.86 respectively while the right hand plot is for 5 combinations of sweep and Mach number at relatively high altitudes. As might be expected the maximum relative responses at the most inboard wing station occur for $\Lambda_{LE} = 26^{o}$ for the transonic conditions and at the highest altitude where the penetration beyond buffet onset is the greatest. Even so, the buffet loads are no more than 4 percent of the maneuver loads in shear and no more than 5 percent in bending moment. At the most outboard station the relative responses are much higher, about 10 to 12.5 percent for shear and 18 to 20 percent for bending moment.

The effect of wing leading-edge sweep at subsonic speeds is such that at the inboard station the relative responses are reduced as the sweep increases while near the tip the

relative response at $\Lambda_{LE} = 50^{o}$ is about the same as that for $\Lambda_{LE} = 26^{o}$. At $\Lambda_{LE} = 72.5^{o}$ a significant reduction in relative response occurs at all four wing stations.

At M = 1.20 the relative responses are very small and are essentially identical for $\Lambda_{LE} = 50^{o}$ and $\Lambda_{LE} = 72.5^{o}$.

CHARACTER OF THE RESPONSES

In the Phase I study it was found that the spectral content of the structural responses changes with sensor type, sensor location and angle of attack. The peaks in the various spectra were identified with natural vibration modes of the aircraft, some symmetric and some antisymmetric.

Reference 5 presented some example power spectra which showed, for example, that wing shear, bending moment, and torsion responses exhibited quite different spectra. Also outboard locations on the wing respond more to higher frequency vibration modes than do the inboard stations. Finally, the pilot's seat vertical accelerometer response shifts toward higher frequency modes as angle of attack is increased.

Horizontal tail response spectra were not obtained during Phase I, but it was inferred that horizontal tail modes caused significant contributions to the fuselage buffet accelerations.

Power spectra obtained during Phase II for the higher wing sweeps in general show similar trends to those obtained in Phase I at leading-edge-sweep of 26 degrees. Therefore, the discussions of the power spectra in the body of this report are limited to:

(1) presentation of the horizontal tail spectra corresponding to the M = 0.80 wind up turn data for $\Lambda_{LE} = 26^{o}$ discussed in the Phase 1 Report (Reference 1)

(2) comparisons of example spectra showing the effects of wing sweep and

(3) explanations of some of the anomalies that appear in the rms data.

The spectral content of the structural responses is related to the natural vibration modes. Summaries are presented of the natural vibration mode frequencies as determined from ground vibration tests and also as calculated using a finite element representation of the aircraft structure for each wing sweep. These data are useful for interpreting the power spectra Discussion of the narrow-band time history analysis is included because some interesting results were obtained even though the basic intent of the analyses was not accomplished and useful damping data were not obtained.

Natural Vibration Modes

The measured natural vibration modes and their associated frequencies are presented in Tables 10 through 12 for wing sweeps of 26, 50, and 72.5 degrees. These data were obtained during extensive ground vibration tests conducted on aircraft in the F-111 development program and are taken from References 6 and 7. In addition, calculated modes were determined for specific flight conditions for use in the prediction method

Table 10

MEASURED F-111A NATURAL VIBRATION MODES, $\Lambda_{LE} = 26^{\circ}$

Predominant Mode (Airplane No 12 Tests)	Frequency - Hz			
	Fuse Empty, Wing Empty		Fuse Full, Wing Empty	
	Symmetric	Antisymmetric	Symmetric	Antisymmetric
Wing First Bending	5 2	7 6	5 1	7.1
Fuselage First Vertical Bending	8 6	---	8 0	---
Fuselage First Lateral Bending	---	---	---	8 7
Wing Fore and Aft Bending	7 9	9 3	8 8	8 7
Wing Second Bending	16 9	29 2	17 8	29.0
Wing-Horizontal Tail	---	16.2, 17.5	---	17 5
First Wing Torsion	25 2	25 4	25.7	26 1
Horizontal Tail First Bending	13 6	13 3	13 8	13 1
Horizontal Tail Fore and Aft	15 2	15 3	16 3	16 2
Horizontal Tail Pitch	34 4	37 3, 31.0	30 9	29.5, 36 1
Vertical Tail Bending	---	9 9	---	9.6
Vertical Tail Torsion	---	28 0	---	11.7
Rudder Rotation	---	32.7	---	28 3
Rudder Torsion	---	45.0	---	44.8
Rotating Glove				
Leading Edge Bending	27 4			
Yaw	44 3			
Pitch	50 9			
Aft End Bending	63.8			
Spoiler Modes (From Airplane No. 1 Tests)				
Spoiler No 1			46,56,62	53,60
Spoiler No 2			55,65,72	68

Table 11
MEASURED F-111A NATURAL VIBRATION MODES, $\Lambda_{LE} = 50^{\circ}$

PREDOMINANT MODE AIRPLANE NO. 12 TESTS	Frequency - HZ Fuse Full Wing Empty		Fuse Full Wing Full	
	Symmetric	Antisymmetric	Symmetric	Antisymmetric
Wing First Bending	5.0	6.6	4 1	6.0
Fuselage First Vertical Bending	8.0	-	7 9	-
Fuselage First Lateral Bending	-	8.9	-	8 9
Wing Fore and Aft Bending	8.7	7 3	5 8	5.2
Wing Second Bending	17 5	28.9,30.6	13 0	26 1
Wing - Horizontal Tail	15 8	16 5	-	14.7
Wing First Torsion	26.4	26 1	23.8	24.5
Horizontal Tail Bending	13.3	12 8	13.1	11.9
Horizontal Tail Fore and Aft	16.3	16 6	16.2	16.5
Horizontal Tail Pitch	21.4,33.7	29.8,35 9	31 8,35.6	29.3,36.5
Vertical Tail Bending	-	9.7,11.5	-	9.7,11.6
Vertical Tail Torsion	-	27.6	-	27.5
Rudder Rotation	-	32 0	-	32.6
Rudder Torsion		45 0		45 4
Airplane 13 Tests (Close Tolerance Hor Tail Bushings)				
Horizontal Tail First Bending	13.3	12 8	-	-
Horizontal Tail Fore and Aft	16 9	17.0	-	-
Horizontal Tail Pitch	34 2,39 0	37.9,43 2	-	-
Horizontal Tail Second Bending	-	47.2,52 4	-	-

Table 12
MEASURED F-111A NATURAL VIBRATION MODES, $\Lambda_{LE} = 70^{\circ}$

PROMINANT MODE AIRPLANE NO. 12 TESTS	Frequency - HZ			
	Fuse Full Wing Empty		Fuse Full Wing Full	
	Symmetric	Antisymmetric	Symmetric	Antisymmetric
Wing First Bending	5 0	5.8	3 8	4 9
Fuselage First Vertical Bending	8 0	-	7 8	-
Fuselage First Lateral Bending	-	9 0	-	8 3
Wing Fore and Aft Bending	8 0	7 3	5.6	5 6
Wing Second Bending	17 4	30 0	12.9	26 4
Wing - Horizontal Tail	16 1	16 6	-	14 4
Wing Torsion	26 2	27.1,28.7 29 4,31 0	23 7	24.5
Wing - Flap	-	-	-	29.4,29.6
Horizontal Tail Bending	13 3	12.6	-	-
Horizontal Tail Fore and Aft	16.2	16.5	-	-
Horizontal Tail Pitch	31.8,35 2	29.6,36.3	-	-
Vertical Tail Bending	-	9 7	-	-
Vertical Tail Torsion	-	27 7	-	-
Rudder Rotation	-	31 9	-	-
Rudder Torsion	-	44 5	-	-

development and evaluation portions of the contracted investigation The calculated modes are presented in Tables 13 through 20. Further discussion of the analytical effort appears in References 8, 9 and 10.

Narrow-Band Time Histories

Toward the end of this investigation a brief effort was made to obtain damping coefficients for a few of the most dominant wing modes of vibration. The scope of that study was previously presented in Table 9. This effort was not successful, but some important information regarding the character of the responses was obtained.

Some example filtered time histories which were run at a paper speed of 10 mm/sec are presented in Figure 33. The upper two records are vertical accelerations at the right wing tip for frequency ranges of 4 to 6 and 6 to 8 hertz, respectively. The next two records are bending moment response at Wing Station 1 in the same two frequency ranges and the bottom record is bending moment at Wing Station 2 in the frequency range from 16 to 18 hertz. These particular time histories are from the M = 0.80 wind-up turn at Λ_{LE} = 26 degrees for which the rms values of response are quite large (Reference 1).

The first impression one gets from these records is that the responses build up and decay in a random aperiodic manner.

Table 13

CALCULATED F-111A SYMMETRIC VIBRATION MODES

$\Lambda_{LE} = 26^{o}$ GW = 266,044N (59,800 lb)

Mode No.	Mode Description	Frequency - Hz
1	First Wing Bending	4.794
2	First Fuselage Vertical Bending	7 013
3	Horizontal Tail Bending + Sec. Wing Bend + Sec Fus. Bend.	13.930
4	Horizontal Tail Bending + Second Wing Bending	14 828
5	Second Wing Bending	17 010
6	Third Fuselage Bending + Wing Torsion	22 853
7	First Wing Torsion	24 064
8	Horizontal Tail Second Bending	27.521
9	Third Wing Bending	30 666
10	Horizontal Tail Torsion	33 893
11	Fuselage Fourth Bending + Second Wing Torsion	37.573
12	Second Wing Torsion	39.229

Table 14

CALCULATED F-111A SYMMETRIC VIBRATION MODES

$\Lambda_{LE} = 26^{o}$ GW = 293,138N (65936 lb)

Mode No.	Mode Description	Frequency - Hz
1	First Wing Bending	4 792
2	First Fuselage Vertical Bending	6.870
3	Wing - Horizontal Tail (in-phase) + Sec. Fuse Bending	13 894
4	Wing - Horizontal Tail (out of phase)	14.721
5	Second Wing Bending	17 110
6	Third Fuselage Bending + Wing Torsion	22 665
7	First Wing Torsion	24.024
8	Horizontal Tail Second Bending	27.197
9	Third Wing Bending	30 446
10	Horizontal Tail Torsion	33 884
11	Fourth Fuselage Bending + Wing Second Torsion	37 551
12	Second Wing Torsion	39 076

Table 15

CALCULATED F-111A SYMMETRIC VIBRATION MODES

$\Lambda_{LE} = 50^{\circ}$ GW = 331,392N (74,515 lb)

Mode No.	Mode Description	Frequency - Hz
1	First Wing Bending	4 908
2	First Fuselage Vertical Bending	6 736
3	Wing - Horizontal Tail (in-phase) + Fuselage Second Bending	13 529
4	Wing - Horizontal Tail (out of phase)	15.218
5	Second Wing Bending	16.762
6	Third Fuselage Bending + Wing Torsion	21.836
7	First Wing Torsion	24.217
8	Horizontal Tail Second Bending	25 987
9	Third Wing Bending + Horizontal Tail Pitch	31.293
10	Horizontal Tail Pitch	33.869
11	Horizontal Tail Bending + Third Wing Bending	37 618
12	Wing Second Torsion + Horizontal Tail Pitch	39.377

Table 16

CALCULATED F-111A SYMMETRIC VIBRATION MODES

Λ_{LE} = 72 5 GW = 268,673N (60,419 lb)

Mode No.	Mode Description	Frequency - Hz
1	First Wing Bending	4 849
2	First Fuselage Vertical Bending	6 913
3	Wing - Horizontal Tail (in-phase) + Fuselage Second Bending	14 391
4	Wing - Horizontal Tail (out of phase)	15 425
5	Second Wing Bending	17 794
6	Third Fuselage Bending + Wing Torsion	22 927
7	First Wing Torsion	24.571
8	Horizontal Tail Second Bending	27 448
9	Third Wing Torsion + Horizontal Tail Pitch	31.927
10	Horizontal Tail Pitch	33.898
11	Second Wing Torsion	39.260
12	Horizontal Tail Torsion	39.856

Table 17

CALCULATED F-111A ANTISYMMETRIC VIBRATION MODES

$\Lambda_{LE} = 26^{o}$ GW = 266,044N (59,800 lb)

Mode No.	Mode Description	Frequency - Hz
1	First Wing Bending	7 417
2	First Fuselage Lateral Bending	8.119
3	Vertical Tail Bending + Wing Bending	10 887
4	Horizontal Tail Bending + Wing Bending	12 290
5	Second Fuselage Lateral Bending	15 720
6	Wing - Horizontal Tail	18 510
7	Third Fuselage Lateral Bending	21 947
8	Wing Torsion + Bending	22.983
9	Wing Torsion + Horizontal Tail Pitch	25 081
10	Vertical Tail Torsion	25.678
11	Vertical Tail Torsion + Second Wing Bending	26 029
12	Second Wing Bending	27 179
13	Fuselage Lateral Bending + Second Wing Bending	31 249
14	Horizontal Tail Pitch	31 990
15	Fuselage Lateral Bending + Second Wing Torsion + Hor Tail Torsion	36 377

Table 18

CALCULATED F-111A ANTISYMMETRIC VIBRATION MODES

$\Lambda_{LE} = 26^{\circ}$ GW = 293,138N (65,936 lb)

Mode No.	Mode Description	Frequency - Hz
1	First Wing Bending	7.284
2	First Fuselage Lateral Bending	7.863
3	Vertical Tail Bending	10 699
4	Horizontal Tail Bending + WingBending	12 078
5	Second Fuselage Lateral Bending	15.663
6	Wing - Horizontal Tail	18.183
7	Third Fuselage Lateral Bending	21 636
8	Fuselage Lateral Bending + Wing Bending	22.586
9	Wing Torsion + Horizontal Tail Pitch	24 647
10	Vertical Tail Torsion	25.260
11	Vertical Tail Torsion + Second Wing Bending	25.595
12	Second Wing Bending	26.881
13	Fuselage Lateral Bending + Second Wing Bending	29 033
14	Horizontal Tail Pitch	31.460
15	Fuselage Lateral Bending + Second Wing Torsion + Hor Tail Pitch	35.189

Table 19

CALCULATED F-111A ANTISYMMETRIC VIBRATION MODES

$\Lambda_{LE} = 50^{\circ}$ GW = 331,392N (74,515 lb)

Mode No.	Mode Description	Frequency - Hz
1	First Wing Bending	6.917
2	First Fuselage Lateral Bending	7.795
3	Vertical Tail Torsion + Wing Bending	10 844
4	Horizontal Tail Bending + Wing Bending	12 290
5	Second Fuselage Lateral Bending	15 070
6	Wing - Horizontal Tail	17 815
7	Horizontal Tail Pitch + Vertical Tail Torsion + Wing Bending	21 185
8	Third Fuselage Lateral Bending	22 354
9	Wing Torsion + Horizontal Tail Pitch	23 794
10	Vertical Tail Torsion	25 264
11	Vertical Tail Torsion + Second Wing Bending	25.915
12	Fuselage Lateral Bending + Second Wing Bending	27 925
13	Second Wing Bending	29 479
14	Horizontal Tail Pitch	31.498
15	Fuselage Lateral Bending + Second Wing Torsion + Hor. Tail Torsion	34 660

Table 20

CALCULATED F-111A ANTISYMMETRIC VIBRATION MODES

Λ_{LE} = 72 5° GW = 268,673N (60,419 lb)

Mode No	Mode Description	Frequency - Hz
1	First Wing Bending	6 036
2	First Fuselage Lateral Bending	7.973
3	Vertical Tail Bending + Horizontal Tail Bending	10 739
4	Horizontal Tail Bending + Wing Bending	12.385
5	Second Fuselage Lateral Bending	16.542
6	Wing - Horizontal Tail (out of phase)	17 408
7	Wing - Horizontal Tail (in-phase)	20 631
8	Vertical Tail Torsion + Wing Torsion	23 599
9	Third Fuselage Lateral Bending + Vertical Tail Torsion	24 085
10	Vertical Tail Torsion	25 462
11	Vertical Tail Bending	25.973
12	Fuselage Lateral Bending + Wing Torsion	29 300
13	Wing Second Bending	30 429
14	Horizontal Tail Pitch	31 581
15	Fuselage Lateral Bending + Wing Second Bending + Hor Tail Torsion	36 404

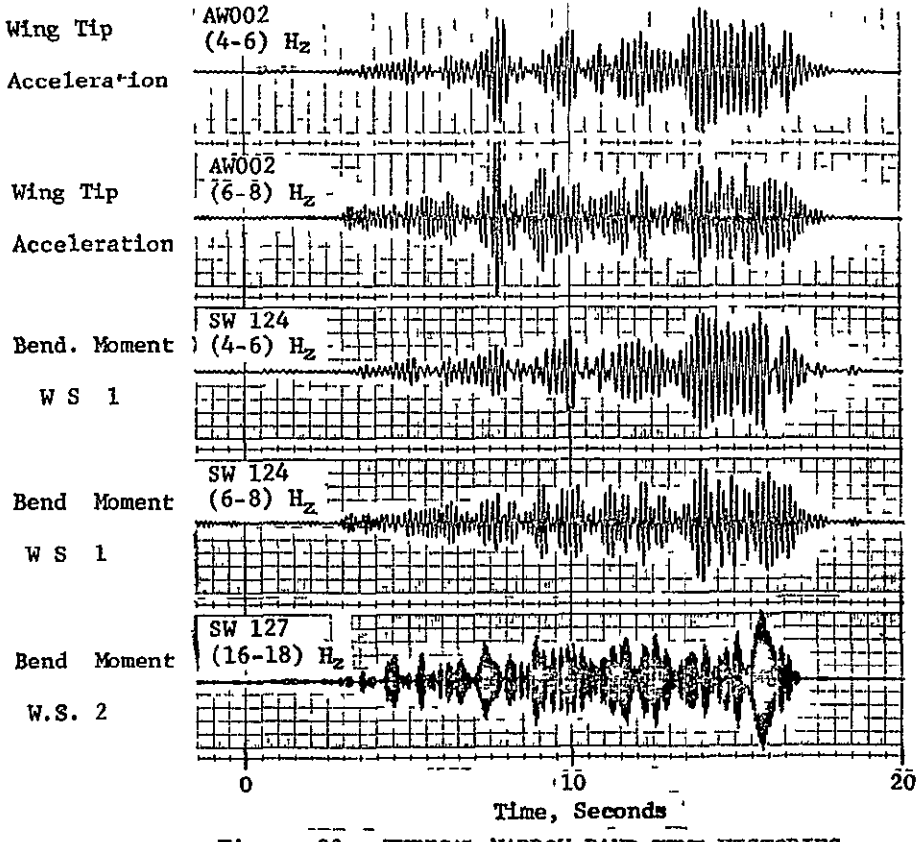

Figure 33 TYPICAL NARROW BAND TIME HISTORIES

The ground vibration tests had indicated that in the frequency range from 4 to 8 hertz three wing vibration modes are likely to be present in the responses. The modes are first symmetric and first antisymmetric wing bending and first fuselage vertical bending coupled with first symmetric wing bending. In the range from 16 to 18 hertz three modes can also be expected. The modes are antisymmetric wing-tail modes (wing motion in-phase and out-of-phase with tail motion) and the second symmetric wing bending mode.

Time histories were also run at higher paper speeds and the frequencies checked at several points on each record. Actually 10 distinct frequencies are present in the range from 5.25 to 7.70 hertz and 6 frequencies in the range from 16.0 to 18.0 hertz. Apparently several asymmetric modes occur rather than the "pure" symmetric or antisymmetric modes and the wing motion is continually shifting from one adjacent mode to another. There is no apparent cycle or trend to the frequency shifts although some of the frequencies do occur several times during the maneuver.

The interference of one adjacent model response on another precluded obtaining meaningful variations of damping characteristics with angle of attack; but the narrow band time histories were a useful tool for diagnosing what is happening.

Horizontal Tail Power Spectra for $\Lambda_{LE} = 26^{o}$

Power spectra for the horizontal tail dynamic loads are presented in Figures 34 and 35 for two data samples represented by nominal angles of attack of 7.1 and 12.2 degrees, respectively, for the nominal Mach number of 0.80 and an altitude of 6035 meters. These data samples are the same as were presented in the Phase I report (Reference 1) for the wing and fuselage responses. Shown are the power spectra for vertical shear and bending moment at the root and hingeline torque for both left and right horizontal tails.

The plotted data have been normalized by a scale factor which is the sum of the values over the range of frequencies from 1 to 100 hertz. The values plotted at 0 and 1 hertz are fictitious and were used to establish the plot format using an automatic plotting routine. If a data point falls on the lower bound of the plot for other frequencies, the value is either at or below the lower bound of the dynamic range of the recording/processing system.

This plot format serves several purposes. First, all of the dynamic data fall within a four decade band. Second, the scale factor can be easily converted to either U.S. Customary or S.I. units. Finally, human errors in the data processing usually occurred in recording the gains during processing and could be easily detected and corrected.

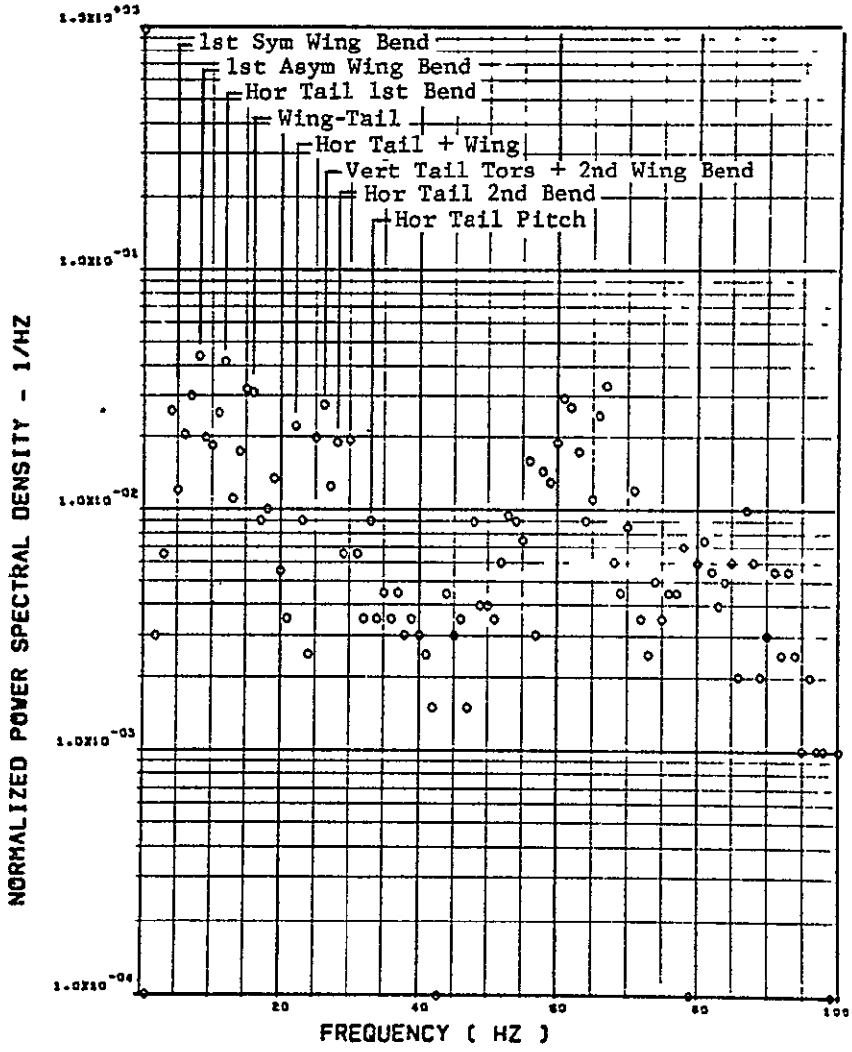

(a) ST077 SHEAR, L/H HORIZ TAIL ROOT

Figure 34. HORIZONTAL TAIL SPECTRA
$\Lambda_{LE} = 26^{o}$, M = 0.80, $\alpha_{NOM} = 7.1^{o}$

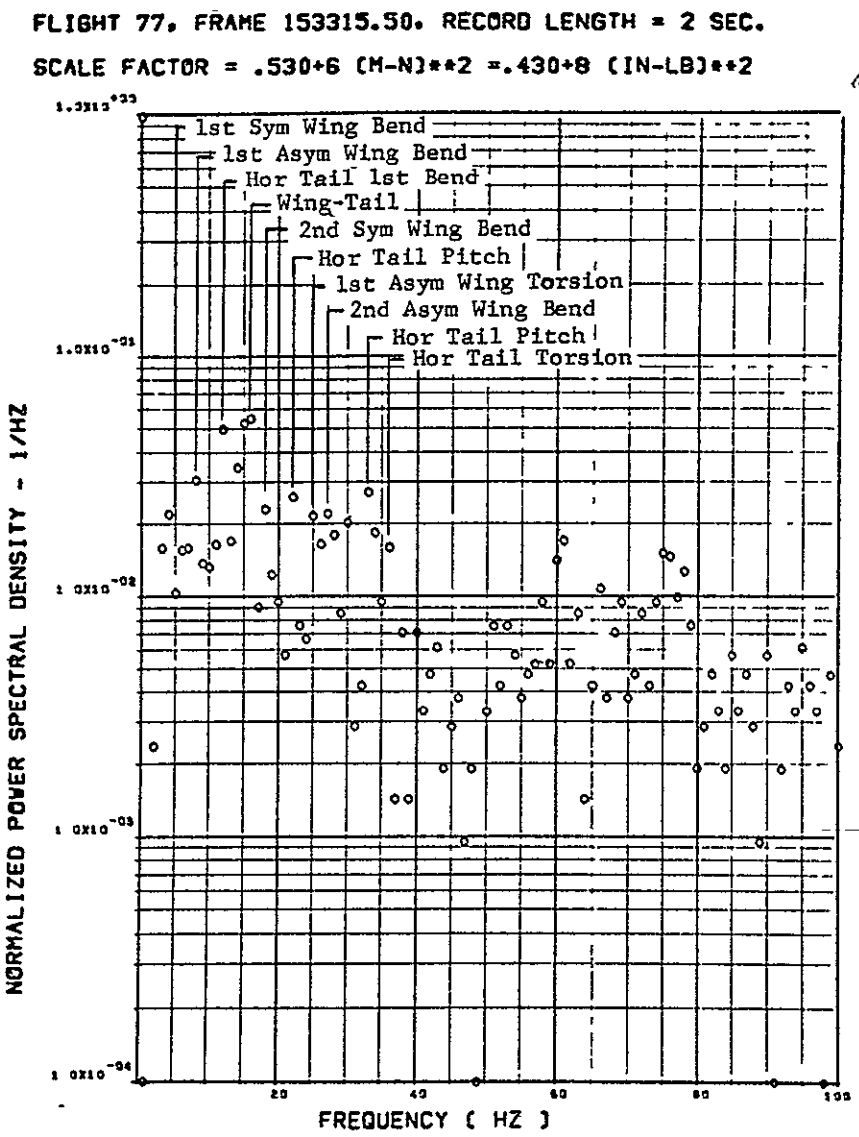

(b) ST078 BEND. MOM. L/H HORIZ TAIL ROOT

Figure 34. Continued

FLIGHT 77. FRAME 153315.50. RECORD LENGTH = 2 SEC.

SCALE FACTOR = .415+6 (M-N)**2 =.337+8 (IN-LB)**2

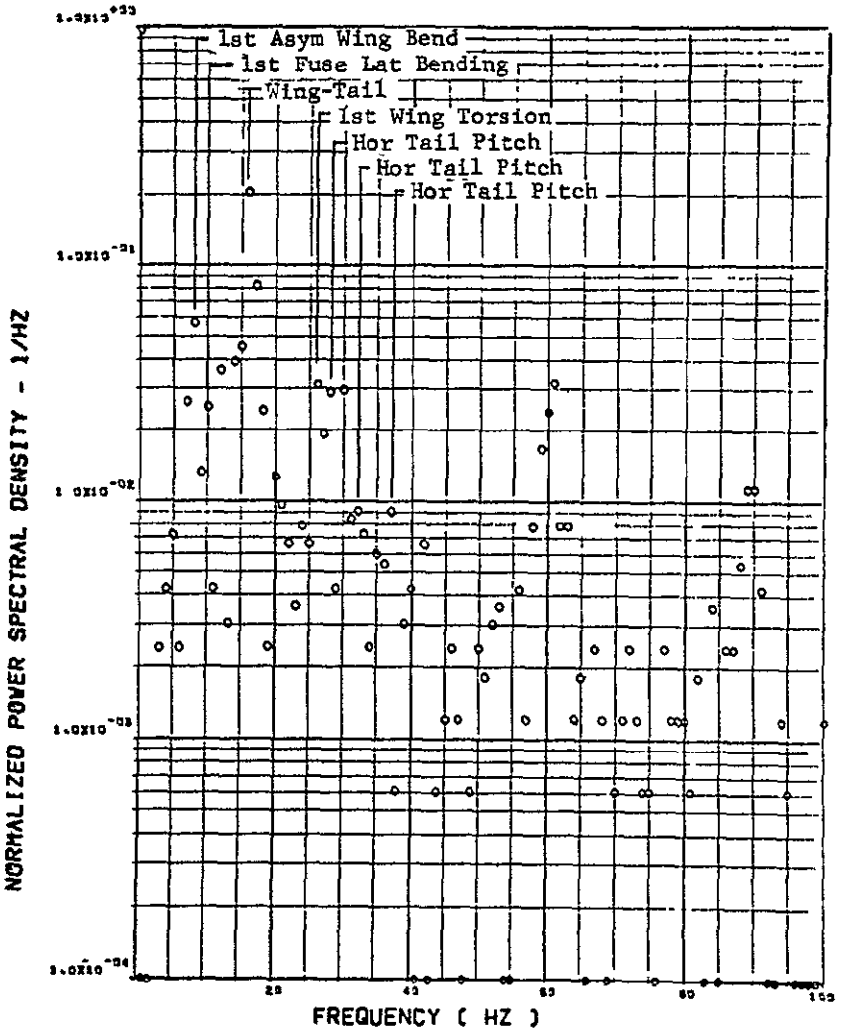

(c) ST135 TORSION. L/H HORIZ TAIL HINGE LINE

Figure 34. Continued

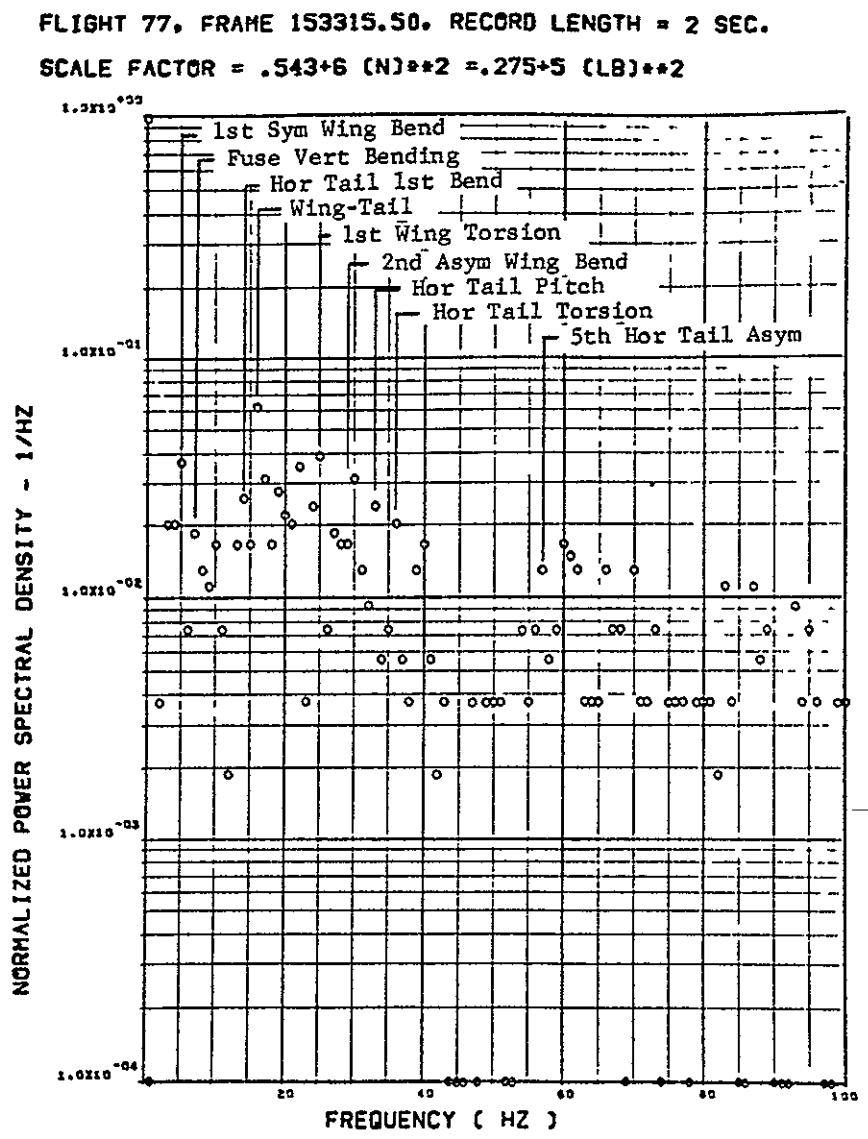

(d) ST072 SHEAR, R/H HORIZ TAIL ROOT

Figure 34. Continued

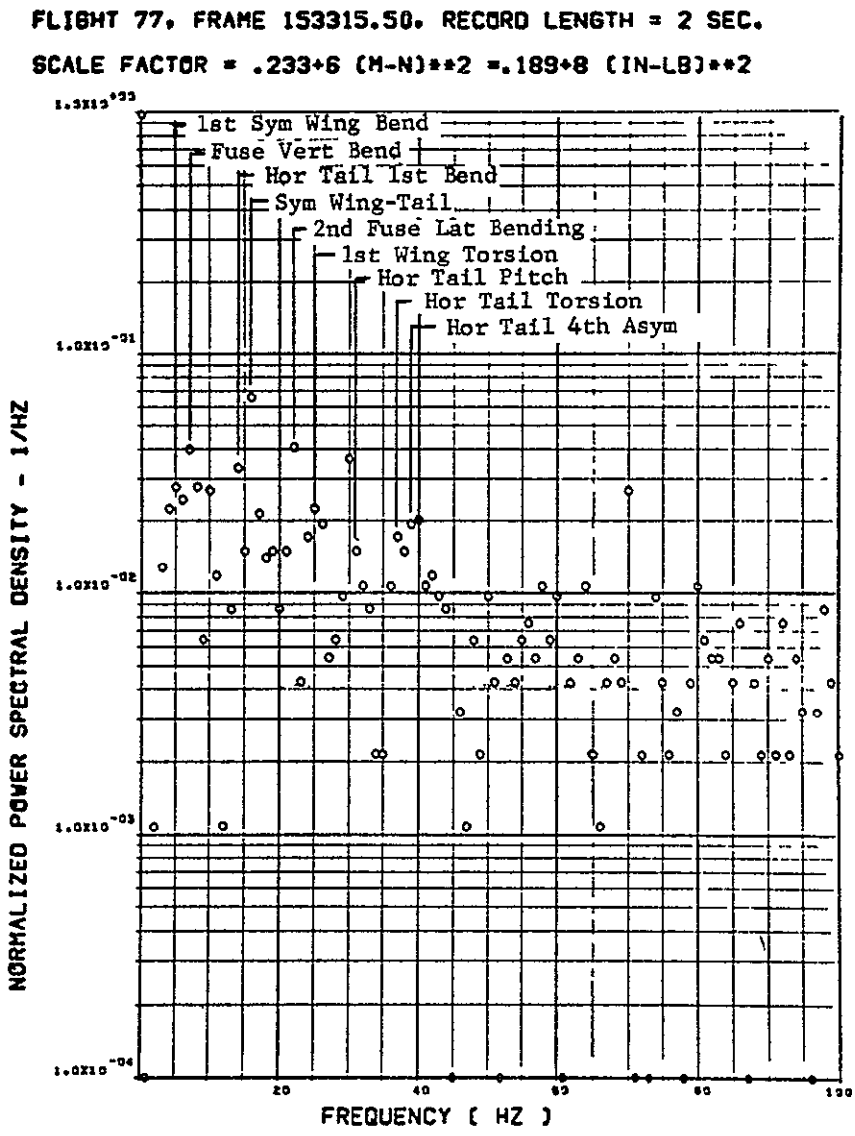

(e) ST073 BEND. MOM. R/H HORIZ TAIL ROOT

Figure 34. Continued

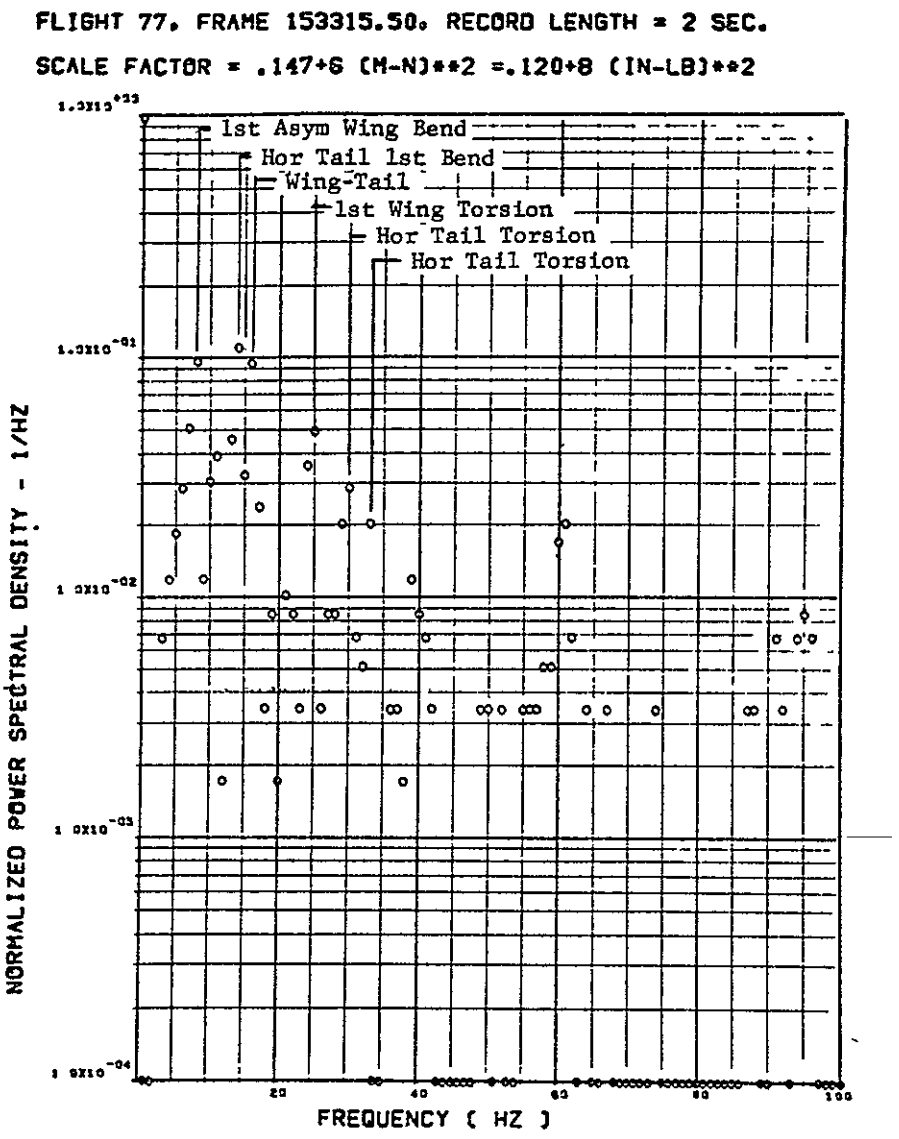

(f) ST118 TORSION, R/H HORIZ TAIL HINGE LINE

Figure 34. Concluded

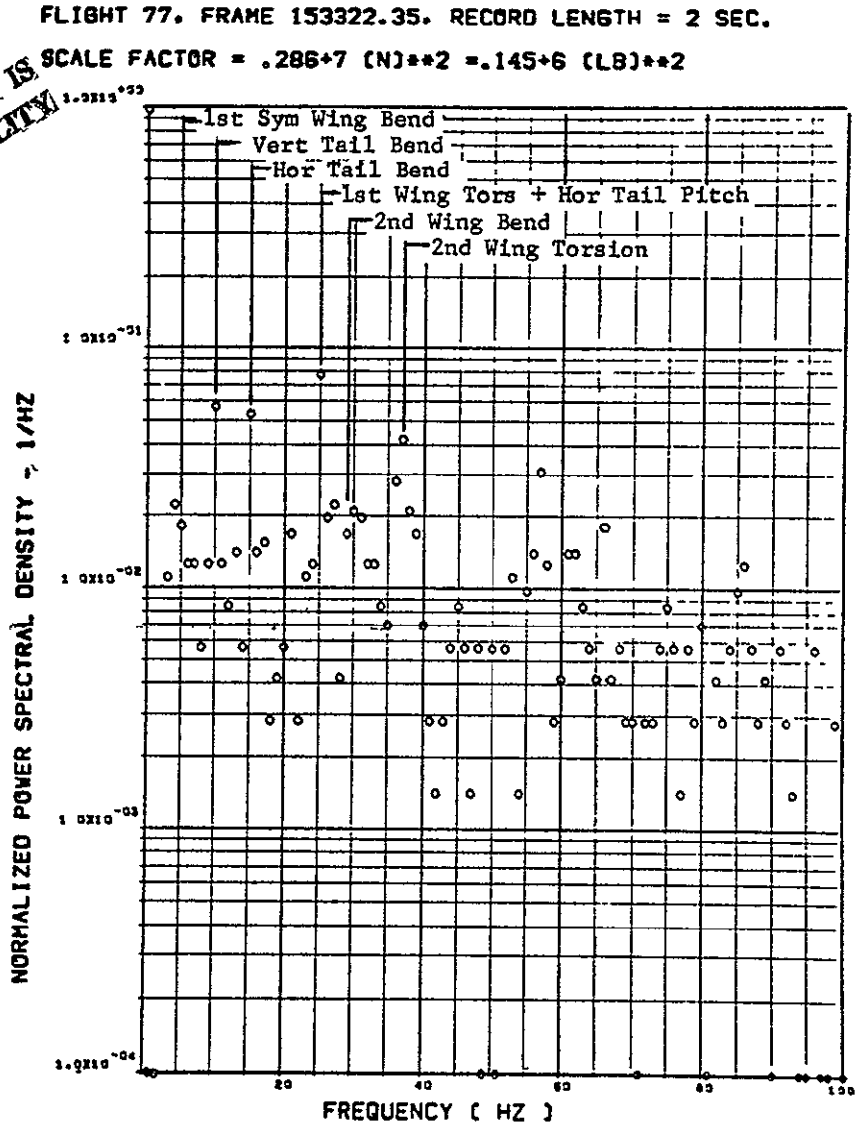

(a) ST077 SHEAR, L/H HORIZ TAIL ROOT

Figure 35. HORIZONTAL TAIL SPECTRA
Λ_{LE}= 26°, M = 0.80 , α_{NOM} = 12.2°

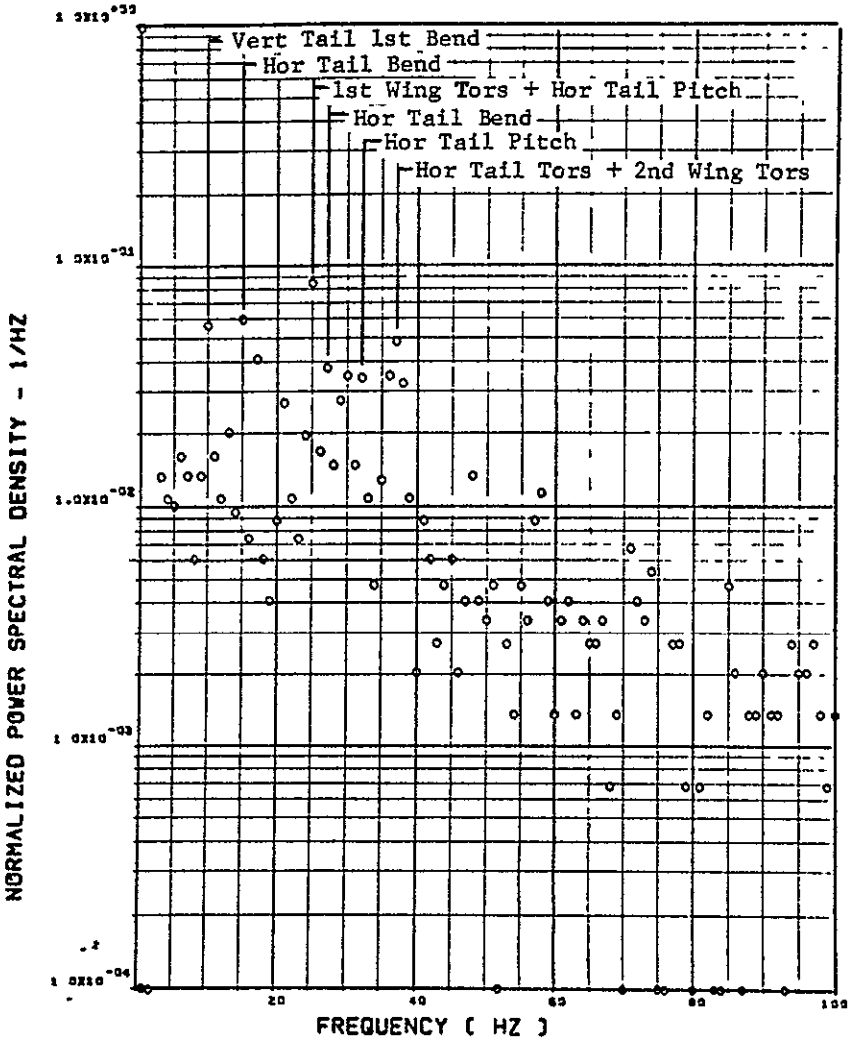

(b) ST078 BEND. MOM. L/H HORIZ TAIL ROOT

Figure 35. Continued

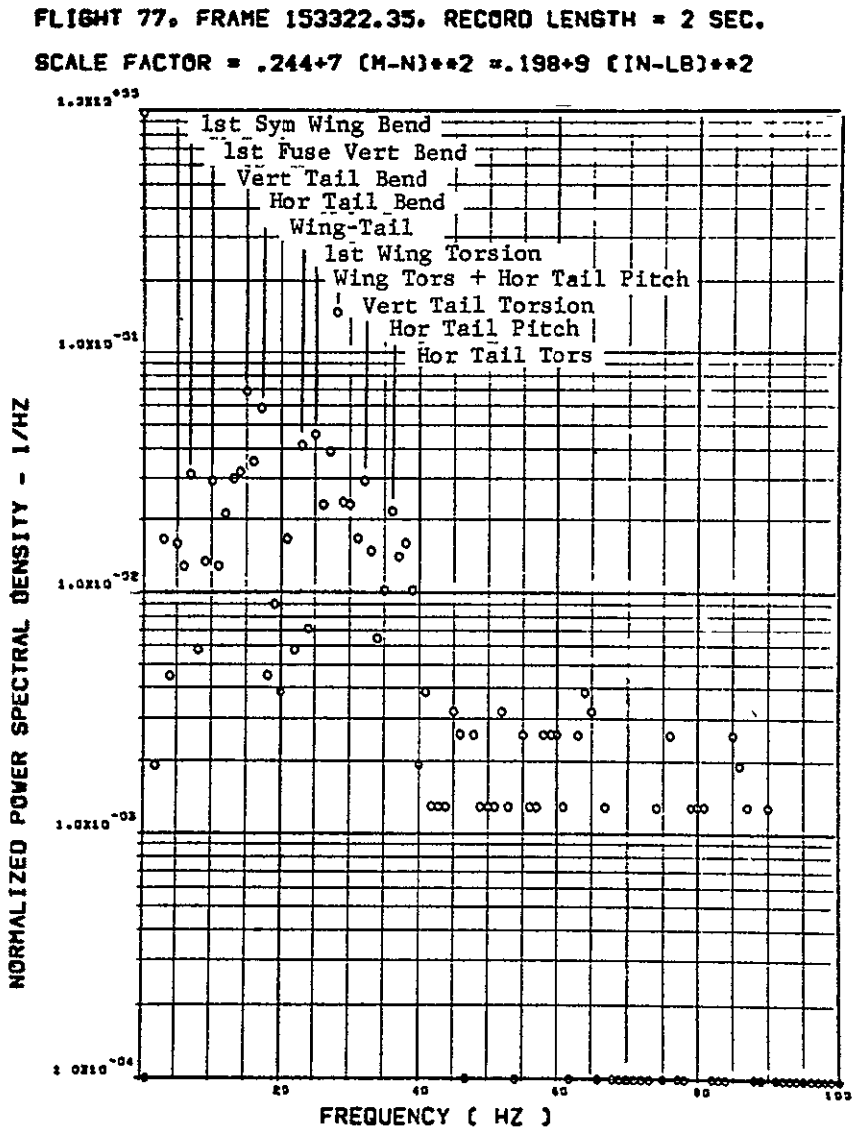

(c) ST135 TORSION. L/H HORIZ TAIL HINGE LINE

Figure 35. Continued

FLIGHT 77. FRAME 153322.35. RECORD LENGTH = 2 SEC.

SCALE FACTOR = .525+7 (N)**2 =.265+6 (LB)**2

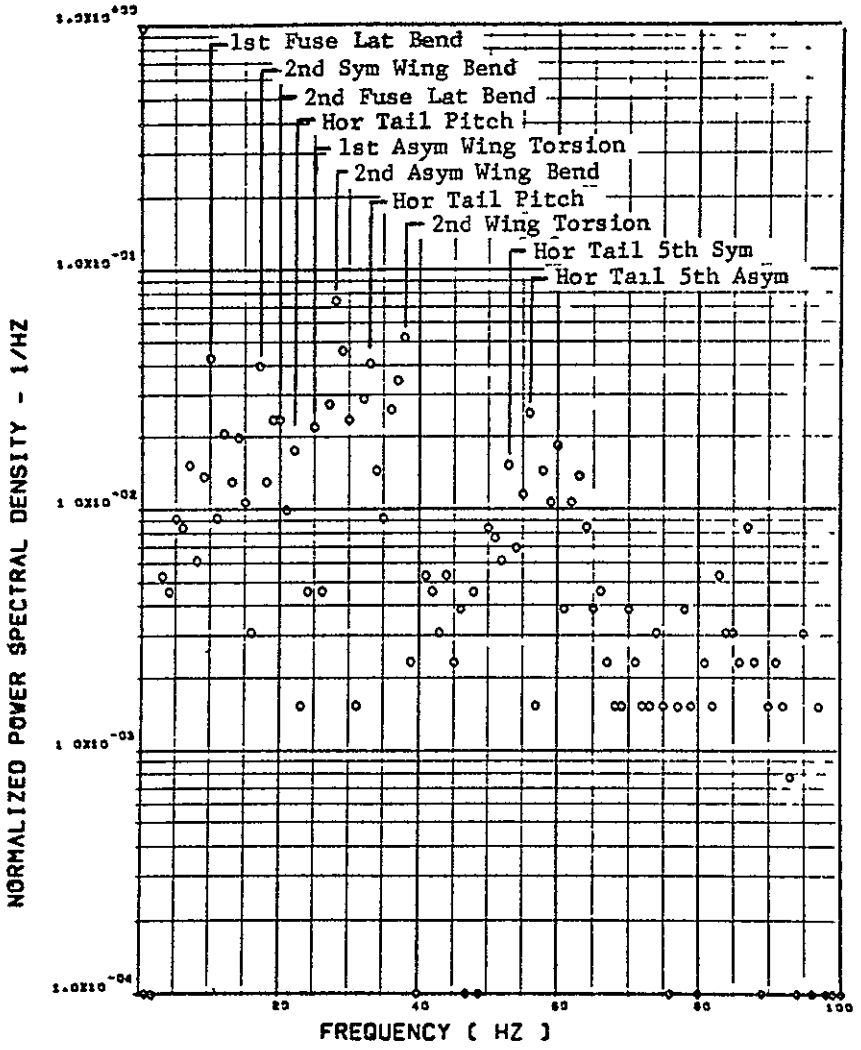

(d) ST072 SHEAR. R/H HORIZ TAIL ROOT

Figure 35. Continued

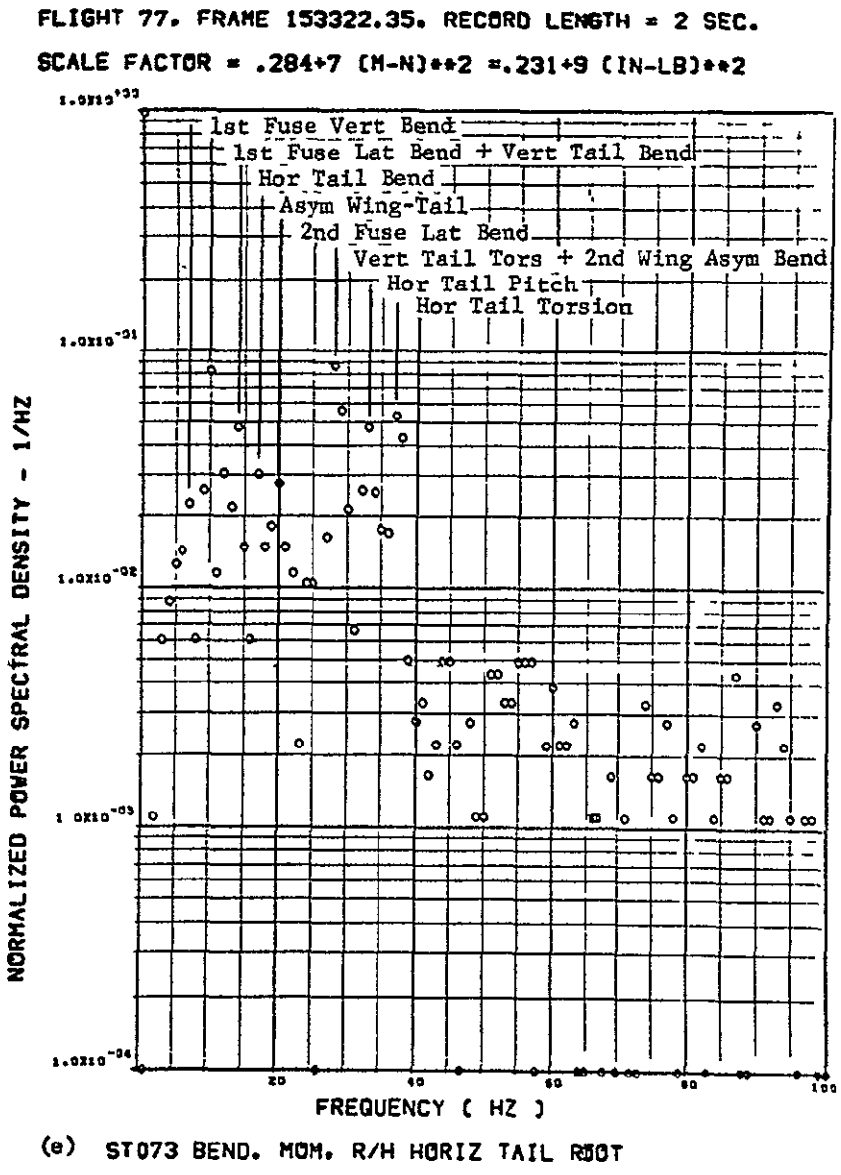

Figure 35. Continued

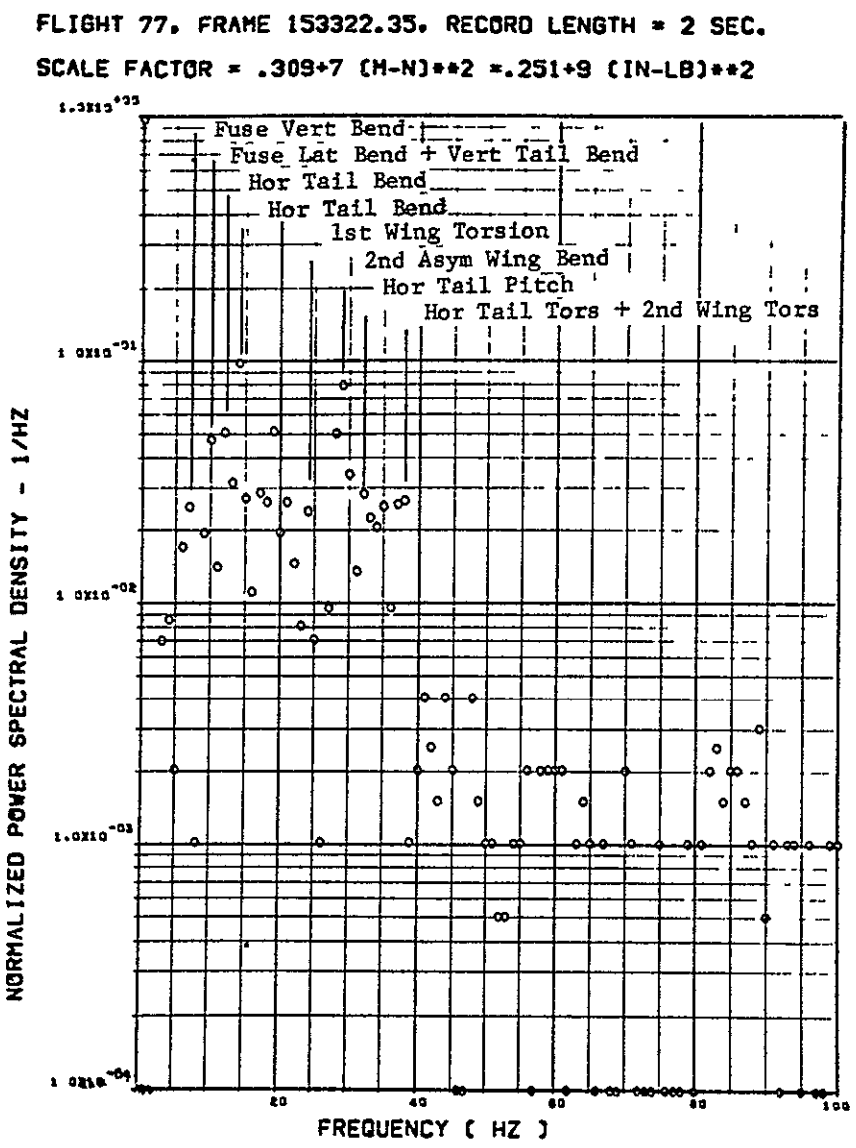

Figure 35. Concluded

In Phase I wing and fuselage responses which occurred at the frequencies listed below were tentatively associated with horizontal tail motion.

Frequency, hertz	Vibration Mode
12	first horizontal tail bending
16	wing-tail
26-28	second horizontal tail bending
31-33	horizontal tail pitch (torsion)
36	horizontal tail pitch
38-39	horizontal tail plus second wing torsion
43-44	horizontal tail pitch
52-53	horizontal tail symmetric fifth mode
57-58	horizontal antisymmetric fifth mode

Figures 34 and 35 are annotated with the vibration modes associated with the peaks in the spectra. Each of the frequencies listed above appear in one or more of the spectra although in some cases the amplitudes are quite small. In addition, small differences in frequencies apparently occur between the left and right tails for some of the modes.

One apparent difference in the spectral content of the responses for the two angles of attack is the growth in response in lateral fuselage bending modes at 10 and 20 hertz for the higher angle of attack relative to response

in other modes. The high responses at 28 hertz indicate that the horizontal tail second bending may be coupling with a vertical tail torsion mode.

Effects of Wing Sweep

It was expected that the spectral content of the structural response would change somewhat with wing sweep because the separated flow fields are different and the natural vibration mode shapes are also somewhat different. In order to better show the effects the power spectra described in the following comparisons are not normalized. Data are presented showing comparisons for wing bending moments at all four wing stations, torsion moment at Wing Station 3, and the pilot's seat and center of gravity accelerometers.

Wing Bending Moment

Figures 36a through 36d present side by side comparisons of power spectra for wing bending moments measured at each of the four wing stations for three wing sweep angles. The data are represented by lines in these comparisons rather than discrete data points for clarity. The range of frequencies is from 2 to 45 hertz because those limits applied to data from wing stations 2 and 4. The angles of attack are such that the flow separation is well developed at each sweep angle.

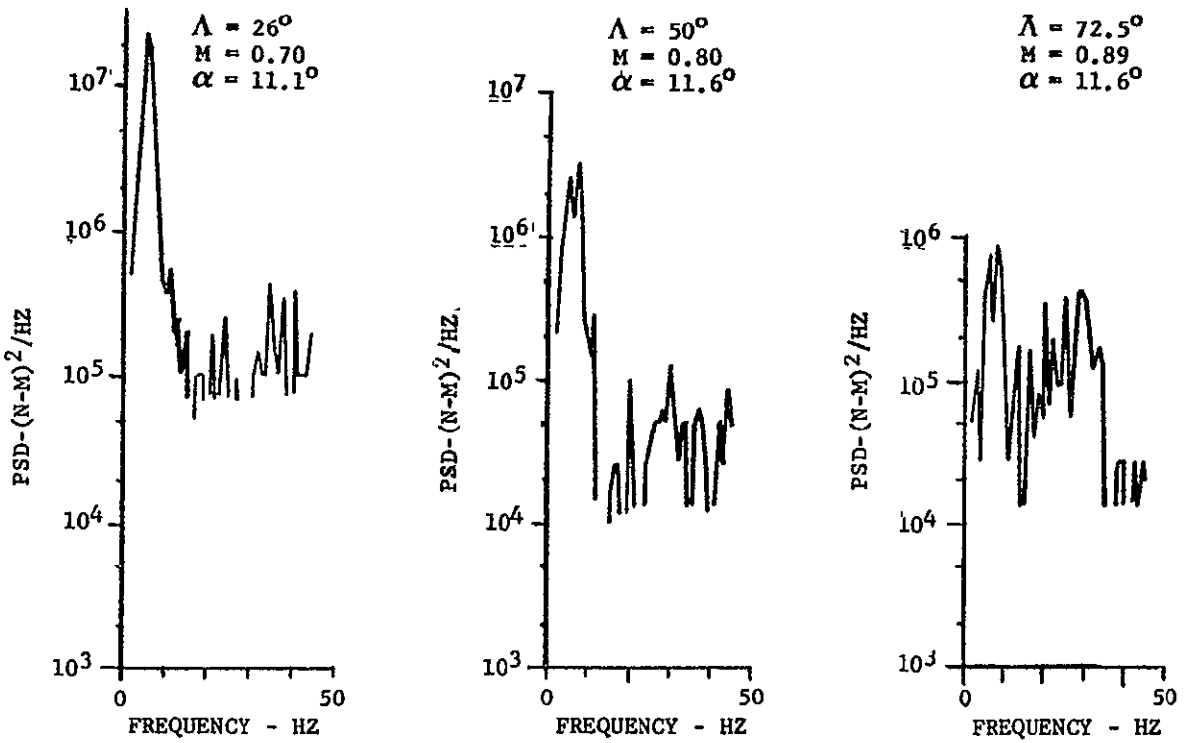

(a) Wing Station 1

Figure 36. COMPARISONS OF WING BENDING MOMENT SPECTRA AT THREE WING SWEEPS

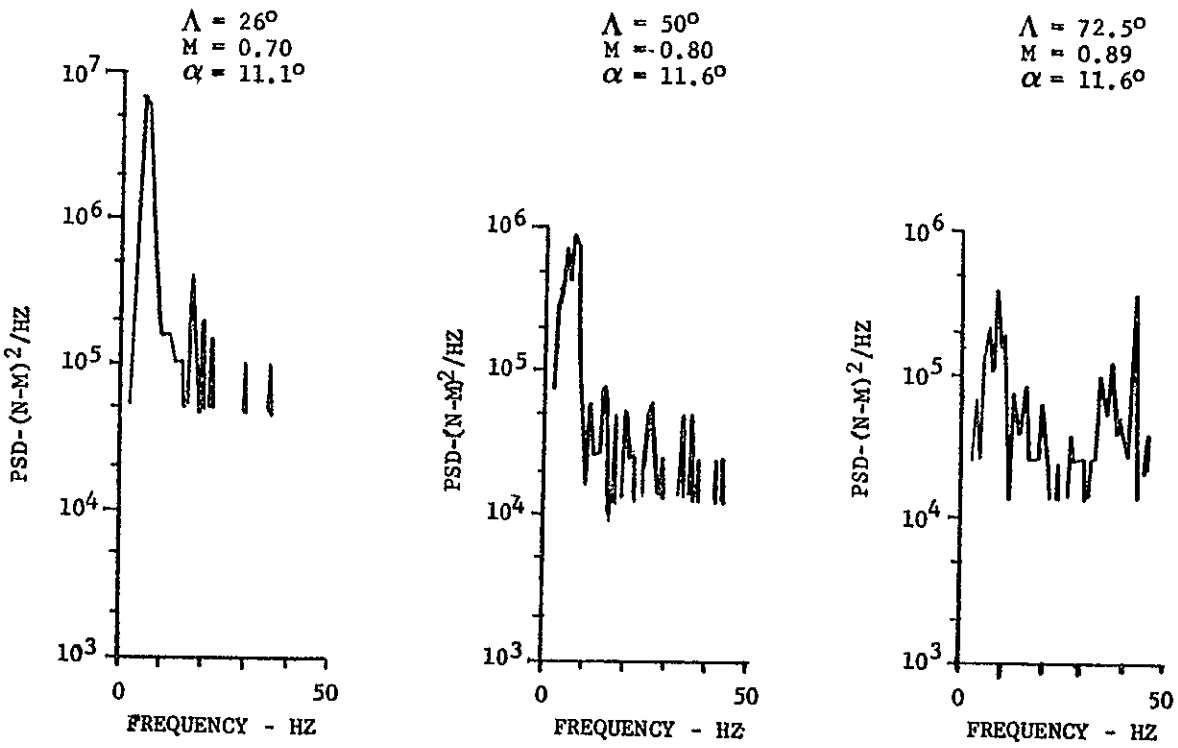

(b) Wing Station 2

Figure 36. Continued.

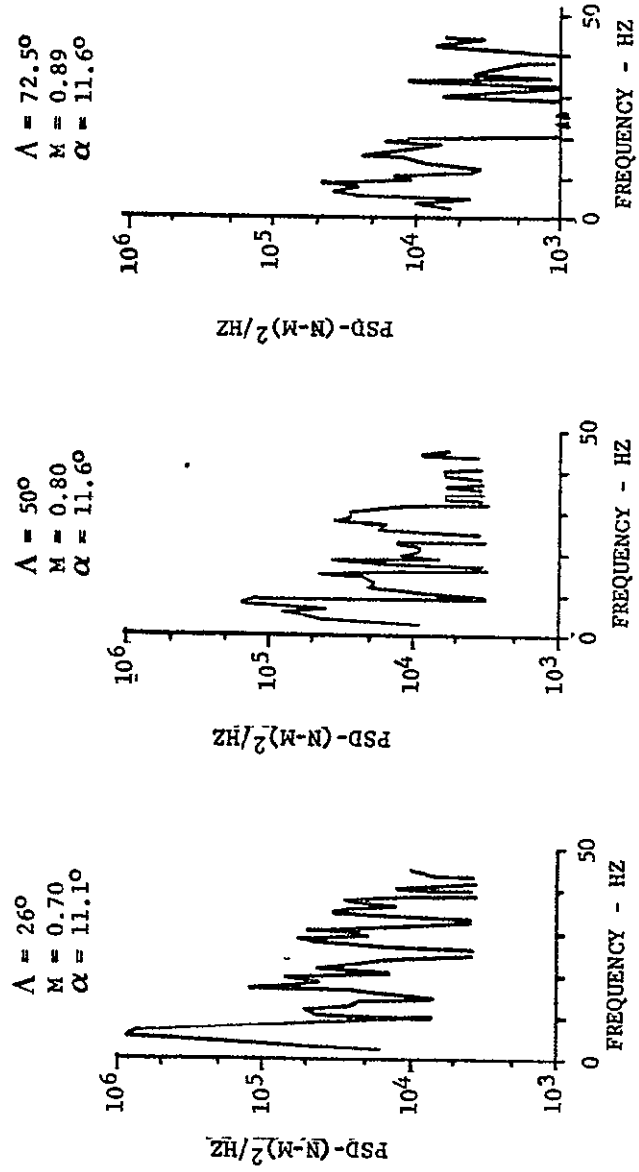

(c) Wing Station 3

Figure 36. Continued

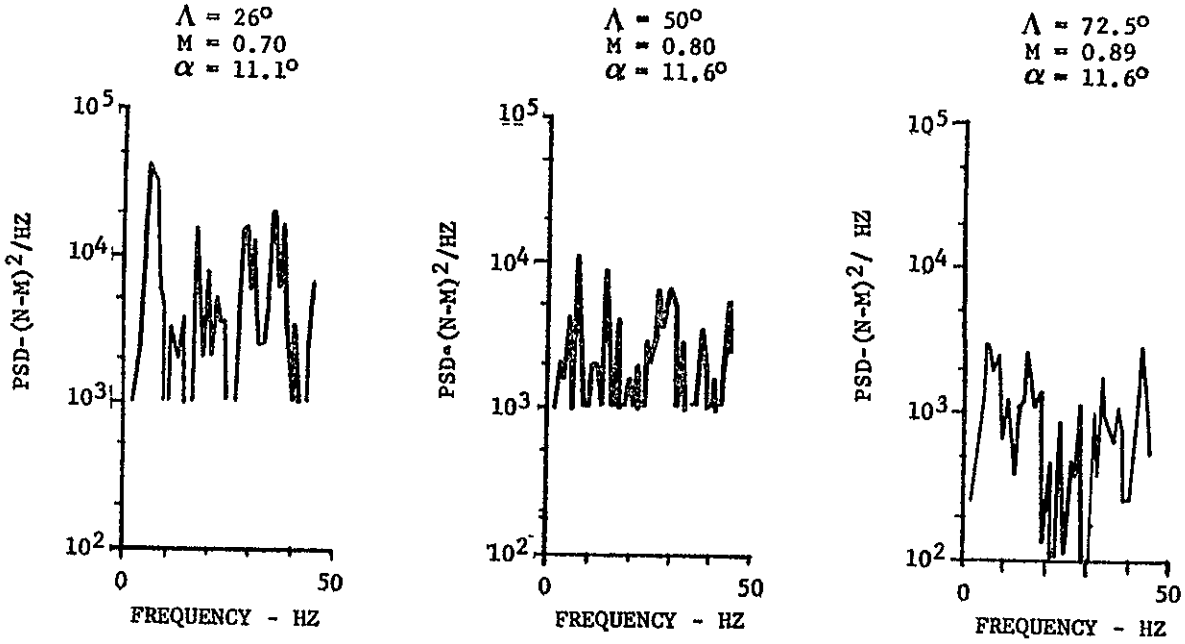

(d) Wing Station 4

Figure 36. Concluded

At Wing Station 1 (Figure 36a) there is a marked decrease of the response in the dominant first wing bending modes as wing sweep is increased from 26 degrees. In addition there is a decrease of response in the higher frequency modes between 26 and 50 degrees sweep but an increase between 50 and 72.5 degrees-sweep. As a consequence the relative response in the higher frequency modes at maximum sweep is appreciable. These general trends also exist at Wing Station 2 but as expected the level of response is reduced from the levels at Wing Station 1. At Wing Stations 3 and 4 the higher frequency modes including wing-tail second symmetric and second antisymmetric wing bending and several horizontal tail modes produce major contributions to the response at all three wing sweeps. The level of response decreases progressively with increasing wing sweep at Wing Stations 3 and 4.

The character of these responses can be directly related to the type of flow separation which has occurred. At 26 degrees sweep the critical separation occurs at the trailing edge between wing stations 3 and 4 and progressively moves forward in that region with angle of attack. For the condition presented the separation has just reached the leading edge and has started to spread rapidly spanwise. High Reynolds number test data obtained with the 1/6-scale semispan model

indicate that significant excitation occurs at low frequencies which induces response in the low frequency wing modes.

At 50 degrees sweep the flow separation is of the leading edge type which forms a vortex sheet that breaks down well forward on the wing at the condition analyzed. Again significant excitation at low frequencies causes the response in the low frequency modes.

At maximum sweep the flow separation forms a well organized leading edge vortex which produces excitation over a broad band of frequencies but at a lower level than occurs at the lower sweeps. There is little chordwise correlation of the pressure fluctuations. As a consequence the overall response is lower than at the lower wing sweeps.

Wing Torsion

A comparison of the spectral content of the torsional response at Wing Station 3 for the three wing sweeps is presented in Figure 37. The lines on this plot represent envelope curves which connect the peak responses rather than the detailed spectra and the range of frequencies extends from 2 to 100 hertz. These comparisons show that for the conditions analyzed here the torsional response occurs over a broad band of frequencies for all the wing sweeps rather than being concentrated primarily in the first wing torsion modes as was the case for 26 degrees wing sweep at M = 0.80.

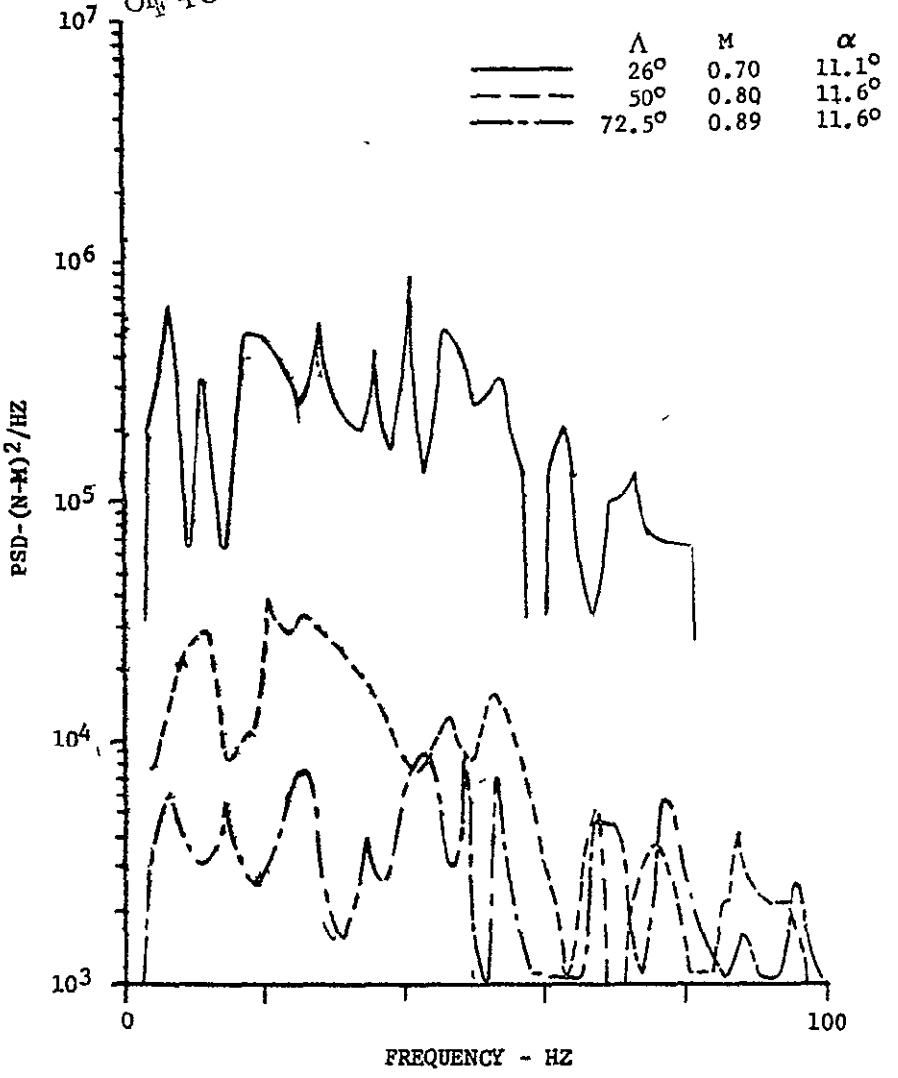

Figure 37. ENVELOPES OF SPECTRAL PEAKS FOR THREE WING SWEEPS - TORSION MOMENT AT WING STATION 3

It is of interest to note the response in the 35 to 60 hertz frequency range which apparently affects the response at the center of gravity.

Pilot's Seat Acceleration

Comparisons of envelope curves connecting the peak spectral responses of the Pilot's Seat vertical accelerometer are presented in Figure 38 for the three wing sweeps. In addition a curve for 26 degrees sweep at M = 0.80 is shown. By far the major share of the response occurs in the range from 2 to 50 hertz for all the cases although an isolated peak of substantial level occurs above 60 hertz. It is of interest to note that although the first and second fuselage vertical bending modes contribute to the response there are equally significant contributions in the first and second wing torsion modes at higher frequencies. In fact at 26 degrees sweep at M = 0.80 the responses due to wing torsion-bending coupling are so large that the crew designated the response as heavy buffet. The spikes that occur above 60 hertz have not been identified with a particular vibration mode and apparently are not sensed by the crew.

Center of Gravity Acceleration

Comparisons of envelope curves of the spectral response measured by the center of gravity accelerometer are presented in Figure 39

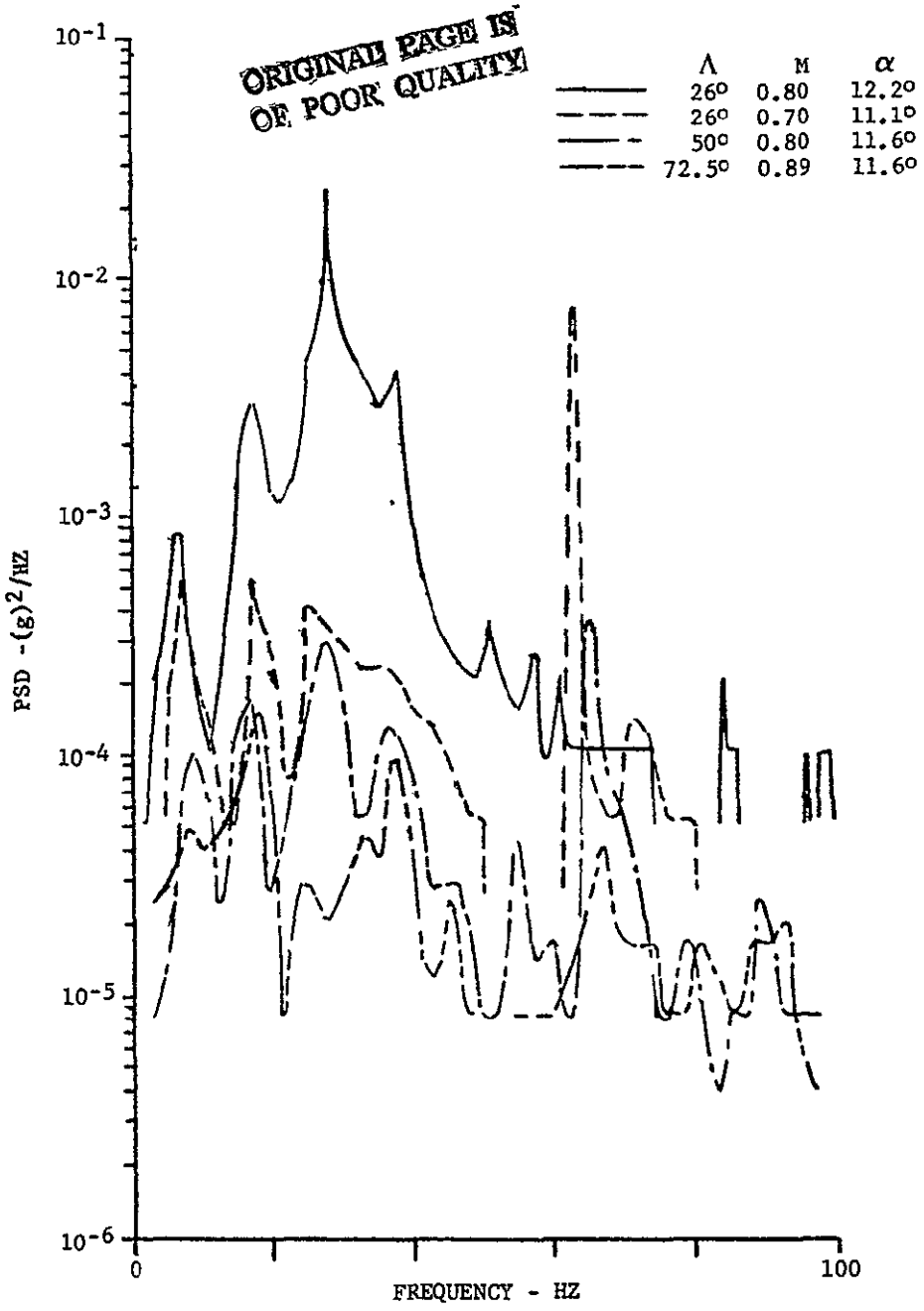

Figure 38. ENVELOPES OF SPECTRAL PEAKS FOR THREE WING SWEEPS - PILOT'S SEAT VERTICAL ACCELERATION

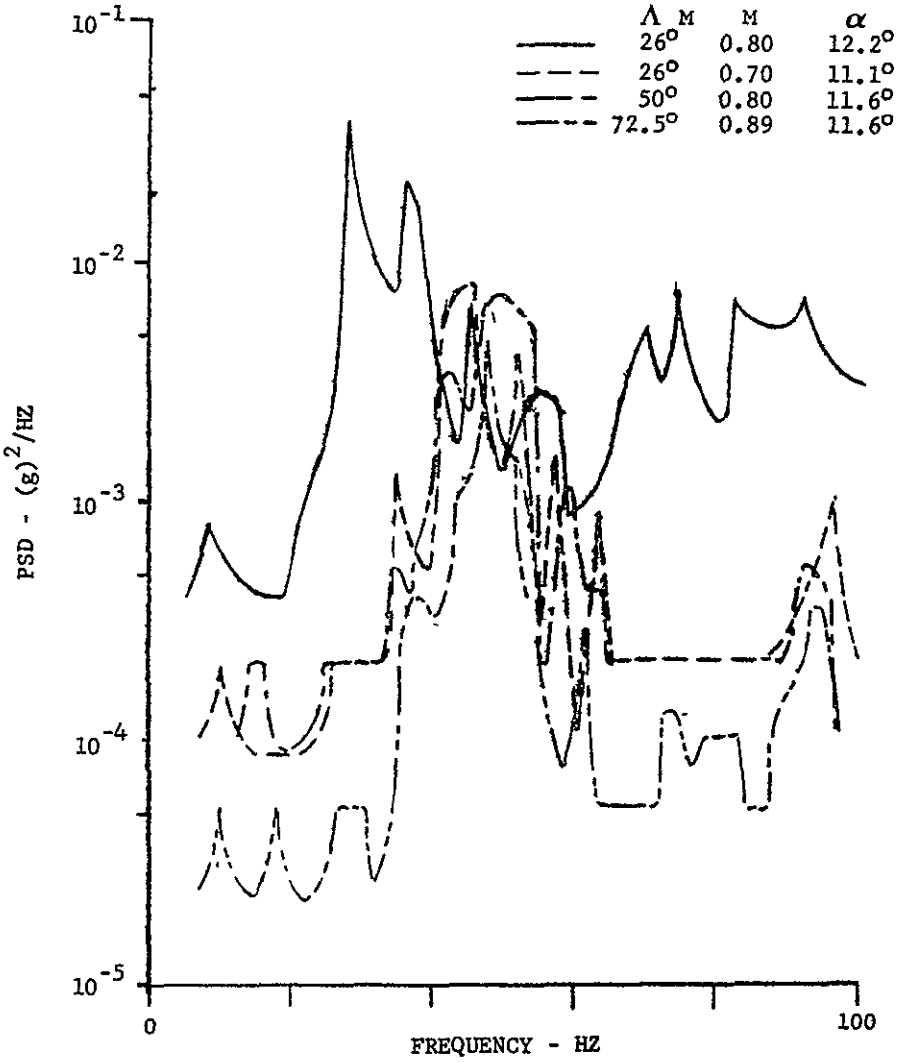

Figure 39. ENVELOPES OF SPECTRAL PEAKS FOR THREE WING SWEEPS - CENTER OF GRAVITY VERTICAL ACCELERATION

With the exception of the $\Lambda_{LE} = 26^{o}$, M = 0.80 case the major portion of the responses occur in the frequency range from 35 to 60 hertz and the levels are significantly higher than those measured at the pilot's seat. Initially it was thought that horizontal tail motions were causing the high response but examination of the horizontal tail spectral data showed that tail motion for some of the frequencies was very small. Further examination of the wing responses particularly those in torsion at Wing Station 3 indicated a close correlation between the wing torsion response and the center of gravity accelerations in that frequency range. Torsion data at Wing Station 3 were not available for the $\Lambda_{LE} = 26^{o}$ M = 0.80 wind-up turn. However, data from a pullup at $\Lambda_{LE} = 26^{o}$ M = 0.80 at lower altitude showed significant correlation between center of gravity acceleration and wing torsion response in the 25 to 40 hertz frequency range

SECTION 8

CONCLUDING REMARKS

The substance of this report deals with Phase II of an investigation of flight buffeting of the F-111A aircraft. It is appropriate, however, to summarize conclusions drawn from the flight data analyses performed during both Phase I and Phase II.

The objectives of the overall investigation were threefold:

(1) to establish the feasibility of applying stochastic analysis methods to structural vibration data obtained during moderate to high-g maneuvers of the aircraft.

(2) to develop a more detailed understanding of the structural response of the aircraft to buffet and thereby provide guidance for establishing an improved method of predicting the structural response.

(3) to provide flight data to evaluate the prediction method.

When measured against these objectives the investigation has been a fruitful endeavor.

At the outset of the program there was some doubt that stochastic analysis methods would be appropriate because of the transient nature of the maneuvers. However, by breaking down each maneuver time history into several short segments the variations of angle of attack and Mach number within a data sample were kept reasonably small in most cases.

In this way the statistical requirements appropriate to power spectral analysis are approximately satisfied with respect to stationarity of the data. The short duration time samples of course reduce the confidence level in the results in a statistical sense, but the results have indicated quite good agreement between power spectra from different data samples taken under nominally the same conditions of angle of attack and Mach number.

In future flight test programs it would be beneficial if data samples of longer duration could be obtained at nominally constant conditions of angle of attack and Mach number.

The capability of the F-111A aircraft to be configured to different aerodynamic shapes via its variable wing sweep feature has been of significant benefit with respect to developing an understanding of the buffeting response of different classes of aerodynamic vehicles.

The primary finding of the investigation is the fact that the aircraft structural response to buffet during moderate-to-high-g maneuvers is very complex. Many of the natural structural vibration modes can be excited to significant levels of response. As a consequence the early methods of analysis and prediction which assumed that the first-wing-bending mode response as measured at the wing

"root" is of primary concern are woefully inadequate in assessing the variations of buffeting intensity with angle of attack and Mach number.

Even though the root bending loads are the largest of those measured in absolute magnitude, they are relatively small (4 to 5 percent) in terms of the quasi-steady loads produced during a high-g maneuver. From a structural design viewpoint the dynamic loads near the wing tip due to buffet are much larger relative to the maneuver loads (15 to 20 percent) and include higher frequency vibration modes which could contribute to fatigue damage, particularly fatigue of secondary structure.

Dynamic wing torsion loads at low wing sweep were found to be much larger than anticipated from previously published information, particularly at conditions for which shock-induced separations are present. This finding could have a significant impact on advanced wing-design efforts which have concentrated on developing quasi-two-dimensional flow over a major portion of the wing span. It is precisely that type of flow which can produce large torsion responses when shock-induced separation does occur.

In contrast to the low wing sweep case, the more three-dimensional flow separations associated with higher wing leading-edge sweep produce smaller structural responses

(especially torsion), and particulary so if the sweep is high enough for well organized leading edge vortex type flow separation to occur. If leading edge vortex "bursting" occurs ahead of the wing trailing edge then a significant increase of structural response will take place. One can infer from these results that it may be possible to significantly reduce buffeting by using complex wing planforms which produce significant amounts of vortex lift.

The vibrational environment at the crew station due to buffet is of vital importance for fighter aircraft. The present investigation showed that the higher frequency wing bending and wing torsion modes produced the most significant increases in vertical and lateral accelerations at the pilot's seat with increasing angle of attack during the high-g maneuvers. It appears that aerodynamic design to reduce dynamic wing torsion and structural design to minimize crew station normal and lateral motions at frequencies near the second wing bending modes and the wing torsion modes would have significant payoff in terms of crew comfort.

One vibration mode which can contribute significantly to the structural response sensed by the crew is trailing edge flap pitch. In the present investigation that mode

tended to couple with second wing torsion to produce large responses at the pilot's seat. It would appear fruitful in future aircraft designs to tailor the structural design to decouple trailing edge flap or trailing edge control modes from the basic wing modes if possible.

The decision to perform spectral analysis of the accelerations and dynamic loads at several locations on the aircraft for a few selected maneuvers rather than concentrate on a few items of measurement and look at many maneuvers appears in retrospect to have been a wise one. The detailed spectra have not only helped in the formulation of the prediction method, but are also vital to the evaluation process. It is recommended that future flight investigations of other aircraft include a broad array of sensor types and locations such as used in this program in order to further develop the data base for understanding structural response to buffet.

REFERENCES

1. Benepe, D.B., Cunningham, A.M., Jr., and Dunmyer, W.D., An Investigation of Wing Buffeting Response at Subsonic and Transonic Speeds: Phase I F-111A Flight Data Analysis. Volume I - Summary of Technical Approach, Results and Conclusions, NASA CR-152109, May 1978.

2. Benepe, D.B., Cunningham, A.M., Jr., and Dunmyer, W.D., An Investigation of Wing Buffeting Response at Subsonic and Transonic Speeds: Phase I F-111A Flight Data Analysis. Volume II - Plotted Power Spectra, NASA CR-152110, May 1978.

3. Benepe, D.B., Cunningham, A.M., Jr., and Dunmyer, W.D., An Investigation of Wing Buffeting Response at Subsonic and Transonic Speeds: Phase I F-111A Flight Data Analysis. Volume III - Tabulated Power Spectra, NASA CR-152111, May 1978.

4. Chudyk, D.W., Transonic Wind Tunnel Tests of a 1/24-Scale F-111A and EF-111A, Airplane No. 59, CALSPAN Corporation Report No. AA-4003-W-23, April 1974.

5. Benepe, D.B., Cunningham, A.M., Jr., and Dunmyer, W.D., "A Detailed Investigation of Flight Buffeting Response at Subsonic and Supersonic Speeds," AIAA Paper 74-358, Presented at the AIAA/ASME/SAE 15th Structures, Structural Dynamics and Materials Conference, Las Vegas, Nevada, April 17-19, 1974.

6. Nevius, H.E., F-111A Ground Vibration Test-No Wing Stores (Airplane 12), General Dynamics Fort Worth Division Report FZS-12-167, 5 August 1966, and Supplement 1, 1 August 1967.

7. Nevius, H.E., F-111A Ground Vibration Tests-No Wing Stores (Airplanes 1-11), General Dynamics Fort Worth Division Report FZS-12-060, 1 March 1965.

8. Cunningham, A.M., Jr., Waner, P.G., Watts, D. and Benepe, D.B., "Development and Evaluation of a New Method of Predicting Aircraft Buffet Response," AIAA Paper 75-69, Presented at the 13th AIAA Aerospace Sciences Meeting, Pasadena, California, January 20-22, 1975.

9. Cunningham, A.M., Jr., Benepe, D.B., Watts, D., and Waner, P.G., A Method for Predicting Full Scale Buffet Response with Rigid Wind Tunnel Model Fluctuating Pressure Data. Volume I - Prediction Method Development and Assessment, NASA CR-3035.

10. Cunningham, A.M., Jr., Benepe, D.B., Watts, D., and Waner, P.G., A Method for Predicting Full Scale Buffet Response with Rigid Wind Tunnel Model Fluctuating Pressure Data. Volume II - Power Spectral Densities for Method Assessment, NASA CR-3036.